



Title	Microwell assist biosensor for neutrophils response cells using localized surface plasmon resonance and luminol - based electrochemiluminescence sensing application
Author(s)	Mohamed Ali, Riyaz Ahmad Bin
Citation	大阪大学, 2019, 博士論文
Version Type	VoR
URL	<a href="https://doi.org/10.18910/72374">https://doi.org/10.18910/72374</a>
rights	
Note	

*The University of Osaka Institutional Knowledge Archive : OUKA*

<https://ir.library.osaka-u.ac.jp/>

The University of Osaka

# Doctoral Dissertation

Microwell assist biosensor for neutrophils response cells using localized surface plasmon resonance and luminol - based electrochemiluminescence sensing application

RIYAZ AHMAD BIN MOHAMED ALI

December 2018

Department of Applied Physics,  
Graduate School of Engineering,  
Osaka University

## Table of contents

Table of contents .....	1
Abstract.....	4
Table of Figure .....	8
List of table.....	11
List of commonly used abbreviations .....	12
1 CHAPTER 1: INTRODUCTION.....	13
1.1 Biosensor system in general .....	13
1.1.1 Bio-receptor region.....	15
1.1.2 Bio-transducer region .....	17
1.1.3 Signal amplification, processing and display.....	17
1.1.4 Important of cell based biosensor study .....	18
1.2 Single – cell based biosensor analysis.....	21
1.2.1 Bulk analysis versus single cell analysis .....	22
1.2.2 Single cell analysis.....	23
1.2.3 Single cell capture - microwell approach .....	26
1.2.4 Integration of microwell array into biosensor .....	28
1.3 Introduction to human immune system .....	29
1.3.1 Neutrophils in general and its importance .....	31
1.3.2 Neutrophils extracellular traps (NETS).....	33
1.3.3 Reactive oxygen species (ROS).....	35
1.3.4 The need of single neutrophils study and its study approach .....	36
1.4 Introduction to optical – transducer biosensor .....	37
1.4.1 LSPR sensing principle.....	38
1.4.2 The LSPR quantification for cell application .....	40
1.5 Introduction to electrochemistry biosensor .....	40
1.5.1 The basic of electrochemiluminescent (ECL) .....	42
1.5.2 ECL imaging application .....	43
1.6 Concept of thesis approach .....	44

2	CHAPTER 2 : ONE-STEP NANOIMPRINTED HYBRID MICRO-/NANO-STRUCTURE FOR LOCALIZED SURFACE PLASMON RESONANCE DETECTION.....	47
2.1	Introduction .....	47
2.2	Experimental setup .....	51
2.2.1	Fabrication of nano-porous alumina oxide.....	51
2.2.2	Fabrication of SU-8/AAO mold template .....	52
2.2.3	One-step NIL and gold sputtering for LSPR activation .....	52
2.2.4	Characterization of gold-sputtered COP chip .....	53
2.2.5	Trapping and isolation of fluorescent beads .....	54
2.2.6	Real-time cell monitoring via LSPR .....	54
2.3	Results and discussion .....	55
2.3.1	Morphology characterization of AAO mold and COP film .....	55
2.3.2	LSPR absorbance response evaluation of COP film .....	57
2.3.3	Biomolecule detection with COP film .....	58
2.3.4	Performance in trapping of fluorescent beads on COP film .....	59
2.3.5	Real-time monitoring of absorbance response from cell secretions.....	60
2.4	Conclusion.....	61
3	CHAPTER 3 : HYPERSPECTRAL IMAGING WITH LSPR OBSERVATION FOR SINGLE NEUTROPHILS CELLS	62
3.1	Introduction .....	63
3.2	Material and methods.....	68
3.2.1	Fabrication of the gold sputtered plasmonic substrate.....	68
3.2.2	Fabrication of PDMS microwell array (MWA) sheet.....	70
3.2.3	Assembly of MWA plasmon chips.....	72
3.2.4	Optimization of MWA sheet thickness .....	72
3.2.5	Hyperspectral imaging system .....	73
3.2.6	Extraction of neutrophils from raw blood .....	74
3.2.7	Neutrophils isolation using MWA plasmon chips .....	75
3.2.8	Verification of PMA induced neutrophils of fibrin release .....	77
3.2.9	Real-time LSPR observation of neutrophil extracellular traps (NETs) .....	77

3.3	Results and discussion .....	78
3.3.1	Optimization of MWA plasmon chips .....	78
3.3.2	Neutrophil isolation capability.....	79
3.3.3	PMA induced fibril release from neutrophils.....	80
3.3.4	Real-time LSPR imaging observation of neutrophils.....	82
3.4	Conclusion.....	85
4	CHAPTER 4 : LUMINOL BASED ECL FOR ROS DETECTION FROM NEUTROPHILS CELLS. ....	87
4.1	Introduction .....	87
4.2	Fabrication of Luminol based ECL biosensor .....	90
4.3	ECL imaging using microarray electrode.....	92
4.3.1	Effect of Ph buffer .....	93
4.3.2	Peak versus area under the curve analysis for continuous testing.....	94
4.3.3	Effect of potential voltage.....	96
4.3.4	Effect of alternative current (AC) by altering the frequency .....	97
4.3.5	Effect of H <sub>2</sub> O <sub>2</sub> concentration.....	97
4.4	Real time monitoring of neutrophils cells.....	98
4.4.1	Neutrophil cell preparation.....	98
4.4.2	Real time neutrophil observation .....	99
5	CHAPTER 5 : CONCLUSION AND FUTURE WORK. ....	101
5.1	Conclusion.....	101
5.2	Future remarks.....	103
6	Reference.....	104
	List of publications .....	112
	List of attended scientific conference.....	113
	Acknowledgement .....	114

## Abstract

Neutrophil has been considered as primary soldier in innate immune system for eliminating invading pathogens. Neutrophil being abundant immune host cell in human blood vessel, several differentiation mechanisms is known to take place engulfing microbes pathogens such as phagocytosis, degranulation, cytokine production and neutrophil extracellular trap (NETs) production. An imbalance in NETs formation (NETosis) and its reactive oxygen species (ROS) produce are associated with autoimmune, inflammatory, metabolic, vasculitis and other diseases. Since every cell possess unique differentiation character, it is very important to monitor individual neutrophils' NETosis and ROS production release. Single cell analysis technique provides remarkable capacity for understanding sole cell characteristic rather than commonly used average measurement from bulk population cells. Therefore, by manipulating neutrophil into singular manner, it is possible to further understand cell biology mechanism for the improvement of early disease diagnosis and regular healthcare activities.

In this work, single cell analysis of neutrophils cell activity of formation of NETs and the release of ROS was quantified using localized surface plasmon resonance (LSPR) and luminol – based electrochemiluminescence (ECL) observation technique was performed, respectively. Neutrophil cells were extracted from healthy blood donor and suspended in D-PBS(-) media. For NETosis analysis, simple microengraving platform was realized with microwell array (MWA) sheet on plasmonic sensing substrate for LSPR observation. Introduction of microwell structure provide good segregation phenomena without perturb surrounding cells. Activated neutrophil cell undergoes single cell isolation before quantified using hyperspectral imaging system for absorbance spectrum observation. Real time monitoring of NETs release and its absorbance spectrum change are reported in this study. On the other hand, the ROS release was realized by using microwell enhanced luminol based ECL biosensor. Here, neutrophil cells were introduced between dual electrode (working and counter electrode) before trapping using microwell structure. The quenching of ECL imaging localized inside microwell electrode was examine as successful reaction between produced ROS and luminophore electrochemical reaction. As extension of this study could monitor the degradation of the NETs release

and ROS production which can be proven useful for autoimmune disease detection and pathogenesis elucidation.

The first chapter of this study will discuss in detail on the introduction of biosensor, relating its important with detection technique and introduction of targeted cell neutrophils will be discussed in detail. Neutrophil cell is abundant among leukocyte (about 40% to 70%) in human blood vessel with 6 to 8 hours of lifespan before apoptosis. Even though their lifespan is short, neutrophils cell able to mobile and reach site of inflammation where other cells could not able to do so. Neutrophil cell able to eliminate pathogens through various mechanisms such as phagocytosis, degranulation and NETs formation. Further discussion on the sensing device with microwell array to trap whole cell was discussed in this chapter.

In the second chapter of this study, introduction of LSPR-based biosensor and single step imprint fabrication process will be discussed. LSPR phenomena occurs when the frequency of the incident electromagnetic radiation matches the natural frequency of the electron cloud around the noble metal (e.g. gold, silver, copper) nanostructures, which leads to resonant oscillations of the electrons and sharp absorption of light at this frequency. Any variation in the refractive index (RI) near the nanoparticle surface due to biomolecules attachment, will lead to instantaneous changes in the LSPR-induced absorption peak wavelength. This could then provide high sensitive and real-time proteomic sensing capability. To realize an LSPR chip with hybridized micro- and nanostructures using a single material via nano imprint, an SU-8 patterned alumina mold was prepared. Subsequently a photolithographically patterned SU-8 layer was formed on top of the porous alumina mold surface. The SU-8 layer acts as a micro level spacer during the thermal nanoimprint process, which enables the simultaneous production of micro- and nano- patterns on a single COP film substrate. Sensitivity of prepared LSPR was showing slope of 304 nm/RIU. The response of this plasmonic chip to various concentrations of the anti-IgA antibody (10 ng to 500 ng/ $\mu$ L) in serum free media (SFM) was measured. It found that, prepared MAPS chip able to sense with limit of detection of 10ng/ $\mu$ L of anti IgA. In Pichia

pastoris cells trial analysis, a red shift of 6.9 nm was observed over 12 h, which is likely due to the protein secretion from the cells.

In the third chapter, neutrophils cells obtained from whole-blood samples from healthy human donors were trapped, isolated, and stimulated on a novel microarray plasmon sensing chip (MAPS) and the corresponding spectral shift was then observed. To achieve this objective, first a LSPR-based chip was prepared that comprised of a perforated polydimethylsiloxane (PDMS) sheet that forms the MWA and a gold-capped nanopillar-structured cyclo-olefin polymer (COP) substrate that serves as the LSPR sensing platform. The use of the PDMS here allows forming inexpensive arrays of densely packed microarray to isolate individual neutrophil cells into specific confinement that allow room for the extent of fibril and NET release to be studied. Therefore, hyper-spectral imaging platform provides a rapid, high-throughput, and continuous observation of heterogeneous responses of each individual cell. The developed MAPS chips allow single cell isolation of neutrophils from 150  $\mu\text{L}$  suspension ( $6.0 \times 10^5$  cells/mL) with an efficiency of 36.3%. To demonstrate the utility of the chip, trapped cells were incubated between 2 to 4 hours after introducing with phorbol 12-myristate 13-acetate (PMA) before measurement. Under observation using a hyperspectral imaging system that allows high-throughput screening, the neutrophils stimulated by PMA solution show a significant release of fibrils and NETs after 4 hours, with observed maximum areas between 314–758  $\mu\text{m}^2$ . An average absorption peak wavelength shows a redshift of  $\Delta\lambda = 1.5$  nm as neutrophils release NETs.

In the fourth chapter of this thesis, the quantification of ROS release from activate NADPH oxidase within extracellular region of neutrophils is studied. Any excessive production of ROS due to various reason such as binding of anti-neutrophils cytoplasmic auto-antibodies (ANCA) or other possibility during degranulation can lead for induce of inflammation such as vasculitis disease. Therefore, it is essential for understanding the progression of ROS in term of quantification measurement parallel with NETs formation. Since ROS particles has high activity, very short lifespan and extremely low concentration, the luminol based ECL biosensor who processes high sensitivity was used. In this study,



gold sputtered working electrode (height 90nm) was prepared with additional Su8 layer that provide microarray structure for individual cell isolation purpose. Pre-cut PET spacer (height 50 $\mu$ m) was added to act as solution channel. Later, both electrode and channel was sandwiched with pre milled holes (as inlet and outlet) on an ITO glass that act as counter electrode. Active neutrophils cells with luminol solution was added and potential voltage was applied before its photon activity was recorded.

Prepared luminol solution with ROS (source from neutrophils cell) substance follows coreactant ECL pathway, luminol was oxidized under influence of potential (+1.2 to +1.6V) releasing an electron while combining with ROS radical such as  $O_2^-$  (rare) and  $H_2O_2$  species. This combination allows to form excited state before returning to metastable or ground state by releasing photon energy in form light. The acquired excited energy information can be further analyse as quantification of ROS that released by neutrophils cells. Several parameter factor was analysis including depended of buffer pH, potential voltage value, type of waveform (DC and AC) and  $H_2O_2$  concentration was executed. It found that buffer with pH alkali 9 shows highest activity compared with others (7.8, 8.0, 8.5) while suitable potential was found between +1.2V to +1.5V for direct voltage (DC). For  $H_2O_2$  concentration detection, prepared electrode shows lowest detection of 100nM for +1.4V DC voltage. For single neutrophil cell observation, the first 10 minutes signal was found slight increase about (4.45%) in intensity measurement, while at 30 minutes, the value dropped about 1.2% in term intensity. Therefore, it shows that prepared electrode shows high sensitive detection of neutrophil cells.

In the fifth chapter, as a wrap of main chapters above, the conclusion of finding and future remarks will be included in details.

## Table of Figure

Figure 1-1: Simplified representation of a bio-sensing system.....	14
Figure 1-2: Concept of bio-receptor.....	15
Figure 1-3 : Transducer working principle. ....	17
Figure 1-4 : Non inverting operational amplifier (Op-amp) circuit that helps to amplify .....	18
Figure 1-5 : Various whole cell interaction with biosensor.....	20
Figure 1-6 : Signal secretion released into extracellular region due to stimulant. ....	22
Figure 1-7 : Comparison between conventional bulk analysis and single cell analysis. ....	23
Figure 1-8 : Schematic overview of manipulator[12].....	24
Figure 1-9 : Fluorescence activated cell sorting (FACS) setup[12]. ....	24
Figure 1-10 : Various microwell size and shape for cell trapping application.....	26
Figure 1-11 : Microwell preparation and cell seeding procedure on prepared microwell .....	28
Figure 1-12 : Human immune cells system division.....	29
Figure 1-13 : Neutrophil cell structure.....	31
Figure 1-14 : Possible mechanisms of neutrophils cells.....	32
Figure 1-15 : Phagocytosis mechanism performed by activated neutrophil cell.....	32
Figure 1-16 : Illustration of suicidal NETosis mechanisms forming NETs.....	34
Figure 1-17 : The NETosis formation release NETs into surrounding. ....	34
Figure 1-18 : Electron valance of ROS formation. ....	35
Figure 1-19: Optical biosensor sensing approach. ....	38
Figure 1-20 : Schematic diagram explaining the principle of LSPR shift. ....	38
Figure 1-21: Electrochemical biosensor working electrode, counter electrode .....	41
Figure 1-22 : The schematic diagram of LSPR imaging for single neutrophil cell. ....	45
Figure 1-23 : The schematic diagram of Luminol based ECL quantification for ROS application. ....	46
Figure 2-1 : Schematic illustration of hybrid nano-/micro structured plasmonic substrate.....	47
Figure 2-2 : The schematic design of prepared AAO mold. ....	52

Figure 2-3 : Full fabrication procedure for microwell enhanced LSPR substrate.....	53
Figure 2-4 : The AFM image of prepared AAO mold. ....	56
Figure 2-5 : Successful SU8 micro-poles on nanostructured AAO mold. ....	56
Figure 2-6 : The SEM image of imprinted microwell enhanced LSPR substrate. ....	57
Figure 2-7 : a) Absorbance LSPR peak shows red-shifted. b) average sensitivity of LSPR .....	58
Figure 2-8 : a) The absorbance response of 500 ng/mL anti-IgA antibody in .....	59
Figure 2-9 : Microscopy observation of the trapped beads into microwell.....	60
Figure 2-10 : Number of fluorescent beads trapped in each prepared microwell. ....	60
Figure 2-11 : a) Real-time absorbance observation of healthy P. pastoris cells .....	61
Figure 3-1 : Activated neutrophils cell are isolated using microwell enhanced LSPR substrate...	62
Figure 3-2 : Possible mechanisms of neutrophils cell. ....	63
Figure 3-3 : Single cell analysis provide individual response. ....	65
Figure 3-4 : Neutrophils cells are trapped into microwell array before stimulated .....	68
Figure 3-5 : Anodic porous alumina structure (AAO) mold.....	69
Figure 3-6 : Preparation of LSPR substrate using nanoimprint method. ....	70
Figure 3-7 : Photomask design with microwell diameter 60 $\mu$ m and pitch 100 $\mu$ m.....	70
Figure 3-8 : SU8 mold coated on silicon wafer.....	71
Figure 3-9 : PDMS material was injected into SU8 micro pattern before apply heat & pressure.	71
Figure 3-10 : Cured PDMS layer was carefully removed to form perforated microwell array. ....	72
Figure 3-11 : The full assembly of plasmon chip with perforated layer on top .....	72
Figure 3-12 : Hyperspectral imaging system setup. ....	73
Figure 3-13 : Substrate image corresponding to TBPF system in graph representative.....	74
Figure 3-14 : Isolation procedure for neutrophil cells from raw blood. ....	75
Figure 3-15 : Cell trapping observation.....	76
Figure 3-16 : MWA plasmon chips trapping capability. ....	76
Figure 3-17 : Beads trapping capacity of varies thickness range of 30 $\mu$ m, 60 $\mu$ m and 90 $\mu$ m. ...	79

Figure 3-18 : Neutrophils trapping efficiency using 60 $\mu\text{m}$ thick MWA PDMS sheet. ....	80
Figure 3-19 : The fibril releases from neutrophils cells under stimulation of PMA .....	81
Figure 3-20 : Real time LSPR observation of single neutrophils cells with PMA (+) and .....	82
Figure 3-21 : Real time monitoring for 30 single cell neutrophils in PMA (+), PMA (-).....	84
Figure 4-1 : Mechanism pathway of neutrophils differentiation.....	87
Figure 4-2 : Suicidal NETosis mechanism by neutrophil cell. ....	88
Figure 4-3 : The full assemble of microwell enhance luminol based ECL setup. ....	90
Figure 4-4 : The specific design using acrylic sheet.....	91
Figure 4-5 : The experimental setup of microwell enhanced luminol based ECL substrate.....	92
Figure 4-6 : pH response in range of 7.84, 8, 8.5 and 9.02. ....	93
Figure 4-7 : Repetition performance at 10 cycle.....	94
Figure 4-8 : The area under curve representation of 10 <sup>th</sup> cycle.....	95
Figure 4-9 : The peak versus area under curve analysis.....	96
Figure 4-10 : The potential response of DC voltage from 1.0 V to 1.7V. ....	97
Figure 4-11 : The frequency based AC response.....	97
Figure 4-12 : The limit of detection of lumniol based ECL for 1.4V DC. ....	98
Figure 4-13 : Neutrophil cell isolation from raw blood.....	99
Figure 4-14 : The real time ROS ( $\text{H}_2\text{O}_2$ ) measurement from activated neutrophil cell. ....	100

## List of table

Table 1 : Types of interaction.....	16
Table 2 : Cell organelle and its task.....	19
Table 3 : Component of the human immune system .....	30
Table 4 : Proposed ECL pathway generation.....	43
Table 5 : Comparison between commercially available technique. ....	48
Table 6 : The peak analysis for 10 repeated cycle.....	94

## List of commonly used abbreviations

AAO	Anodizing alumina oxide
AC	Alternative current
COP	Cyclo-olefin polymer
DC	Direct current
D-PBS(-)	Dulbecco's phosphate-buffered saline
ECL	Electrochemiluminescence
LOD	Limit of detection
LSPR	Localized surface plasmon resonance
MPO	Myeloperoxidase
MWA	Microwell array
NADPH	Nicotinamide adenine dinucleotide phosphate
NE	Neutrophils elastase
NETosis	Neutrophil extracellular traps progression
NETs	Neutrophil extracellular traps
NIL	Nanoimprint lithography
PAD4	Protein arginine deiminases
PDMS	Polydimethylsiloxane
PMA	Phorbol-12-myristate-13-acetate
PMN	Polymorphonuclear
RI	Refractive index
ROS	Reactive oxygen species
SFM	Serum free media

## **1 CHAPTER 1: INTRODUCTION.**

### **1.1 Biosensor system in general**

The first reported bio sense-able technology, dates back as early as 1906 by M. Cremer [1] who demonstrate concentration of an acid in solution is proportional with electrical potential that arise between parts of fluid located on the opposite sides of glass membranes. The first appropriate biosensor was pioneer by Leland C. Clack who developed oxygen detection electrode in 1956 until remembered as 'Clark Electrode'[2]. Further development in biosensor field, Clack introduce amperometric enzyme electrode for detection of glucose in 1962 and follows by discovery by Guilbault and Montalvo [3], for first potentiometric biosensor for urea detection in 1969.

Since then, numerous development was conducted performing broad spectrum application causing bio-sensor was defined as any self-depend bio-analytical device that possess ability to detect chemical substance (analyte) consist of bio-molecules component that consolidates with transducer surface which yield in electrical signal as response. Produced signal can be used to detect or quantified concentration of targeted analyte with help of targeted bio-receptor that initially placed on transducer surface. Such phenomena allow biosensor own unique ability to recognize its targeted analyte before providing its variable response signal that can be evaluate or investigate any further. Manipulation of bio-receptor region and transducer elements allows further expand of biosensor technology providing wide range of area coverage such as point-of-care diagnose/monitoring and disease progression, food processing and safety authenticity industry, drug discovery, pollutants-environmental observation, forensics, detection of biological warfare and biomedical research field.

To fulfil those requirement, several important characteristics that biosensor need to possess including stability, reproducibility, selectivity, sensitivity and linearity. This is important to have such a reliable biosensor that could produce output at its best. Stability element in any biosensor is important where it maintain ambient without perturb surrounding element. This can ensure produce output can be trusted at any point of time. Another equally important requirements of a biosensor

are selectivity and sensitivity. As commonly understood, selectivity involve ability for a biosensor to detect specific analyte in vase sample mixture. In classic approach, interaction of antibody and its pair antigen provide good example of adequate biosensor success. In any point, due to success interaction occur, biosensor should able to start sense and produce its relevant output to indicate limit of detection (LOD). Having low scale of LOD providing good sensitivity to its user. Linearity output can be a good indication of accuracy that measured response of various different sample concentration. Depending on the linearity of tested biosensor one can categories into certain field of range. Reproducibility can play most important card for manufacturing sector where similar performance biosensor can be produce over and over without any failure. This ensure produce biosensor output can be trust and further use as evidence for any diseases detection or other applications.

In general, any biosensor consists of 3 main components, i.e. i) bio-receptor region with active analyte, ii) bio-transducer element, iii) signal amplifier and processor (electronics) with display function. The schematic representation of a working biosensor system has been illustrated in Figure 1-1. Combining each and every section forms series of chain event that propagate applicable electrical signal (optical signal in some case) that could be calibrated for certain level of quantification interpretation. This interpretation capability provides information evidence for end user to perform prompt decision especially disease progression and prevention purpose. Detailed discussion on each part are as follows.

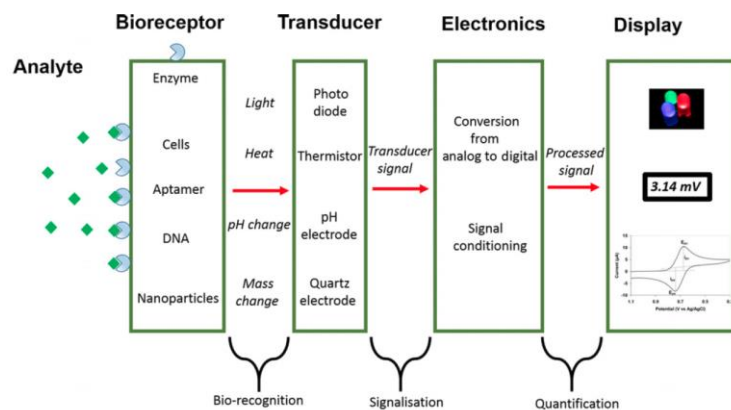


Figure 1-1: Simplified representation of a bio-sensing system [4].



### 1.1.1 Bio-receptor region

Analyte can be defined as substance that need to be detected, while bio-receptor layer consists provide specific counter analyte substance as shown in Figure 1-2. Immobilized interface using simple covalent bonding was formed to capture and further hold any targeted analyte with bio-receptor molecules. This allows unique selectivity and high sensitivity capability for biosensor. Successful analyte – receptor binding provides measureable situation for transducer to react accordingly in form of corresponding response such as light, pH change, heat or even mass change.

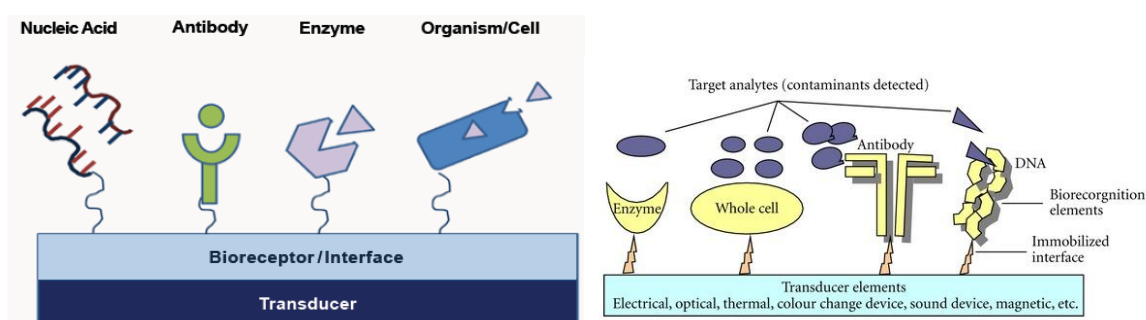
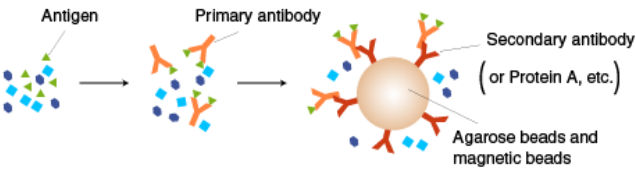
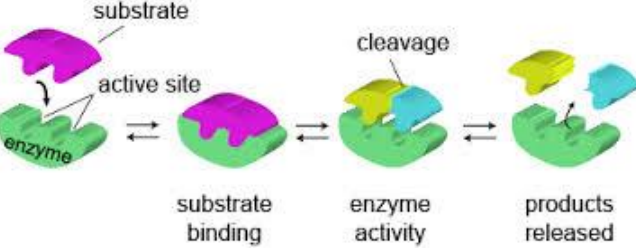
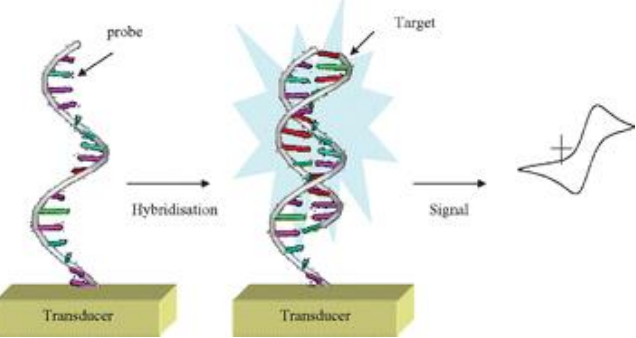
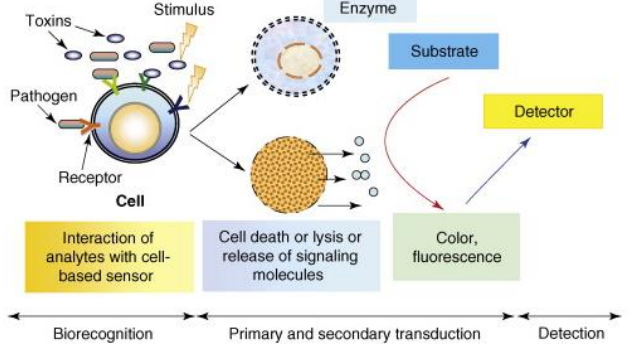


Figure 1-2: Concept of bio-receptor.[5, 6]

There are several types of bio-receptor molecular interaction often used such as antibody/antigen, enzymes/ligands interaction, nucleic acid interaction and cellular/ cells integration. Mechanism of each interaction has been simplified as shown in Table 1. Each interaction provides unique selection capability that can be manipulated for targeted sensing purpose.

Cellular interaction study uses whole cell structure as bio-receptor where this approach provides huge benefit as it is simpler to immobilize, unique specific activity and versatile providing wide range response with corresponding external stimulants. This allows researcher to use cells for several study including stress condition, toxicity, autoimmune and other condition that benefit for effect of drugs monitoring analysis. Most cells provide excellent attachment with transducer surface due to its large surface area and adhesive capability. Living cells that been isolated from tissues are usually need appropriate surrounding of suspending media which include nutrient media, growth factor, gases and others for continue survival.

Table 1 : Types of interaction

Type of interaction	Analyte	Bio-receptor	Illustration of possible interaction
Antibody – antigen	Antigen	i) primary antibody ii) secondary antibody	 <p>Image credit : MBL life science.</p>
Enzymes - ligands	Ligands	Enzymes	 <p>Image credit : Schmoop/ Socratic.</p>
Nucleic acid (DNA) [7]	Target	Probe	
Cellular[8]	i) stimulant ii) toxics iii) pathogens	Whole cell	 <p>Biorecognition      Primary and secondary transduction      Detection</p>

Healthy cells that been perturb with stimulant such as toxics, pathogen or chemical stimulant can evoke sudden or gradual response by cell death, lysis, secreting signal molecules (i.e. protein, peptides, amino acids, nucleotides, steroids, fatty acid derivatives or even gases), cytokines, fibril structure

release and some others. Corresponding transducer provide adequate response which can be used as tool for time lapsing monitoring purpose.

### 1.1.2 Bio-transducer region

As mention earlier, the bio-transducer works as surface holder that will responsible to convert bio-sensing signal that originated from bio-receptor region which consist of physical quantity change; such as chemical, optical, mass or temperature into corresponding electrical or optical signal. The basic working principle are as shown in Figure 1-3. It is also important for transducer element possess stable surface structure for ease of immobilization assay that lead into higher sensitivity biosensor.

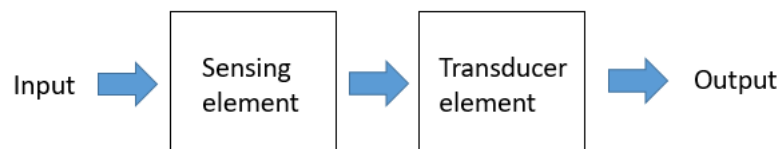


Figure 1-3 : Transducer working principle.

In general, bio-transducer can be further categories into four main types, i.e. electrochemical, optical, pH electrode and piezo-electric. Each transducer provide output that can used by following chain for further analysis process. In this study, two types of transducer; electrochemical and optic will be discussed later.

### 1.1.3 Signal amplification, processing and display

Electrical signal that been obtain from bio-transducer are usually in from of raw analogue signal where can further categories into voltage, current, resistance, intensity. In matter of week signal response usual in micro scale, produced signal might undergo signal amplification with higher gain ratio. Most of the analogy signal amplification uses operational amplifier (op-amp) circuit to amplify input signal. The basic amplification are shown in Figure 1-4. Signal that insert in positive input will be amplify to higher voltage depending on the gain value consists of value of resistor as;

$$A = \frac{V_{Out}}{V_{In}} = 1 + \frac{R_f}{R_{in}}$$

This allows user to process and quantified measurement with ease. However, such arrangement might produce saturation output value depending on the operation voltage insert into the amplifier or higher background signal that may limit overall detection. Good balance of gain is needed to avoid any signal surplus/saturation. On other hand, produced raw analogue signal can be digitalized using analogue-digital converter, where this allows user to analysis produced data and recorded any response. Computer was used widely as aid for analysis and display purpose.

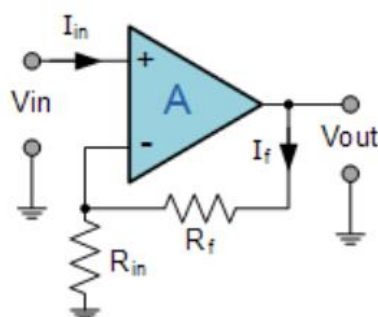


Figure 1-4 : Non inverting operational amplifier (Op-amp) circuit that helps to amplify input signal reciprocal to its gain.

#### 1.1.4 Important of cell based biosensor study

Cell is basic function unit of any life. Human cells works by providing basic structure to the body, absorb nutrients and convert into energy for maintaining specialized human daily function for good health. To obtain this objective, cells possess many parts that carry different tasks and body function which known as organelles in general. As describe earlier, organelles which bound inside cell structure perform certain specialized yet important tasks to support its survival. Below are some of organelles inside human and its task as describe in Table 2. Differ with molecular based analysis where it promotes single type detection, whole cell analysis can provide broad spectrum of analyte detection

ability. Cell – based biosensor provide advantage by allowing living cells to be used directly on transducers for cellular physiological parameter detection, drug effect analysis, toxicity test and others.

Table 2 : Cell organelle and its task

Name	Description	Function
Cell membrane	i. Flexible boundary formed around the cell. ii. Bi-layer of proteins and lipids.	i. Separates the cell from outside environment. ii. Selectivity permeability.
Mitochondria	Power generator for cell	Make energy out of food.
Nucleus	Contain DNA (information to make protein).	Control cell activity.
Chromatin	i. Granular material within nucleus. ii. DNA bound to protein	Condenses to form chromosome at the time of cell division.
Chromosome	i. Distinct threadlike. ii. Contains genetic information.	i. Control the cell activity ii. Contain information that can be use by next generation.
Ribosome	Made of RNA and protein	Protein synthesis
Golgi Apparatus		Make, process and package of protein.
Lysosome	Contains hydrolytic enzymes	Digestive food down
Endoplasmic Reticulum	Network of ribosomes around cells	Used to transport activity

Whole cell analysis can provide fast and sensitive for in situ cell monitoring observation. These kind of biosensor allows non-invasive analysis of many different kind of cellular response ranging from cell adhesion, cell barrier function, cell communication, signalling, virus infection, migration, proliferation and cell apoptosis, and differentiation. Illustration of this cellular response are shown in

the Figure 1-5. These stimulated whole cell will provide cellular response, while bio-transducer will provide its quantified signal for user.

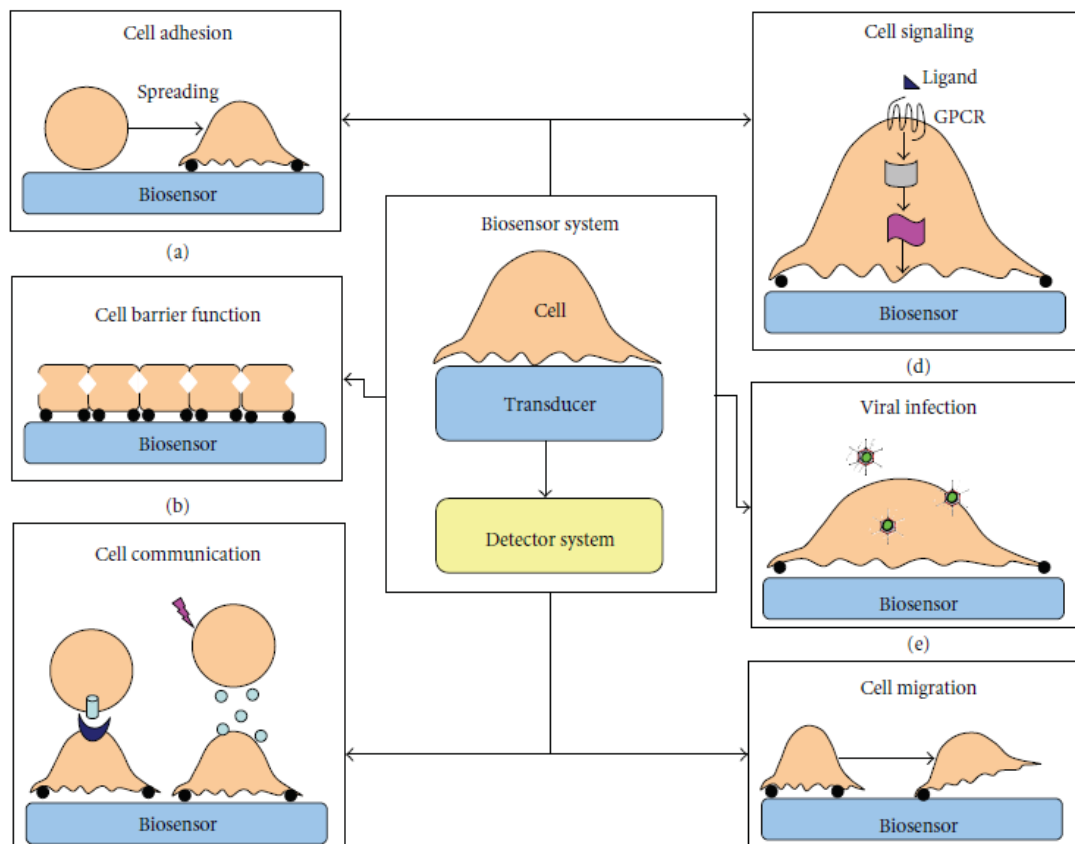


Figure 1-5 : Various whole cell interaction with biosensor[9].

One of interesting method to study immune cells response is to provoke with known microbe that could have stimulate its nucleus to attack (defence process) and phagocytes harmful substance to maintain good health. By provoking such condition, immune cells could response promptly by providing first-hand information secreting reaction molecules as response where is this part of native cellular living mechanism. Therefore, it is much convenient for researcher to use whole cell to study its physiological changes for continuous monitoring. However, several difficulties might be experienced in order to obtain this goal including safer and stable response cells, sensor sensitivity and broad selectivity detection. Vase development are being conducted synergy with existing bio-

technique such as micro-/ nanotechnology and microfluidics for simpler, smaller, more sensitive with higher screening capability biosensor.

## 1.2 Single – cell based biosensor analysis

Biosensor was developed in the aim of improving the quality of life. Conventional available biosensor has contributed impressive development as demand increases for new or improved detection method for disease prevention, diagnose rare type disorder, improving food safety, controlling biotechnological process and others such as biological warfare activities. Several modifications on bio-receptor and bio-transducer can made into sensible biosensor device that provide room of analyte interaction and change in signal interpretation for user to quantified any detection changes. To enhance the performance of these biosensor devices, it is essential to achieve success coupling between biological molecular analyte and bio-transducer region such as through living cells were directly immobilized on the transducer's surface as shown in Figure 1-6. Whole cell that been expose with activator stimulant will response by secreting counter signal molecules into the surrounding. The secreted signal molecules can be in form of proteins, peptides, amino acids, nucleotides, steroids, fatty acids derivatives and others. This type of response helps to keep communicate with other targeted cells or tissue to regulate their behaviour or needs. Secreted signal usually distributed around the cell environment depending on time taken for the cell to process. The protein secretion around whole cell phenomena are been illustrated as in Figure 1-6. Successful interaction of secreted protein with sensing region will produce Therefore, it is essential for researcher to sense and quantified biological signal produced at extracellular environment of whole cell due to chemical stimulants using biosensor device.

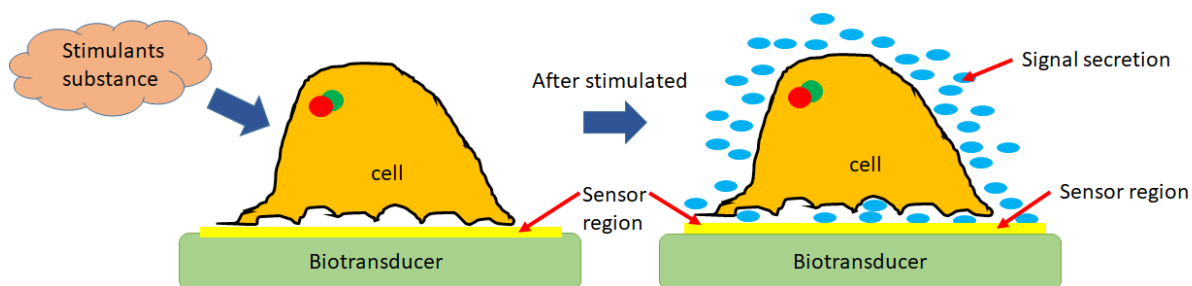


Figure 1-6 : Signal secretion released into extracellular region due to stimulant.

### 1.2.1 Bulk analysis versus single cell analysis

In the conventional cell based analysis method, biosensor usually uses cell in heterogeneity population to study its cell behaviour towards stimulants on sensor platforms. Heterogeneity behaviour of cells are referring to behaviour of cells such as molecular secretion and signally upon in the present of identical stimulant environment condition. This process can be also including by variation in cell division, drug efficiency, cell cycles stage or age, phenotype due to stochastic nature of gene expression, receptor expression, concentration of a critical metabolite or ion[10-15]. Each of these condition cells do present differently and its response characteristic might be different as well. Using bulk analysis approach, collected data of population of cells often include collective average data of vast population of cells that been detected by sensor. As mention earlier, even though similar cells are used in bulk cell analysis, but it may possess different type of characteristics that is unique and difference from each other as shown in Figure 1-7. Therefore, these population data recorded could not represent unique bio-response analyte produced from single unit cell that function differently from the majority population cells. It is not really clear why certain cells behave differently to the provide stimulant, but it does happen such way[16]. Certain type of sub set cell such as limited and rare type subsets cell response might not able to quantified as shown in illustration Figure 1-7.

On the other hand, single cell analysis sensing allows individual cell interaction response record without or less disturbance from nearby surrounding cells in various field study such as differences in proliferations, drug or protein molecular response, cell moment or division, and others. Single cell analysis provides opportunity to increase knowledge and understanding at the level of individual cell,



aiming for better understanding of human body[16]. Such situation is possible as cell undergoes sorting or capturing procedure before quantification takes place. Through this cell isolation, some limited or rare type of subset cell might able to be identify its secretion response together with common type individual cells. Such phenomena allow to explore and solves life science and biomedical field complications.

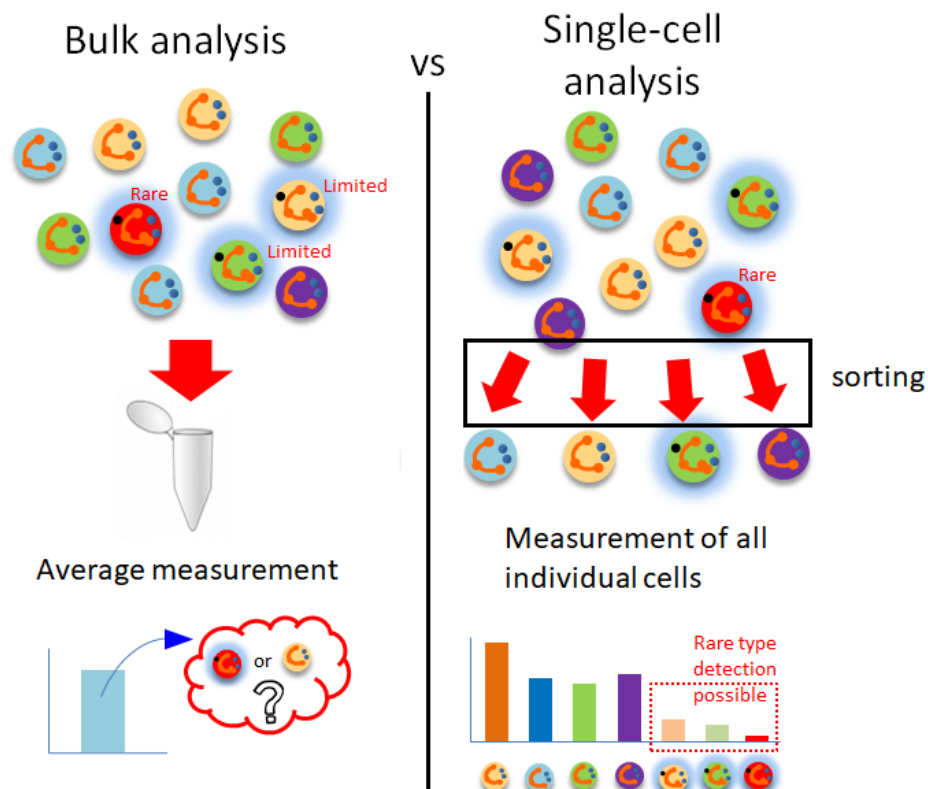


Figure 1-7 : Comparison between conventional bulk analysis and single cell analysis.

### 1.2.2 Single cell analysis

There are few common method was used to sort and analysis captured single cell. The flow cytometry (FC) is among the popular method which was initially developed in 1960s. The FC allows huge number of cells to be analysed according to their size, granularity and their fluorescence response properties for wide application purpose such as viability, gene expression and protein expression and localization[17]. This type of analysis method provides significant advantage over manual cell sorting method using manipulators. Manipulators is known for its job intense task where

cell needs to be capture using micropipettes using positive or negative pressure line as illustrated in Figure 1-8. Low number of cell sorting ability with higher risk of cell damage are among reason such technique shows far behind capability over FC.

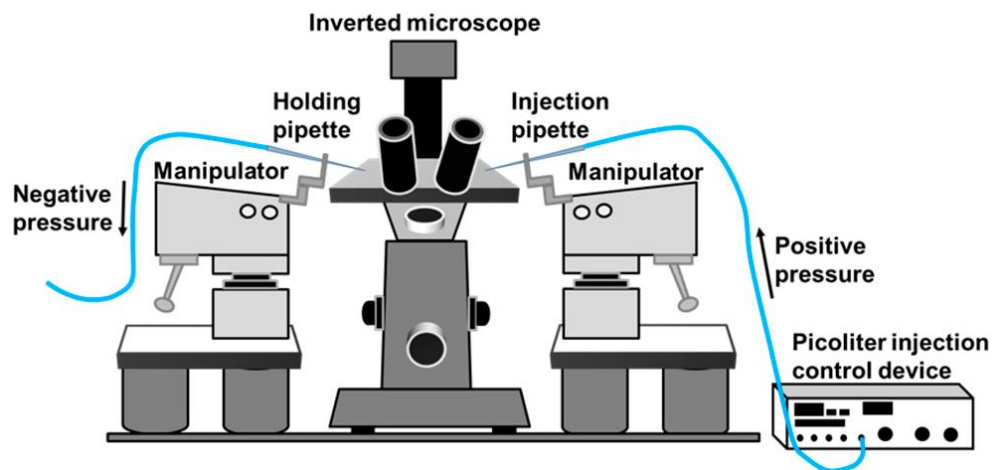


Figure 1-8 : Schematic overview of manipulator[18].

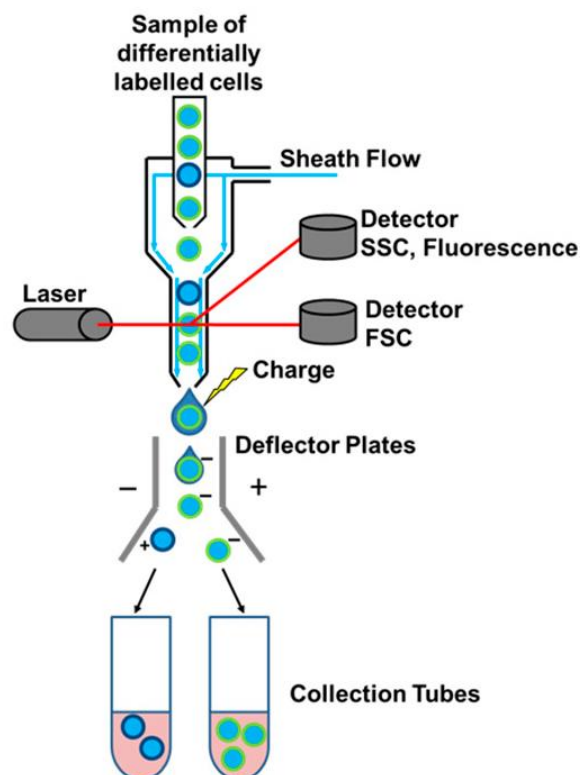


Figure 1-9 : Fluorescence activated cell sorting (FACS) setup[18].

The FC method, it provide high capability for single cell analysis with the usage of florescence-activated material as their primary marker allowing semi- quantitative quantification of protein level response at various timeline laps, in heterogeneity population cells[19, 20]. Stained cells are injected through nozzle into narrow tube before excited laser with specific wavelength was focused at individual cells inside narrow tube as shown in Figure 1-9. The response from each cells are recorded and represented as distribution of group of individual cells. However, though this method, the time line based observation could not able to repeated due to the design of FC technology that observed cells will end as waste material or been sorted into collection tubes using deflector plates before mixed in dedicated collection chamber as illustrated in Figure 1-9. Due to this cell mixing situation, retracing cells for continuous single cell monitoring become a known challenge.

Another frequently used method for single cell analysis is microscopy observation. Since invention in early 17<sup>th</sup> century, microscopy allows intracellular localization analysis with additional time lapse capability for monitoring individual cells' behaviour or physical/chemical response. In order to coop with huge number of cells need to be analyse, this has resultant for introduction of automated microscopy (AM), image cytometry (IC) screening, high content screening/analysis (HCS/HCA) and other. In this approach, interested cells need to be identified (hunting) and log its coordinate point before image was obtained. Automation allows hundreds of images to be obtained over vase number of individual single cell with continuous monitoring capability. Recorded image can be used to analysis cells progression or differentiation over certain period of time without the present of human interaction. Certain type of AM even possesses tracking ability (self-adjust interested cell's coordinate) to overcome cell's nature where its tend to migrate. Even though such tracking capability provide advantage for user to keep in tracking interested cell, migration can induce certain other problem such as lost in identification due to change in shape and size, interference with surrounding cells response, irregularities expand of cell differentiation that perturb nearby cells and others. Therefore, it is essential to introduce certain type of wall of wells that allow proper cell trapping and also provide isolation in order to maintain cell moments and analysis.

### 1.2.3 Single cell capture - microwell approach

There are numerous approaches by bioengineering community who develop microtechnologies synergy with biosensor for high throughput single cell capturing and quantification. These development includes microwells, microtubes, micropallets, microdroplets and integration of microfluidics chip are some of notable approach. The microwell structure approach are among simple yet promising method to passively separate cells by physical manner using mechanical wall structures. Depending on the proposed application of cell accumulation, microwell structure can be formed in numerous method by selecting possible parameter such as shape, size, well depth, number of wells and others.

Size of purposed microwell design parallel with intended cell to be use plays important role in determining number of cell managed to be separated in individual manner. Larger microwell makes more than a cells accommodate into same microwell in result. On the other hand, thigh microwell size cause lower numbers of cell trapping to occur. Therefore, sufficient space needs to be provided for successful cell trapping to happen. There is possible situation where cell was observed to move in and out of the wells due to insufficient depth as barrier issue. Good wall depth provides good protection for trapped cell[21]. Several different size and shape of microwell are represented in Figure 1-10.

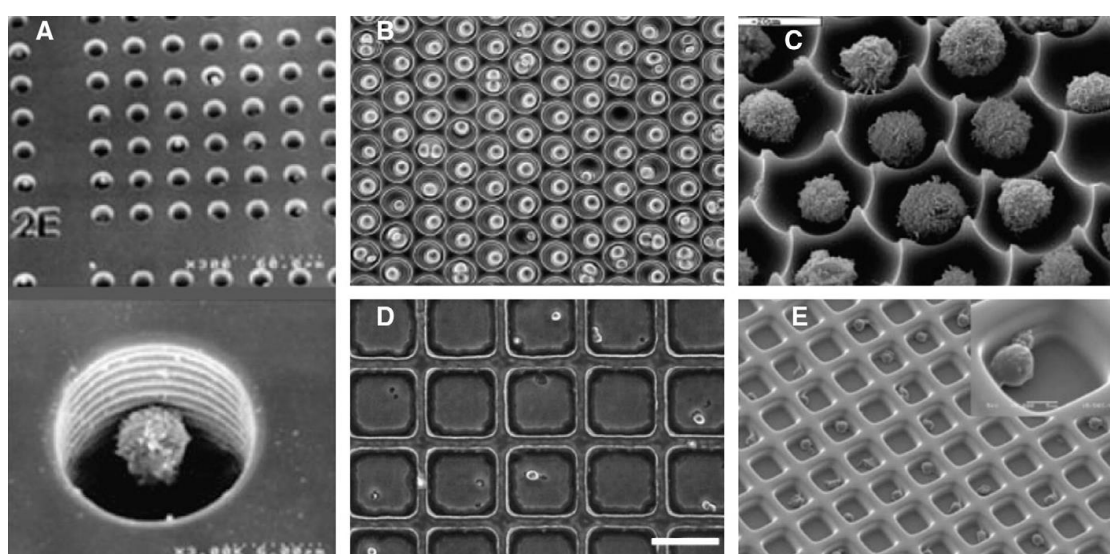


Figure 1-10 : Various microwell size and shape for cell trapping application[21].

There several type of bio compatibility material that been used widely in form of microwell structure such as silicon based polymer, Polydimethylsiloxane (PDMS), Polyethylene glycol (PEG), collagen and silicon. Most of these material, especially PDMS can be reshaped into proper microwell structure using soft lithography technique. PDMS possess excellent quality of clear (optical), non-toxic and inert behaviour[22, 23] on biological samples proving excellent material for imaging application that manipulated with micro – engraving technique forming microwell structure in microfluidic applications. In additional, PDMS material offers an elastic option where this advantage can be used as good sealing properties[24] especially in microfluidic application.

Microwell structure provide simple yet adequate isolation space for cell to be randomly trapped inside microwell through sedimentation process due to gravity or weak fluid force flow inside confined channel. Continues work are carried to improve the single individual cell trapping capability inside microwell which can be noted as single cell trapping efficiency in term of percentage. Study reported by Rettig and Folch[23], optimization of microwell arrays has been focused to increase single cell isolation by altering the diameter and depth design of microwell structure. In the study, microwell structure was prepared with curding PDMS on specifically design soft lithography SU 8 which referred as master mould. Cured PDMS was prepared with dimension of diameter 20  $\mu\text{m}$ , 30  $\mu\text{m}$  and 40  $\mu\text{m}$  with depth size of 16  $\mu\text{m}$ , 21  $\mu\text{m}$  and 27  $\mu\text{m}$ . The diameter to depth are maintain to an approximately ratio of 1. Upon preparation, the curded PDMS was seeded with cells solution and allow for sedimentation for 5 to 40 minutes. Trapped cell are then observed and recorded its trapping efficiency as shown in Figure 1-11. It is found that, this simple preparation of microwell structure able to obtain capturing efficiency about 85% for used type of cell; adherent fibroblasts cells and approximately about 92% for non-adherent rat basophilic leukemia-1 (RBL-1) cells. Such arrangement shows that, microwell array structure possess good candidate for being simple yet effective method for cell isolation purpose.

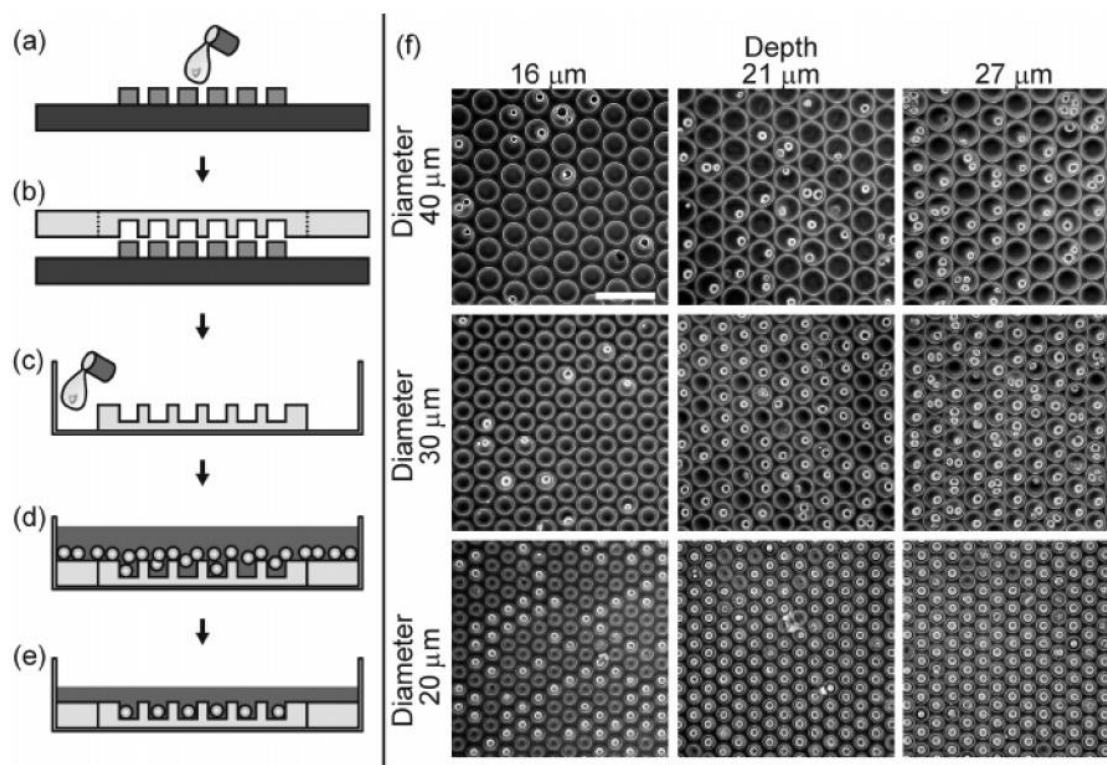


Figure 1-11 : Microwell preparation and cell seeding procedure on prepared microwell array[23].

#### 1.2.4 Integration of microwell array into biosensor

As mention earlier, microwell structure array shows simple yet promising technique to isolate cells into single individual cell manner without perturbing other cells in surrounding. This provide huge benefit for researcher to study cell for differentiation or proliferation in continuous monitoring application. Trapped whole cells can be observed using microscopy to record its surface physical changes due to stimulant. PDMS material provide clear and biological inert properties that could use as advantage together with microscopy observation method. However, through normal microscopy observation technique, it is impossible to observe the chemical molecular secretion changes around cells for real time monitoring purpose. Therefore, it is important to synergy microwell structure into biosensor to enhance its molecular quantification capability together with existing imaging facility. It is crucial for researcher to understand more about type of cellular and its chemical secretion before determine the suitable sensing biosensor need to be used. Further discussion regarding type of cells and its suitable biosensor application are as follows.

### 1.3 Introduction to human immune system

The human body is constantly under treat of pathogenic and non-pathogenic microbes, numerous type of toxics and allergenic substance that present in surrounding. The pathogenic microbes hold ability to propagate, replicate, sustain and threaten human body in general. Human body proposes self-defence known as immune system to safe guard human body from any foreign pathogenic microbes nor toxics. Failure to eliminate these harmful substance, it can cause damage and destruction to the parts of the body causing breakdown in human function or response. Therefore, it is not surprising to known that human immune system owns complex array of protective mechanism for differentiating between beneficial or non-beneficial microbes before eliminate these organisms and toxins. This mechanism includes host cell able to detect cellular features of microbes or toxic before label it as distinct for further destruction without causing damage to its own cells or tissues[25].

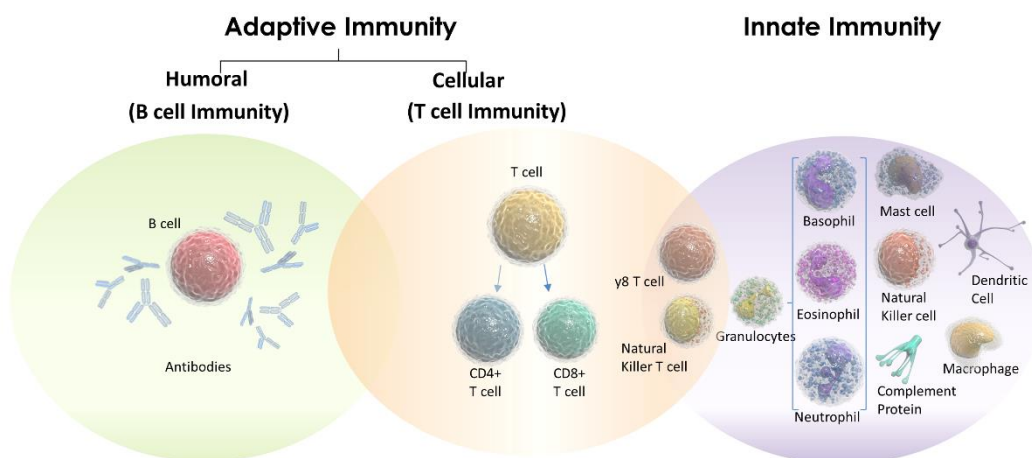


Figure 1-12 : Human immune cells system division (image credit : Oxford Immunitec).

In general, immune systems protect human through two types of layered defence system with increase of speciality as situation become tougher as shown in Figure 1-12. As pathogens breaches human system, the first layer defence system, named as innate immune system will provide rapid yet non-specific type of response. The innate immune system in general recognize molecular patterns that shared by many microbes or toxins that not be present in human body (to differ between good and

destructive microbes). As stronger destructive microbes that able to successfully evade first layer response, the second layer defence system named as adaptive immune system which possess “experienced” immune cell that able to rearrange to assemble antigen-binding molecules with higher specificity targeted to eliminate invader. This improved response (the second layer defence system) then retained in human system as long lived memory cells that allows adaptive immune system to reboot faster from its previous learned experienced and function with specific antigen if similar pathogens appear [26, 27]. This allow for more effective immune protection for human in future. Basic components of immune system are describe in Table 3.

Table 3 : Component of the human immune system

Innate immune system	Adaptive immune system
First layer response	Second layer response
Non-specific response	Highly specific pathogen response
Immediate response after pathogen detected	Require signal from first layer before response
No immunological memory	Immunological memory capable
Short live cells	Long live cells

As the first layer defence, innate immune system provide rapid non-specific response as pathogens invention into human body. This include physical barrier, inflammation, natural killer cells and cellular barriers named as white blood cells. The white blood cells which also known as leukocytes are single cells organisms circulating blood vessel in human body. These leukocyte includes phagocytes (macrophages, neutrophils, dendritic cells), mast cells, eosinophils, basophils and natural killer cells. The leukocyte cells provide protection in human system by identify and eliminate invaders by attacking through surface contact or engulfing before killing microbes, which known as phagocytosis. Phagocytosis allows cells such as neutrophils cell which is most abundant cell constantly travelling



through blood vessel in search for pathogens. Further understanding on the mechanism and its differentiation will be further discussed below.

### 1.3.1 Neutrophils in general and its importance

Apart from physical barriers that possess by innate immune system, neutrophils cell shows its important as first line of defence in human immune system. Neutrophils cell which in size about 11 - 15  $\mu\text{m}$  undergoes granulopoiesis from stem cell differentiation originated from bone marrow. They can be found abundant among leukocyte (about 40% to 70%) in human blood vessel with 6 to 8 hours of lifespan before apoptosis[28]. Neutrophil cell travel inside blood vessel follows chemical substance (known as chemotaxis) such as interleukin-8 (IL-8), C5a, fMLP, leukotriene B4 and others. Eventhough their lifespan is short, neutrophils cell able to mobile and reach site of imflammation where other cells could not able to do so. It belongs to polymorphonuclear (PMN) leucocyte cells family together with low numbers of basophils and eosinophils cells. Regular neutrophil cells contain a nucleus divided into 2 – 5 loops which connected by chromatin. In addition, neutrophils cell contains primary azurophilic granules which found in young cells and secondary granules where this is more specific as getting matured. The primary granules provide capability to generate myeloperoxidase that been used to kill pathogens by possessing the ability to break down pathogens protein and cell wall. The neutrophils cell structure illustration are as shown in Figure 1-13.

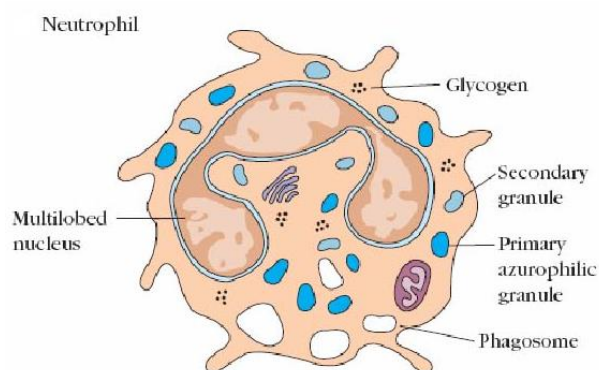


Figure 1-13 : Neutrophil cell structure (Image credit : Online biology notes).

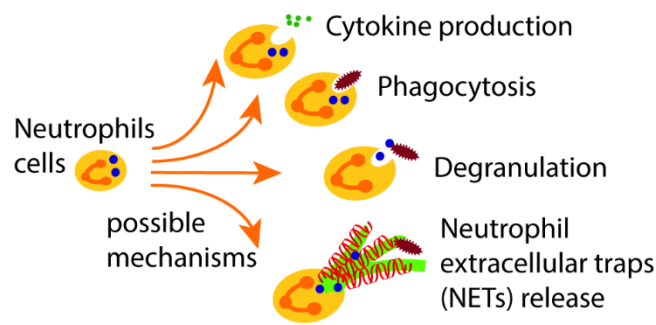


Figure 1-14 : Possible mechanisms of neutrophils cells.

Neutrophils cell are among the first defenders from innate immune system where it migrates to inflammation site for pathogens elimination or cytokines production[29]. At the side of inflammation, neutrophils perform mechanisms as host cell in form of phagocytosis, degranulation, cytokine production and neutrophil extracellular traps (NETs) formation[30] as shown in Figure 1-14. The function reaction of neutrophils that travel inside blood vessel following chemotaxis substance perform adhesion (activated), then migration (diapedesis) into tissues reaching the site of inflammation[31]. In the mechanism of phagocytosis, microbes are engulfed inside neutrophils cell before azurophilic granules perform breaking down proses before undergoes apoptosis. This procedure has been illustrated in Figure 1-15. As host cell, neutrophil also able to undergoes other possible differentiation mechanisms by releasing its granules targeting pathogens which is known as degranulation. Further discussion on the NETs formation are as follows.

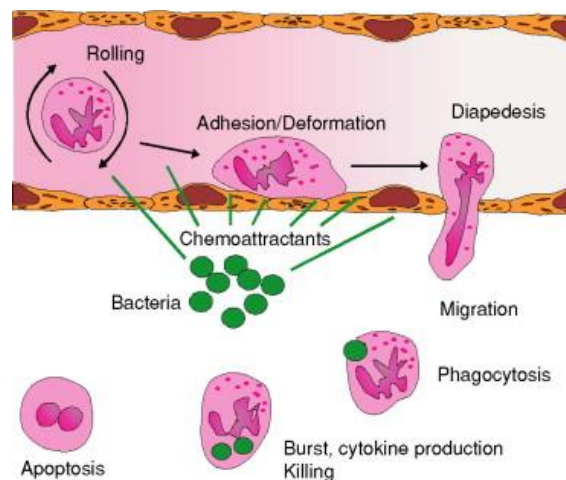


Figure 1-15 : Phagocytosis mechanism performed by activated neutrophil cell[31].

### 1.3.2 Neutrophils extracellular traps (NETS)

As mention earlier, the neutrophil cell able to eliminate pathogens through various mechanisms such as phagocytosis, degranulation and NETs formation. However, the NETs receive attention by discovery of Takei et al. [32] in 1996 where new possible mechanism was reported. As investigating induced neutrophils through phorbol-12-myristate-13-acetate (PMA) solution, they discover significant morphology change on the activated neutrophil. Such discovery suggest new possible pathway of host cell undergoes differentiation other than usual apoptosis and necrosis. In this report, they described that multilobulated nucleus undergoes fusion while chromatin was reduce from its compact structure. The report continues as the extracellular membrane was found burst after 3 hours depending on reactive oxygen species (ROS) availability. This was further detailed its process by Brinkmann et al. [33] and named it as NETosis.

In general, the NETs are DNA structures that released into surrounding due to chromatin decondensation and spreading. This morphology change cause increase in physical size about 3 to 5 times volume than initial size. Several proteins found adhere to NETs structure that include histones and over 30 other components of primary and secondary granules [34]. This released DNA fibril consists of chromatin, histones and glandules has intrinsic antimicrobial activity that would constantly wanted to eliminate any pathogen invaders in present.

The mechanism of formation of NETs or also known as NETosis has 3 models known as now. However, the suicidal NETosis shown most domain [35], yet the molecular reaction is not really full understood by researcher [36] and only this will be covered in this discussion. For suicidal NETosis to formed, the nicotinamide adenine dinucleotide phosphate (NADPH) oxidase inside neutrophils cell was activated within hours of introduction of PMA stimulant as shown in Figure 1-16. This allows for production of reactive oxygen species (ROS) causing activation of protein arginine deiminases (PAD4) resulting chromatin decondensation to occur[37]. The formation of ROS is highly dependable here for chromatin decondensation [38-40] and also behave as second messenger by promoting the

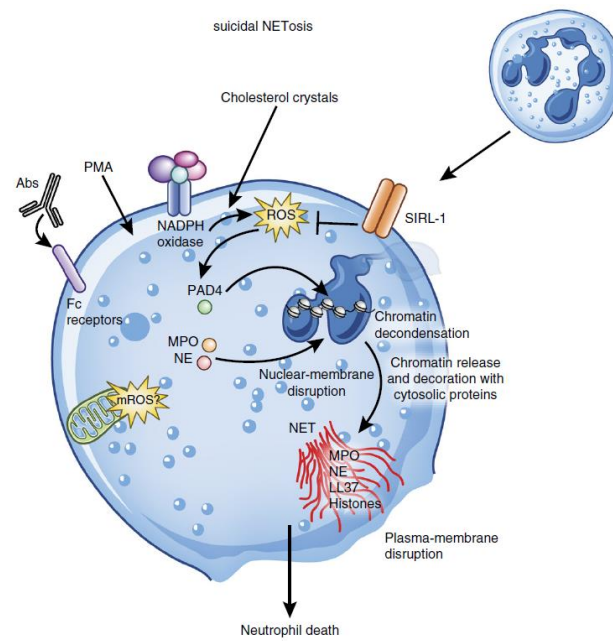


Figure 1-16 : Illustration of suicidal NETosis mechanisms forming NETs[37].

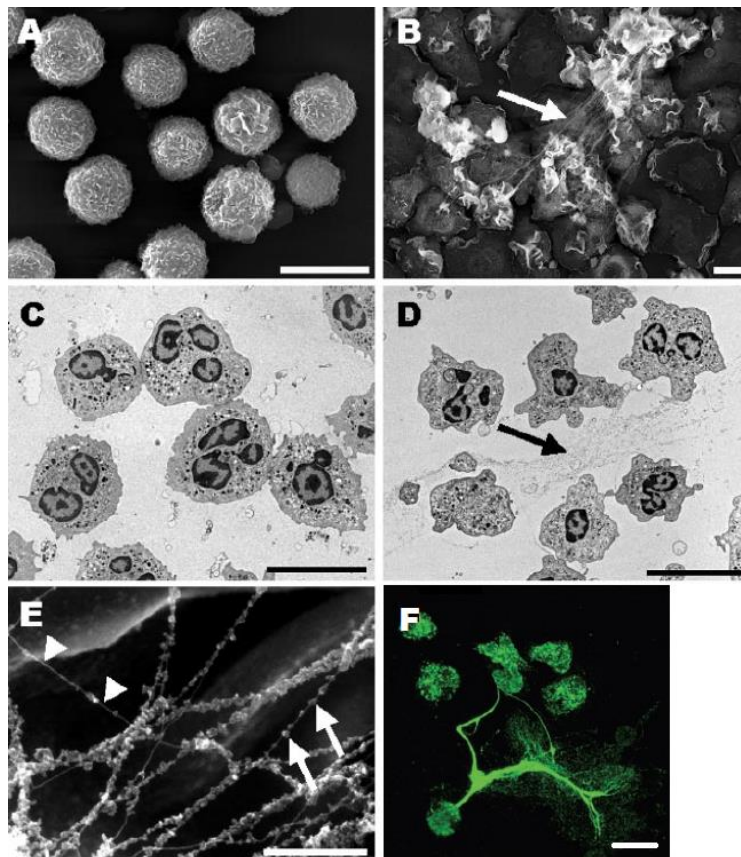


Figure 1-17 : The NETosis formation release NETs into surrounding[33].

gradual separation and loss of nuclear membrane [30]. At this moment, the neutrophils elastase (NE) and myeloperoxidase (MPO) are migrated to help further boost the unfolding of chromatin decondensation. Chromatin starts to agglomerate into cytosol and become decorated with granule toxins and cytoplasmic proteins. Finally, NETs are released through cell membrane pores and cell begin to lysis or apoptosis. As mention earlier, formed NETs has antimicrobial characteristic where pathogen will be eliminated.

The progression flow of NETosis under scanning microscopy image has been reported by Brinkmann et al. [33] as in Figure 1-17. The Figure 1-17a shows the neutrophils cell in resting form. Upon stimulation with PMA, the neutrophils cells undergoes flatten, and several fibril (NETs) was found as in Figure 1-17b and Figure 1-17d. High resolution image on fibril shows size of 15-17  $\mu\text{m}$  and globular domain with diameter of 25  $\mu\text{m}$  as in Figure 1-17e. Activated neutrophils stained for DNA response shows fibril consist of DNA as shown in Figure 1-17f. Further discussion on ROS are as follows.

### 1.3.3 Reactive oxygen species (ROS)

Another important neutrophil cell depended substance is ROS formation during activation mechanisms for microbes elimination through suicidal NETosis formation. Recent study shows ROS plays important role as both intra and intercellular messenger during chromatin decondensation [38-40] and also as cell signalling. Most of the ROS are generated due to electron transport in atomic oxygen with two unpaired electrons in valence band. The sequent reduction of oxygen with addition of free electrons into valence leads for formation of ROS in form of mainly superoxide which acts as

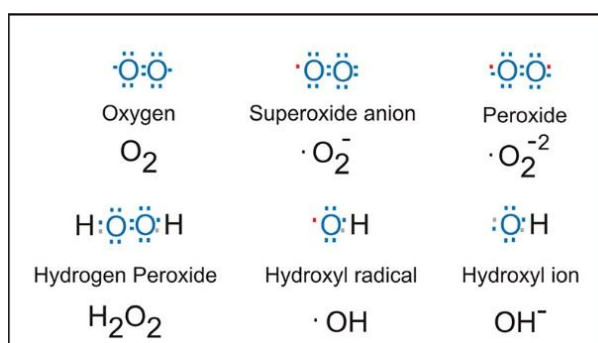
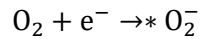


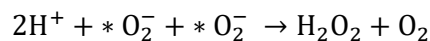
Figure 1-18 : Electron valence of ROS formation (Image credit : BioTeck Instruments/ Paul Held).

precursor for hydrogen peroxide, hydroxyl radical, hydroxyl ion and nitric oxide as shown in Figure 1-18.

The formation of molecular oxygen ( $O_2$ ) produce superoxide ( $*O_2^-$ ) and becoming precursor for most of the other type of ROS[41]. The reduction equation are as follows;



Due to the stability level of  $*O_2^-$  are estimated very low (half-life about 1 - 4 $\mu$ s)[42], this radical needs to dismutase into more stable species. Dismutation of superoxide produces hydrogen peroxide ( $H_2O_2$ ) which have half-life of > 1ms. The equations involve are as follows. Since the hydrogen peroxide radical is stable, it is possible to be used as key for quantification of ROS.



#### 1.3.4 The need of single neutrophils study and its study approach

There are some recent evidence shows NETs formation plays important role in non-infectious diseases. This include such as systemic lupus erythematosus (SLE), rheumatoid arthritis (RA), diabetes, atherosclerosis, vasculitis, thrombosis, cancer, wound healing and trauma[37]. Even though NETs primary task is to defence human body from any type of intruders, the NETs itself can be turned into treat by developing autoimmune diseases where it destroys host tissue. In addition, it also can lead to other dysfunctional outcomes, including metastasis, thrombosis and inappropriate coagulation. On other hand, the production of ROS can be secondary message for the cell signalling and as helping hand for chromatin decondensation for pathogen elimination. However excess production of ROS has been reported causes of vasculitis diseases or even cell apoptosis and necrosis which is uncontrollable cell death. With these emerging reports, it is essential to provide extra attention on NETs formation from single neutrophils cell and ROS production due to NETosis process.

Several approaches employ microscopy as primary observation on neutrophils has been reported. Using microscopy method, the NETosis physical differentiation can be observed and narrative its function. However, it is essential to integrate microscopy observation with bio - sensing capability that

able to portrait real time monitoring of neutrophils cell behaviour. One of promising candidate will be localized surface plasmon resonance (LSPR) where it is possible to be synergy with microscopy apparatus for neutrophil cell observation. Manipulation of LSPR substrate with microwell array will enhance its capability to trap individual neutrophil cells and sensing its NETosis process through label free detection method. However, due to the detection limitation of fast emerging ROS radical though LSPR setup, it more convenient to use luminol based electrochemiluminescence (ECL) for rapid yet reliable ROS quantification. Further discussion on both techniques are as follows.

#### 1.4 Introduction to optical – transducer biosensor

In general, the optical bio-transducer performs by analysing the alteration of properties of light rays, i.e. photon, when free flow analyte interact with bio-receptor molecules. Over this course approach, optical bio-transducer provide great advantage for real-time and label-free detection for many chemical and biological applications. Some of advantages including high specificity, low production cost and great sensitive over free flow analyte. Optical bio-sensor can be further divided into 2 main group of label-free and label-based. For label-free phenomena, the detected signal was generated by direct interaction of analyte with bio-transducer material. The optical shift occurrence due to the analyte interaction can provide real time data analysis advantage without foreign intrusion. On the other hand, label based optical bio-transducer require some external label material that been used as optical signal occurrence including colorimetric, fluorescent or luminescent approach. For example, in fluorescent biosensor, integration of bio-receptor material with fluorescent material that sensitive with targeted analyte. Any successful recognition of analyte through interaction will allows emission of measureable optical signal. Illustration of this type of sensing are as shown in Figure 1-19.

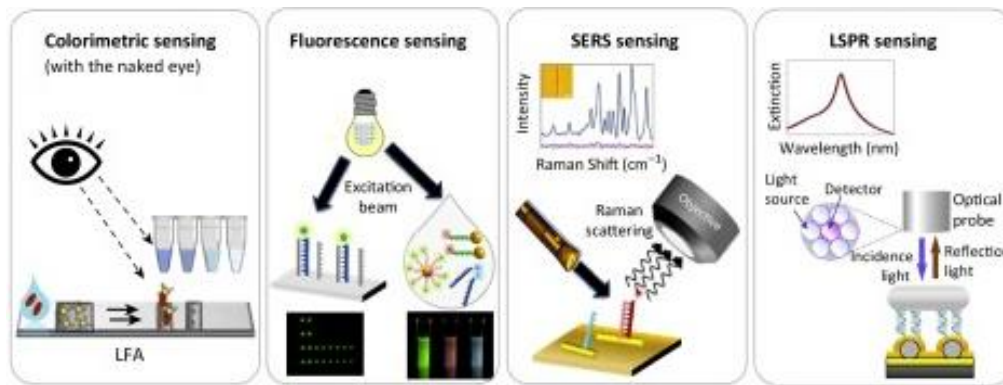


Figure 1-19: Optical biosensor sensing approach[43].

#### 1.4.1 LSPR sensing principle

A localized surface plasmon resonance (LSPR) is the result of the confinement of a surface plasmon in a nanoparticle of size comparable to or smaller than the wavelength of light used to excite the plasmon. The LSPR has two important effects: electric fields near the particle's surface are greatly enhanced and the particle's optical absorption has a maximum at the plasmon resonant frequency. The electric field enhancement allows transmitted light either to be absorbed or to be scattered. This result in absorbance spectrum formation depends on the refractive index (RI) around the nanoparticle.

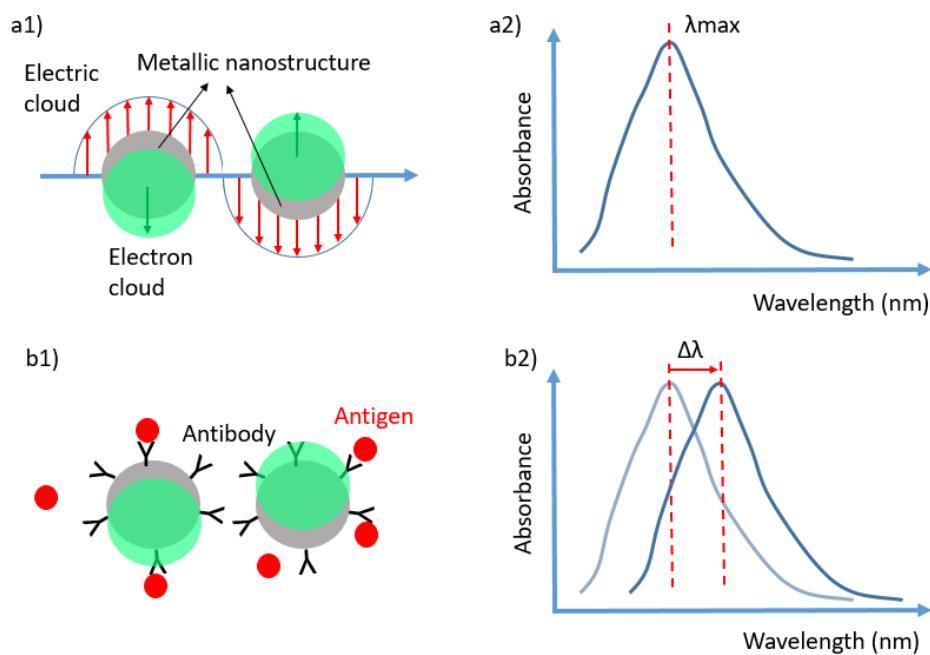


Figure 1-20 : Schematic diagram explaining the principle of LSPR shift.



The initial absorbance spectrum can be clearly seen in Figure 1-20-a2. Several factor that alter absorbance wavelength including metal nanostructure's size, shape, components and others. This provide additional advantage for the researcher to tune needed absorbance wavelength band within visible region for analytical measurement purpose. Also, the metal nanoparticle can be further used to attached with bio molecules such as antibody or protein (surface modification) that able to provide selectiveness in biosensor during experiment as shown in Figure 1-20-b1. Any successful bio molecules bind around the nanoparticles which alter the overall refractive index (RI) which causing the absorbance spectrum to shift either, red-shift (to the right due to increase in RI value) or blue-shift (to the left due to decrease of RI value). Successful shift can be observed as in Figure 1-20-b2. Successful binding occur in the present of plasmonic nanostructure are depending on the change of RI response as the local electromagnetic field,  $E(z)$ [44];

$$E(z) = \exp\left(-\frac{z}{l_d}\right)$$

where  $l_d$  is decay length (nm).

The effective refractive index of the structure is obtaining by integrating the distance-dependant local refractive index;

$$n_{absorbance} = \frac{2}{l_d} \int_0^{\infty} n(z) E^2(z) dz$$

Where  $n(z)$  is[45];

$$n(z) = \begin{cases} n_{sam} & 0 \leq z \leq d_{sam} \\ n_{metal} & d_{sam} \leq z \leq d_{sam} + d_{metal} \\ n_{air} & d_{sam} + d_{sa} \leq z \leq \infty \end{cases}$$

The absorbance shift;

$$\Delta\lambda \approx m(n_{absorbance} - n_{medium}) \left(1 - e^{\frac{-2d}{l_d}}\right)$$

Where  $m$ , represent the local slope (nm/refractive index unit, RIU),  $\Delta n$  as refractive index unit (RIU),  $d$ , as effective thickness of molecular adhesion layer (nm),  $l_d$ , as decay length (nm) and  $m$ , slope of substrate response to the bulk refractive index change.

$$m = \frac{\lambda_{medium_1} - \lambda_{medium_2}}{n_{medium_1} - n_{medium_2}} \quad (\text{unit: nm/RIU})$$

#### 1.4.2 The LSPR quantification for cell application

Since LSPR shows promising method to sense any bio molecular that attached on the plasmonic nano structure, therefore it is able to be applied for cell sensing application. Activated cell that been applied on the surface of plasmonic structure able to secret its protein into surrounding. This bio molecules protein able to attach with metal nano structure that able to change the its overall RI index around the nano particles. This resultant in the shift of absorbance spectrum which can be used to quantified its real time concentration changes without perturbing the cell.

#### 1.5 Introduction to electrochemistry biosensor

Electrochemical biosensor provides bio-recognizable capability by allow selective reaction between targeted analyte with bio-recognition present element by producing appropriate proportional electrical output signal over analyte concentration based reaction. It involved process of reduction and/or oxidation of species at the reaction interface. The species oxidized when the supplied potential is higher than the oxidation potential of the species over the electrode used. Electrochemical biosensor provide advantage over other type of bio-transducer approach including simple assemble, portable, short response time and great selective capability even with small sample amount size. This type bio-transducer contain 3 electrodes for detection, i.e. working electrode, reference electrode and counter electrode as shown in Figure 1-21. However, in some cases, analyte detection was carried without reference electrode where this might affect the overall stability function. Here, the sensing electrode can be made of gold (Au), silver (Ag), Carbon (C), Platinum (Pt)

or other conductive material where most of the reaction occur on these electrode surface. Selection of material provide is important since it determine the tolerable potential that can be handled which known as potential window.

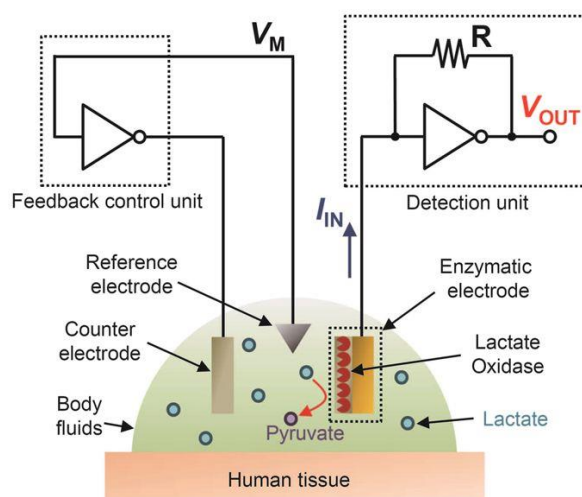


Figure 1-21: Electrochemical biosensor working electrode, counter electrode and reference electrode[46].

By applying certain potential appropriate with material selected, analyst solution can be analysed by studying its response of reduction and oxidation. Most oxidation will occur at the working electrode while opposite reaction occurs at the counter electrode to balance the reaction charge. In this approach, reaction tend to occur at the surface of active electrode where it involves electron to transfer across double layer to produce current or contribute to the double layer potential to produce voltage. Such condition allows one to measure current produced that proportional to reaction based on analyte concentration at fixed potential voltage. Current measure at this point represent direct measure of rate of electrode transfer and reflect reaction occurrence between free analyte and bio-receptor molecules. Some criteria to select proper counter electrode including free from metal degradation and having low resistance allowing faster electrode penetration than working electrode.

As mention above, the application of electrochemistry can be applied further to study molecular biology and bio-molecular interaction from cells. Upon activation of cell secreting signalling protein into environment, the signal protein quantification can be determined with the help of luminance

present as signal detection. This method was referred as electrochemiluminescent (ECL). Further explanation of the ECL are as follows.

#### 1.5.1 The basic of electrochemiluminescent (ECL)

The ECL occur as a result of successful luminescent reaction that been generated due to potential induce causing electrochemical reaction to occur on the working electrode and counter electrode. Since external potential is needed to activated the luminescence reaction, this allows researcher possess ability to control starting reaction and perform accurate detection compared to the electrochemistry method. This allows ECL method represent as powerful analytical tools for environmental observation and biomedical diagnosis.

The ECL process involve reaction to generate luminance as by product. The reaction made possible through two domain pathway known, i.e. annihilation and coreactant pathway. For annihilation pathway, the luminophore undergoes both oxidation and reduction as electrochemical process applied. Successful interaction between oxidized and reduced species produce both ground state and excited state where later it returns to ground state by releasing photon as by product. This type of pathway requires ECL species, solvent and supporting electrolyte in order to generate luminance as by product.

On the other hand, the coreactant ECL pathway it required coreactant substance in present before further reaction can occur. This pathway required the luminophore to be oxidate by losing electron, then react with reduced coreactant substance. Successful reaction between oxidized luminolpore and reduced coreactant produce excited luminol substance and ground state coreactant. The relaxation of excited luminol species allows generation of luminescent as by product. Through coreactant pathway, ECL generation able to be performed in aqueous solution which provide huge benefit for biological studies. Both pathway are simplified as in Table 4.

Table 4 : Proposed ECL pathway generation

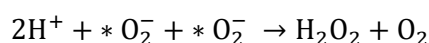
Annihilation pathway		Coreactant pathway (Luminophore : L), (Coreactant : C)	
$R \rightarrow R^+ + e^-$	Oxidation step	$L \rightarrow L^+ + e^-$	Luminophore redox reaction
$R + e^- \rightarrow R^-$	Reduction step	$C + e^- \rightarrow C^-$	Coreactant redox reaction
$R^+ + R^- \rightarrow R + R^*$	Excited state produce	$L^+ + C^- \rightarrow C + L^*$	Excited state formation
$R^* \rightarrow R + \text{Luminace}$	Light emission	$L^* \rightarrow L + \text{Luminace}$	Light emission

Even though there are different pathway for luminol ECL emission, the domain one which is coreactant pathway allows luminol substance to be used as luminophore substance that able to have reaction with the present of hydrogen peroxide. With this advantage, many biological activities that involve transformation or metabolism of hydrogen peroxide can be sensed with high sensitivity level without involving others additional substance. This can be prominent candidate for biological monitoring using biosensor application.

### 1.5.2 ECL imaging application

With high sensitivity detection and controllable reaction time monitoring ability, luminol based ECL quantification shows promising method for biosensor application involving cell application. However, dealing with cells could also introduce some difficulties such as cell migration and also point of interest for observation. Therefore, integration between imaging instruments with ECL observation measurement can provide simple solution to overcome such obstacles. With this approach, the quantification of luminace can be observed strictly at the surface of electrode rather than conventional chemiluminescence approach[47]. With good selection of conducting material, the temporal resolution of targeted cell can be tuned before its ECL detection observed using photon detector.

Using this approach, it is possible for ECL imaging to be applied with cell sensing for ROS secretion from immune cell, neutrophil for continuous monitoring purpose. As mention earlier in subchapter 1.3.3, neutrophil cells differentiate forming NETosis by releasing signal species of ROS in from of hydrogen peroxide with equation.



The luminol ECL able to coreactant with release of hydrogen peroxide (ROS) that allows release of luminance. The quantification of luminance under photo detector was able to provide real time monitoring ability at specific location down to single cell level.

## 1.6 Concept of thesis approach

Neutrophil has been considered as primary soldier in innate immune system for eliminating invading pathogens. Neutrophil being abundant immune host cell in human blood vessel, several differentiation mechanisms is known to take place engulfing microbes pathogens such as phagocytosis, degranulation, cytokine production and neutrophil extracellular trap (NETs) production. An imbalance in NETs formation (NETosis) and its reactive oxygen species (ROS) produce are associated with autoimmune, inflammatory, metabolic, vasculitis and other diseases. Since every cell possess unique differentiation character, it is very important to monitor individual neutrophils' NETosis and ROS production release. Single cell analysis technique provides remarkable capacity for understanding sole cell characteristic rather than commonly used average measurement from bulk population cells. Therefore, by manipulating neutrophil into singular manner, it is possible to further understand cell biology mechanism for the improvement of early disease diagnosis and regular healthcare activities.

In this work, single cell analysis of neutrophils cell activity of formation of NETs and the release of ROS was quantified using localized surface plasmon resonance (LSPR) and luminol – based electrochemiluminescence (ECL) observation technique was performed, respectively. Neutrophil cells were extracted from healthy blood donor and suspended in Dulbecco's phosphate-buffered saline (D-

PBS(-)) media. For NETosis analysis, simple microengraving platform was realized with microwell array (MWA) sheet on plasmonic sensing substrate for LSPR observation. This can be shown in Figure 1-22.

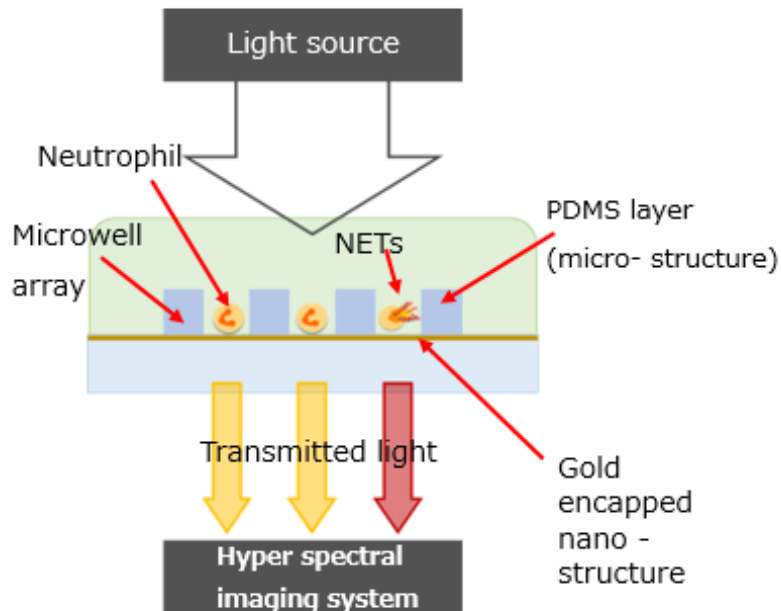


Figure 1-22 : The schematic diagram of LSPR imaging for single neutrophil cell.

Introduction of microwell structure provide good segregation phenomena without perturb surrounding cells. Activated neutrophil cell undergoes single cell isolation before quantified using hyperspectral imaging system for absorbance spectrum observation. The physical change and bio molecular release during NETosis causing the RI to change round the plasmonic structure. This cause the absorbance spectrum wavelength to shift. Real time monitoring of NETs release and its absorbance spectrum change are reported in this study.

On the other hand, the ROS release was realized by using microwell enhanced luminol based ECL biosensor. Here, neutrophil cells were introduced between dual electrode (working and counter electrode) before trapping using microwell structure as shown in the Figure 1-23.

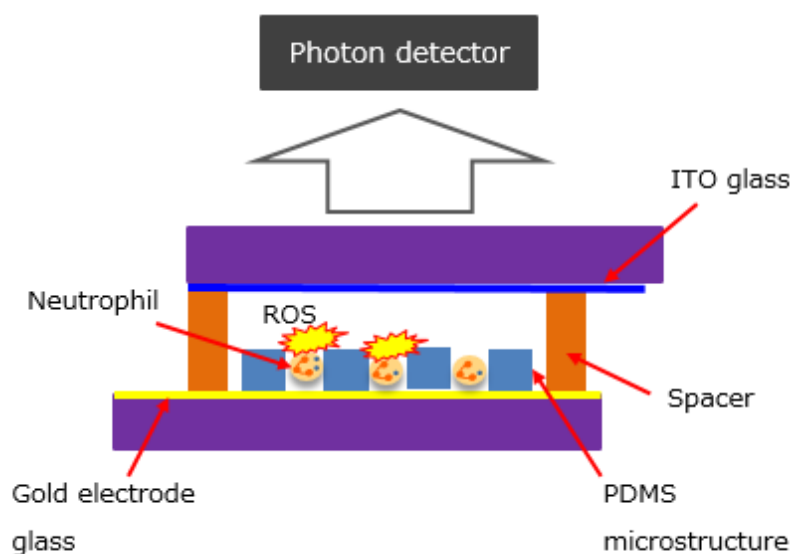


Figure 1-23 : The schematic diagram of Luminol based ECL quantification for ROS application.

As mention earlier, the microwell structure provide room for cell isolation. This allow neutrophil cell to release ROS without been perturb from nearby cells. The quenching of ECL imaging localized inside microwell electrode was examine as successful reaction between produced ROS and luminophore electrochemical reaction. As extension of this study could monitor the degradation of the NETs release and ROS production which can be proven useful for autoimmune disease detection and pathogenesis elucidation.



## 2 CHAPTER 2 : ONE-STEP NANOIMPRINTED HYBRID MICRO-/NANO-STRUCTURE FOR LOCALIZED SURFACE PLASMON RESONANCE DETECTION

In this chapter, single substrate consists of micro-/nano- structured plasmonic substrate was prepared to be used with localized surface plasmon resonance (LSPR) for protein detection as illustrated in Figure 2-1. The synergistic integration of cell-trapping microwell structures with plasmonic sensing nanopillar structures in a single-layered substrate by one-step thermal nanoimprinting was reported in details. Through this integration, prepared device possesses advantage of trapping and isolating cells into certain confined area before activated cell's secretion was able to be sensed the local refractive index change using gold capped plasmonic nanostructure. Reciprocal with the refractive index change with protein secretion from cell, the plasmonic wavelength shift in absorbance spectra was observed. This novel preparation can provide inexpensive, rapid, high reproducibility yet real time label free protein secretion observation.

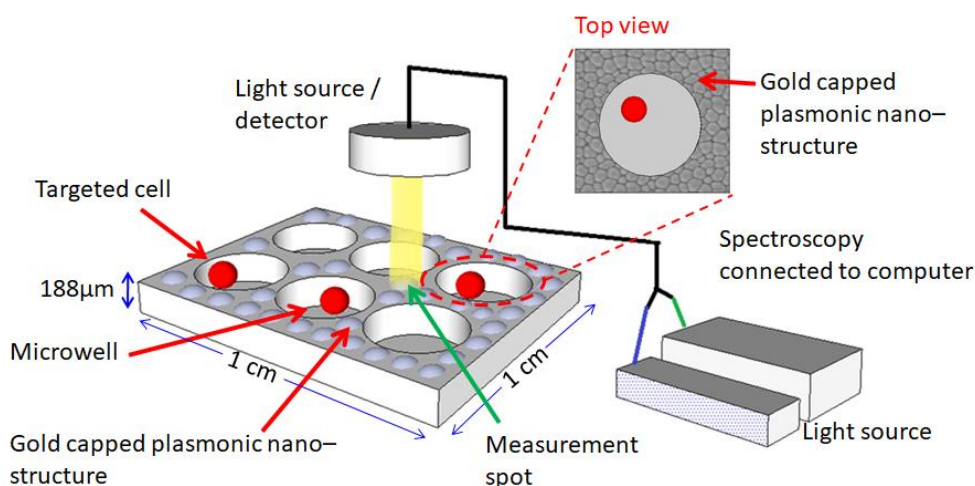


Figure 2-1 : Schematic illustration of hybrid nano-/micro structured plasmonic substrate.

### 2.1 Introduction

The LSPR based biosensors take advantage of biomolecular interactions affecting the refractive index (RI) in the vicinity of the sensing surface during the occurrence of LSPR for spontaneous detection, which is highly beneficial for diagnostic and point-of-care testing (POCT) purposes[48-52].

LSPR occurs when the natural frequency of collectively oscillating conduction electrons in noble metal nanoparticles matches the incident electromagnetic light frequency, causing resonant oscillations of electrons and thus can be read as a sharp absorption of light at this frequency[53]. Any RI changes in the interfacial vicinity due to the biomolecule binding will trigger an immediate response in LSPR-induced light absorption[54, 55]. This has allowed LSPR-based techniques to be used in various analyses involving antigen-antibody interactions and protein surface binding kinetics[56-59]. In addition, LSPR biosensors, especially those integrated with microfluidics, show remarkable potential use in real time bio-sensing device with miniaturization capability and in realizing portable sensing platforms[50, 60].

Conventional methods such as enzyme-linked immunosorbent assay (ELISA) enable sufficient quantification of targeted proteins with its simple parallel array operation and high sensitivity. However, this type of sensing method requires secondary antibodies that bind with targeted analytes and requires complex sample labeling. Another technique, the electrofluorescence method, requires repeated dye staining over time owing to photobleaching of the fluorescent dyes, which makes it inconvenient for continuous cell monitoring[61]. On the other hand, LSPR-based sensing typically uses simple setups and does not require secondary antibodies for detection. In addition, LSPR shows constant responses without losing its intensity, which is highly favorable for real-time observation applications. The comparison has been simplified as Table 5.

Table 5 : Comparison between commercially available technique.

	Electro-fluorescent	ELISA	LSPR
Label	Require fluorescent dye	Require primary and secondary antibodies	Able to perform label free interaction
Sensitivity	High	Very high	High
Preparation	Need regular staining to avoid photobleaching	Complex sample preparation	Simple sample preparation
Time	Almost instant	Overnight	Instant

Real-time cell monitoring enables the immediate detection of proteins secreted by cells for intercellular communication. Analysis of cell activity through protein detection can provide important new information for early detection of infectious diseases and also for regular healthcare purposes. Most conventional analytical methods only measure the average response from a highly heterogeneous population of cells[62]. Therefore, in order not to overlook unique and potentially rare type responses from heterogeneous population cells, it is essential to study cells in form of individual basis and their responses to stimuli independently[63]. However, there are technical difficulties along the pipeline in identifying individual cells from their response activities. To serve this purpose, numerous approaches including LSPR-based cell array analysis have been proposed[49, 64].

LSPR biosensors show great potential as a platform to observe the presence of biomolecules at the single cell level. In a previous study, Oh et al.[53], have demonstrated a three-stage integrated label-free LSPR sensor for real-time detection of tumor necrosis factor (TNF)- $\alpha$  cytokines secreted from cells. The three stages were separately prepared to perform specific dedicated tasks. Their label-free sensing approach showed highly sensitive detection with minimal blood sample volume required. However, with this approach, cells are forced to be trapped between narrow cylindrical gaps through microbeads, allowing the secreted molecules to pass through towards the sensing area. Such an arrangement introduces difficulties in determining the sources of individual biomolecules released. Another study by Raphael et al.[65] provides an excellent LSPR-based approach for observing protein secretion from single cells in real time. Using their system, the spatial and temporal distributions of single cells were evaluated precisely. However, the electron beam lithography (EBL) fabrication procedure that they employed is time-consuming, resulting in the production of relatively small sensing areas. Keeping the cells close within small sensing areas remains a challenge owing to the regular migration of cells. Therefore, an alternative LSPR-based platform is needed to address these limitations.

Nanoimprinting shows promise as a method to mass-produce nanostructured substrates with large working areas[66]. By applying this technology, sub-10 nm designs can be patterned on surfaces with high resolution, high throughput, and good reproducibility at a low cost.[67-69]. Nanoimprinting has been applied to the production of devices such as microfluidics[70, 71], microneedles[72], and lab-on chips devices[73]. In order to fabricate cost-effective disposable biosensors, a cheap mass production technique such as nanoimprinting is required[74, 75]. Therefore, in previous papers, it has been reported in detail on the fabrication of nanoimprinted gold-capped nanopillar structures on cyclo-olefin polymer (COP) substrates for LSPR-based applications[51, 76, 77]. By precisely varying the anodizing conditions, self-organized nanoporous structures can be formed on an alumina mold, which was further used to fabricate a nanopillar-based LSPR biosensor. This method allows the LSPR biosensor to be consistently reproduced.

In this work, to enhance the device biosensing capability, microwells array and a nanopillars structure were integrated into a single substrate; this approach is proposed for plasmonic sensing. Studies have shown that microwell arrays offer promise as versatile platforms for high-throughput continuous long-term cell monitoring[78]. Using these arrays, thousands of individual cells can be trapped within confined areas by simple gravitational sedimentation. Microwell arrays can also limit the regular migration of isolated cells, reducing intrusion from neighboring cells. Thus, the extracellular protein secretion behavior of isolated cells and their released proteins can easily be analyzed and identified. In our proposed device, the microwell structures were fabricated such that individual cells are isolated, while the coexisting nanostructures around the microwell were utilized to sense RI changes in the vicinity owing to protein secretion. The hierarchical structure was successfully realized by a one-step nanoimprint lithography (NIL) fabrication method.

To realize an LSPR chip with hybridized micro- and nanostructures using a single material via NIL, an SU-8 patterned alumina mold was prepared. The nanoporous alumina mold was first fabricated using a two-step anodization method. Subsequently a photolithographically patterned SU-8 layer was

formed on top of the porous alumina mold surface. The SU-8 layer acts as a micro level spacer during the thermal nanoimprint process, which enables the simultaneous production of micro- and nano-patterns on a single COP film substrate. The COP film was chosen for its excellent transparency and its properties to be used as a thermal plastic resin. A thin layer of gold was finally sputtered onto the nanoimprinted COP film, providing plasmonic properties to the device. The optical absorbance, beads trapping capacity, and biomolecular interaction on the prepared gold-sputtered plasmonic device were then investigated. Multiple substrates with uniform plasmonic sensing properties were produced using a single master alumina mold in less than 30 min, which indicated that our method is a cost-effective and hassle-free option to mass produce devices for real-time single-cell monitoring.

## 2.2 Experimental setup

### 2.2.1 Fabrication of nano-porous alumina oxide

Self-organized nanoporous aluminum oxide (AAO) was prepared as a template for nanopillar formation on COP films in this experiment. By precisely controlling the anodizing conditions, pore size and pitch can be adjusted. The fabrication mechanism has been detailed in our previous report[76]. Briefly, the AAO mold was prepared using a two-step anodizing technique. Parallel grained and single-side-polished aluminum was initially sonicated in acetone and pre-etched in an aqueous etching solution containing phosphoric acid (1.16%) and chromic acid (5%, w/v) at 70 °C immediately before use. The first anodizing step was conducted at 80 V for 1 h at 0 °C, before post-etching for 10 min at 70 °C. The second anodizing step was performed at 60 V for 50 s. Lastly, phosphoric acid etching was carried out at 40 °C for 12.5 min to widen surface pore structures. The schematic illustration of prepared AAO mold as shown in Figure 2-2. The resultant mold was used for next preparation.

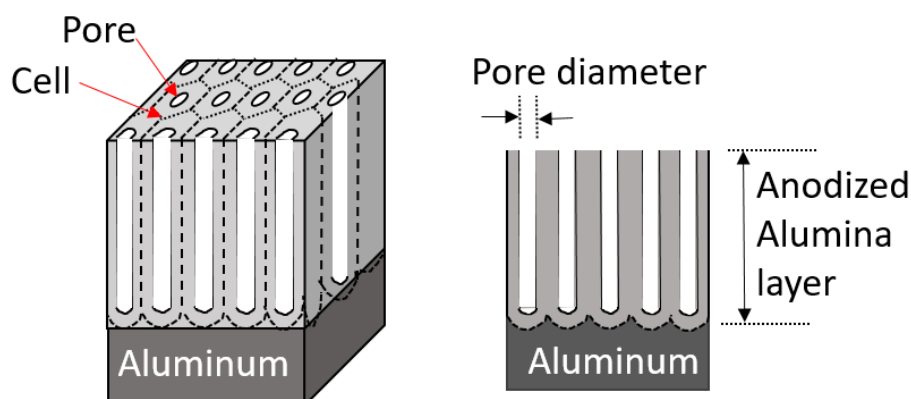


Figure 2-2 : The schematic design of prepared AAO mold.

### 2.2.2 Fabrication of SU-8/AAO mold template

A specifically designed SU-8 layer was formed on the previously prepared alumina mold. This step was conducted to introduce micropoles (specific spacing) during the subsequent thermal nanoimprinting for cell trapping purposes. Several heights and diameters of the SU-8 micropoles were tested in this work. This was carried out to prevent the SU-8 microstructures from coming off during the COP film mold-releasing procedure and clogging of microwells. About 5 mL of SU-8 3010 (Micro Chem) was first spin-coated onto an as-prepared alumina mold in a clean environment at about 2500 rpm for 30 s to form a thin uniform layer of SU-8. Immediately, soft backing was performed on the mold for 10 min at 95 °C. A specifically designed mask prepared in advance was aligned on the cured SU-8 layer. Following this step, the SU-8 layer was exposed to UV for 40 s at 80% brightness using a mask aligner (Mikasa, MA-10). The exposed mold was then hard baked at 95 °C for 5 min before being lifted off using an SU-8 developer. The SU-8-coated alumina mold surface was finally silanized using dilute trichloro(3,3,4,4,5,5,6,6,7,7,8,8,8-tridecafluorooctyl)silane (Wako, 78560-45-9) for 30 min to ease the mold-COP release. After silanization, the mold was returned to a dust-free container until use in following procedures.

### 2.2.3 One-step NIL and gold sputtering for LSPR activation

The SU-8-coated alumina mold describe in the previous section was used to emboss its reverse pattern on a COP film (Zeon, Zf-14) using thermal nanoimprinting equipment (SCIVAX, X-300H). Under

vacuum conditions, a fresh COP film was carefully arranged on the prepared alumina mold before being sandwiched with two identical 4-in. silicon wafers. This ensures a uniform pressure distribution on the mold and COP film. Then, approximately 2 MPa of hydraulic pressure was applied to the COP film at a constant temperature of 160 °C for 10 min. After returning to atmospheric conditions and cooling down to 80 °C, the resultant COP film was removed carefully from the alumina mold. This step is crucial to prevent the SU-8 structure from breaking or coming off together with the COP substrate. The transformed COP pattern was subsequently sputtered with gold using (ULVAC, ACS4000) to form a 68 nm layer of gold on the COP surface. The full fabrication has been illustrated in Figure 2-3.

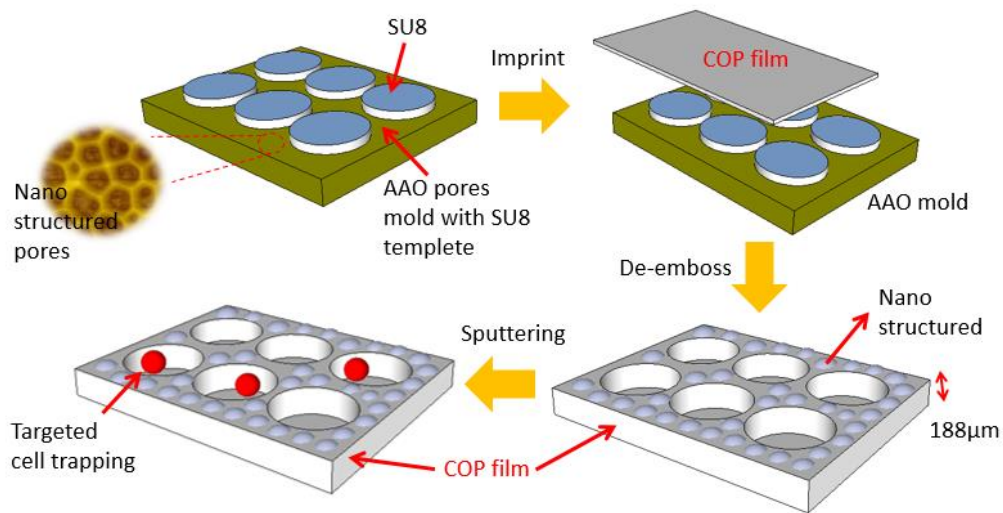


Figure 2-3 : Full fabrication procedure for microwell enhanced LSPR substrate.

#### 2.2.4 Characterization of gold-sputtered COP chip

Morphological evaluation of the gold-sputtered COP film was performed by scanning electron microscope (SEM; FEI Strata, DB235). The AAO mold was examined by atomic force microscope (AFM; Hitachi, SPA400). AFM tips were aligned precisely with the alumina mold in the non-contact mode. From the obtained information, three dimensional (3D) images with cross-sectioned information were regenerated and presented. Using these images, the topographies of the microwells and nanopillars were confirmed.

The absorbance spectrum of the COP film surface was measured with a UV-visible spectrophotometer (Shimadzu, UV-3600). With this observation procedure, the sensitivity of prepared COP films was evaluated in environments with different refractive index, i.e., air ( $n=1.0$ ), water ( $n=1.33$ ), 1 M glucose ( $n=1.35$ ), ethylene glycol ( $n=1.43$ ) and glycerol ( $n=1.47$ ). The shift in LSPR-induced absorption peak wavelength was plotted, as a function of refractive index, and the slope of this curve was used to determine the bulk sensitivity of this as-prepared COP film. In addition, the response of this plasmonic chip to various concentrations of the anti-IgA antibody (10 ng to 500 ng/ $\mu\text{L}$ ) in serum free media (SFM) was measured. For each concentration tested, a bare absorption spectral measurement was taken prior to the addition of pure SFM. Following this, a second measurement was taken 30 min before the anti-IgA antibody was added to its final required concentration. Finally, a third measurement was taken for the construction of a calibration curve.

#### 2.2.5 Trapping and isolation of fluorescent beads

Fluorescent beads were used to study the trapping capability of the microwell structures on the COP film, a fresh stock of fluorescent beads ( $\phi = 15 \mu\text{m}$ , Thermo Fisher Scientific) with excitation and emission wavelengths of 468 and 508 nm respectively was diluted in an aqueous solution of 0.1% Tween 20. This suspension was later adjusted to a concentration of  $2.0 \times 10^4$  beads/mL. About 60  $\mu\text{L}$  of this solution was then dispensed on the plasmonic chip surface and allowed to undergo sedimentation for 30 min. Optical observation was performed using an inverted microscope (Olympus, IX-71) with x10 magnification. Resultant images were recorded using a high-speed (DITECT, HAS-L2) camera. By changing the fluorescence filter, fluorescence images at x20 and x40 magnifications were also obtained. The total number of beads in each microwell was counted and tabulated using a bar graph to evaluate the trapping capability.

#### 2.2.6 Real-time cell monitoring via LSPR

Healthy yeast (*Pichia pastoris*) cells were used for real-time cell observation. This cell model was genetically modified to release the secreted aspartic protease (SAP1) protein after stimulation with a buffered methanol complex medium (BMMY) solution[79]. All the equipment used was cleaned and



autoclaved before cell culture to prevent any contamination. The cells were first pre-cultured in pichia growth media: buffered glycerol complex medium (BMGY) for 24 h. BMGY comprised 1% (w/v) yeast extract, 2% (w/v) peptone, 1.34% (w/v) yeast nitrogen base without amino acids,  $4 \times 10^{-5}$ % (w/v) biotin, 1% (v/v) glycerol, and 100 nM potassium phosphate (pH 6.0)[79]. Pre-cultured cells were centrifuged for 15 min (without brake) at 3000 G and 4 °C.

Next, the supernatant was replaced with BMMY, which consists of 1% (w/v) yeast extract, 2% (w/v) peptone, 100 nM potassium phosphate (pH 6.0), 1.34% (w/v) yeast nitrogen base without amino acids,  $4 \times 10^{-5}$ % (w/v) biotin, and 0.5% (v/v) methanol. The cell suspension was adjusted to a concentration of  $4.0 \times 10^4$  cells/mL.

Prior to LSPR measurements, gold-sputtered COP films were cut into 1 cm x 1 cm pieces. About 30  $\mu$ L of BMMY medium was slowly dispensed on one of the cut films. The initial absorbance measurement was recorded and used as the baseline. Later, about 30  $\mu$ L of cell suspension was added to the BMMY medium already on the COP film. The absorbance spectrum was monitored for 12 h as the cells grew on the COP film surface. The shifts in the absorption peak wavelength were recorded and illustrated in a bar graph.

## 2.3 Results and discussion

### 2.3.1 Morphology characterization of AAO mold and COP film

The microwell enhanced LSPR substrate was prepared as follows. A fresh AAO mold was prepared before applying a patterned SU-8 layer on its surface. This layer serves as a spacer during the nanoimprinting procedure, enabling for the simultaneous formation of microwell structures together with dome-shaped nanostructures in a single COP film substrate. Subsequently, the prepared COP film is subjected to gold sputtering in order to confer plasmonic properties.

Figure 2-4 shows AFM images of the prepared AAO mold. The anodization conditions have been optimized for ease of releasing nanoimprinted COP films from the mold and for dense nanostructure

formation. Under the applied conditions, shallow cavities were formed with an average pitch of 190 nm. The cavity depths (as shown in the cross-section view) were measured to be between 60–85 nm.

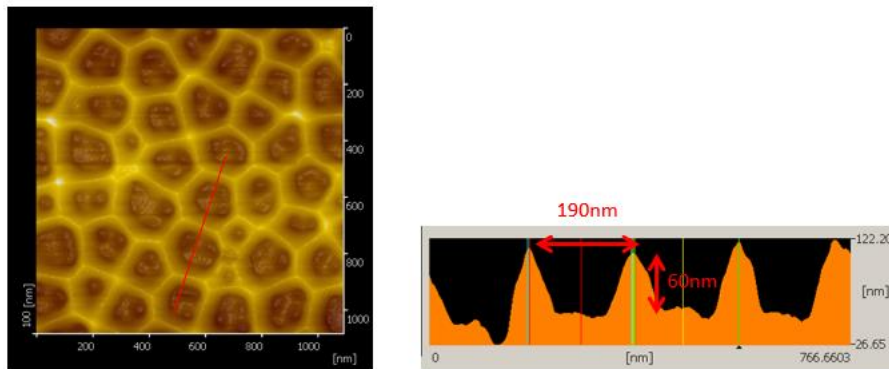


Figure 2-4 : The AFM image of prepared AAO mold.

In this study, several diameters and heights of micropoles on the SU-8 layer were tested. First, a diameter-to-height ratio of 1:1 (60  $\mu\text{m}$ :60  $\mu\text{m}$ ) was tested. At this ratio, several of the SU-8 micropoles, which were needed for microwell formation, broke. This breakage was also observed by optical microscopy observation, which showed the SU-8 micropoles to be broken and twisted. This suggests that the SU-8 micropoles had a relatively high contact surface area, which promotes strong adhesion with the COP substrate during the cooling down and de-embossing steps. This was overcome by reducing the micropole height to 10  $\mu\text{m}$ . In addition, reducing the SU-8 height formed shallower microwells that are more suitable for cell observation in this study. This is because a smaller microwell depth results in a higher likelihood for cell-to-sensing surface interaction during real-time observation. Figure 2-5 shows the SU-8 micropoles after approximately 20 times of nanoimprinting procedure where none of affected micropoles are visible.

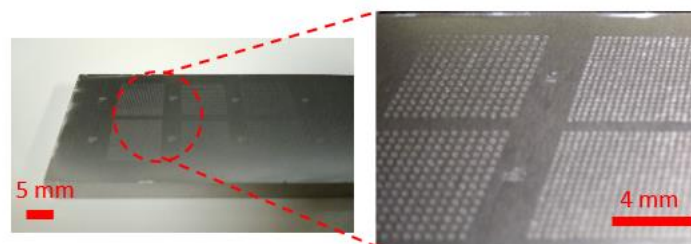


Figure 2-5 : Successful SU8 micro-poles on nanostructured AAO mold.

The SEM images shown in Figure 2-6 show the microwells and dome-shaped nanopillar structures that have been nanoimprinted on a single COP substrate. This formation of microwells among nanostructures has been made possible owing to the addition of the SU-8 spacer on the nanoporous alumina mold. The imprinted COP film shows that the microwells have an average diameter of  $70\ \mu\text{m}$  and a pitch of  $500\ \mu\text{m}$ . In this design, a total of 324 microwells with an average depth of  $10\ \mu\text{m}$  was fabricated in a single imprint procedure. A magnified image shows dense dome-shaped nanostructures with an average pitch of  $190\ \text{nm}$ .

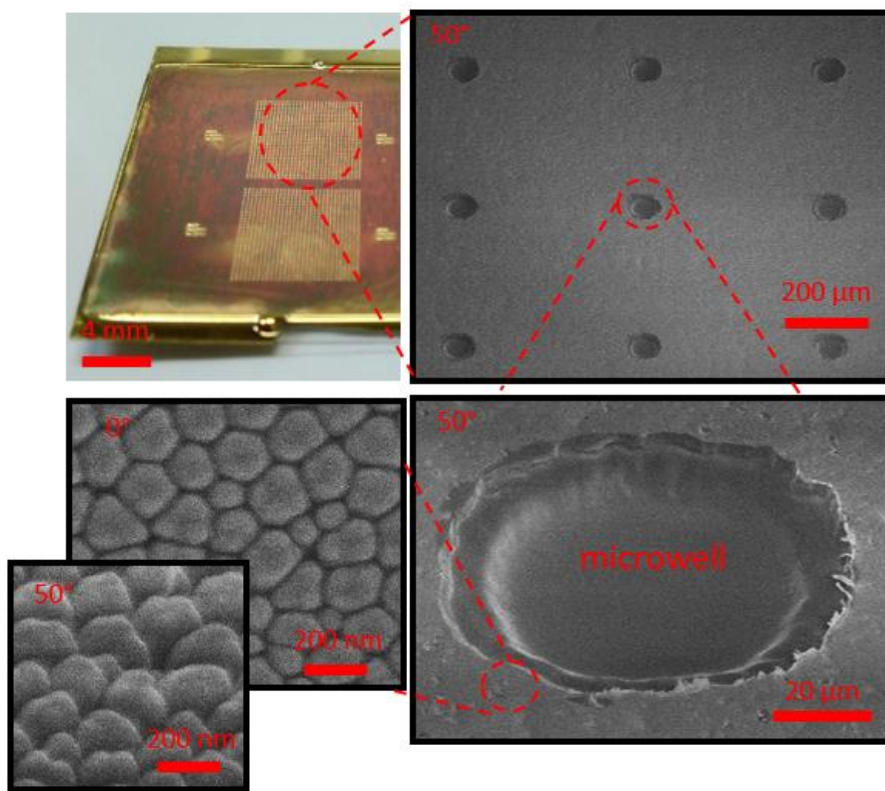


Figure 2-6 : The SEM image of imprinted microwell enhanced LSPR substrate.

### 2.3.2 LSPR absorbance response evaluation of COP film

As-prepared gold-sputtered COP films were measured from their LSPR absorption peak shifts in several different refractive index environments. Each material was dropped on as-prepared substrates, and its absorbance responses were measured. The results show that as the refractive index of the material increases, the LSPR absorption peak is red-shifted and increases in intensity Figure 2-7a. This behavior suggests that the produced gold-sputtered COP substrate exhibits working plasmonic

properties. Furthermore, to determine the bulk sensitivity of the substrate to changes in refractive index, the peak shifts were plotted as a function of refractive index in Figure 2-7b, which showed in a slope of 274 nm/RIU. These results clearly verified that our prepared gold-sputtered COP substrate as an LSPR sensing chip can respond to changes in refractive index with corresponding peak shifts, which is crucial to LSPR-based bio-sensing.

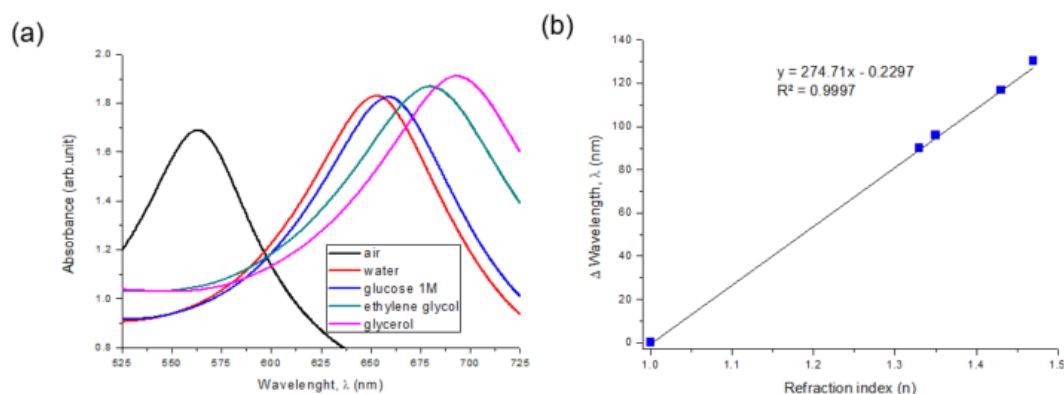


Figure 2-7 : a) Absorbance LSPR peak shows red-shifted. b) average sensitivity of LSPR substrate.

### 2.3.3 Biomolecule detection with COP film

Immunosensing of the anti-IgA antibody was conducted to study the detection of biomolecules using the prepared gold-sputtered COP film. However, in this work, the antibody was not immobilized on the film surface prior to immunosensing. This approach was adopted to allow the free-mode interactions between the gold nanostructures and the target biomolecules during LSPR measurements. The incubation period was 30 min between successive measurements. Figure 2-8a shows the response of the plasmonic chip after the anti-IgA antibody, the target biomolecule, was introduced. The initial absorption peak was observed at 560 nm in air. This absorption peak shows red shifts when SFM was introduced followed by the anti-IgA antibody to a final concentration of 500 ng/ $\mu$ L. Measurement were carried out at several anti-IgA antibody concentrations (10 ng to 500 ng/ $\mu$ L).

Figure 2-8b shows the calibration curve obtained from the responses observed for each target concentration. The results show that the prepared plasmonic device has a linear response with a detection limit of 10 ng/ $\mu$ L. Another study showed that the detection limit for the IgA immunoglobulin

for female adult is in the range of 82 – 470 ng/ $\mu$ L, while that in a male adult in the range of 89 – 624 ng/ $\mu$ L[80]. This IgA level does change depending on certain habits such as alcohol consumption and smoking. A study showed that alcohol consumption in adults leads to an increase in IgA concentration reading variability among light drinkers (78 – 579 ng/ $\mu$ L), moderate drinkers (78 – 733 ng/ $\mu$ L), and heavy drinkers (63 – 569 ng/ $\mu$ L). In addition, adults with smoking habits shows high IgA levels of 74 – 730 ng/ $\mu$ L. In another study[81], the IgA concentrations in diabetic patients (age range; 31 – 40) are 920 – 6700 ng/ $\mu$ L in type 1 diabetes patients and 730 – 3480 ng/ $\mu$ L in type-2 diabetes patients. The control range for this study was recorded at 660 – 3100 ng/ $\mu$ L. With the aforementioned IgA ranges, the detection limit of our prepared plasmonic device is within the desired conditions. Therefore, the as-prepared chip may be used as an alternative platform for cell assay.

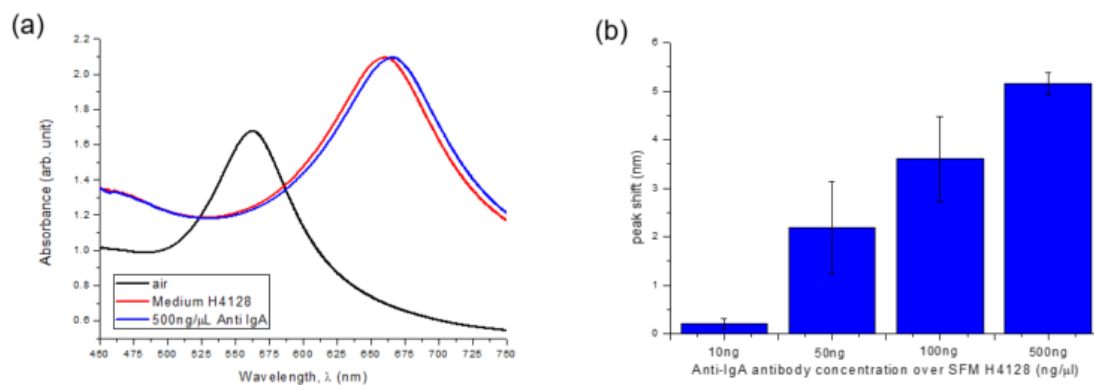


Figure 2-8 : a) The absorbance response of 500 ng/mL anti-IgA antibody in serum free media. b) Calibration curve for concentrations 10 - 500 ng/ $\mu$ L anti-IgA antibody peak absorbance using prepared plasmonic device.

#### 2.3.4 Performance in trapping of fluorescent beads on COP film

The trapping capacity of the shallow microwells on the prepared gold-sputtered COP film was evaluated using 15  $\mu$ m fluorescent beads. It was calculated that approximately 1200 beads were dispensed on the gold-sputtered COP film. Figure 2-9 shows bright-field microscopy observation of the trapped beads. The same area was also imaged by fluorescence microscopy to clearly show that the fluorescent beads were successfully isolated inside the microwells. The number of microwells with single beads trapped is presented in a bar graph in Figure 2-10. From the results, about 14% of the

microwells were capable of trapping single beads. The low percentage of single cell isolation was likely due to the low depth of the microwells. By far this is area subject for compromise since a high cell-to-sensing surface area for interaction is necessary for subsequent experiments.

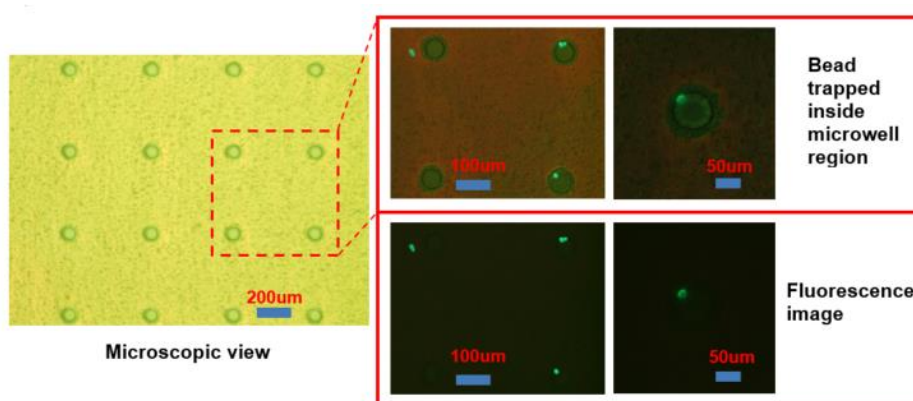


Figure 2-9 : Microscopy observation of the trapped beads into microwell.

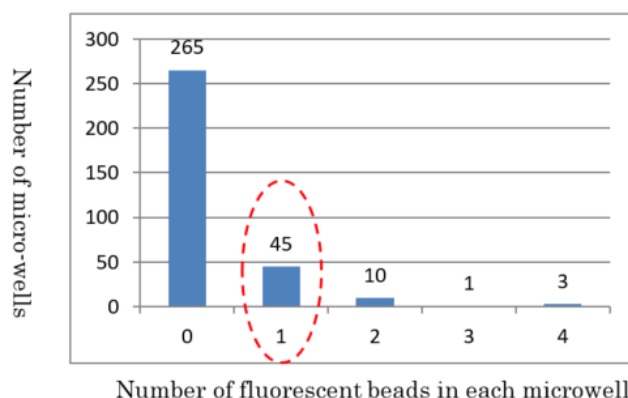


Figure 2-10 : Number of fluorescent beads trapped in each prepared microwell.

### 2.3.5 Real-time monitoring of absorbance response from cell secretions

Real-time LSPR observations of healthy yeast cells (*P. pastoris*) using less than 10 cells per microwell were conducted over omit 12 h. Since yeast cells generally have a lower probability of undergoing apoptosis than human cells, they make excellent candidates for real-time observation. LSPR measurements of the cells on the COP film were carried out every 3 h, and the absorbance responses were recorded and are summarized in Figure 2-11a. In general, the absorbance tend to red shift with time. The absorption peak wavelength shift with time as is illustrated in Figure 2-11b. At earlier stages, gradual shifts of 1-2 nm were recorded. Afterwards, more significant peak shifts were

recorded between 6 and 12 h. After 12 h, the absorption peak red shifted by almost 6.9 nm from its original value. We believe that this peak shift was caused by changes in the local refractive index due to the presence of proteins secreted from the yeast cells on the COP film.

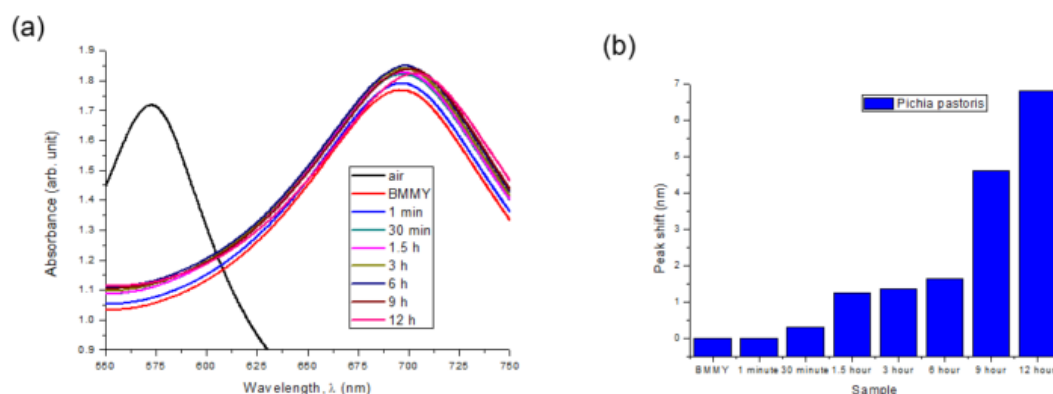


Figure 2-11 : a) Real-time absorbance observation of healthy *P. pastoris* cells using prepared plasmonic device up to 12 h. (b) Time course of absorbance peak wavelength.

## 2.4 Conclusion

Hierarchical hybrid micro-nanostructures with plasmonic sensing capabilities have been successfully fabricated on a single-COP-film substrate via one-step NIL method. This was realized by combining a nanoporous alumina mold with an SU-8 spacer to form a hybrid mold for NIL. With this exquisite design, this substrate is capable of single cell isolation and LSPR detection. The diameter and height of the SU-8 spacer were optimized to obtain the best conditions for smooth de-embossing of the imprinted COP films. Morphological observation by SEM revealed the formation of microwells with a diameter of 70  $\mu\text{m}$  and a pitch of 500  $\mu\text{m}$  along with dome-shaped nanostructures of 190 nm diameter. The gold-sputtered COP film omit exhibits plasmonic properties, with the LSPR-induced absorption peak wavelength red shifting in response to an increases in the local refractive index. The bulk sensitivity of this substrate was found to be 274 nm/RIU. A limit of detection of 10 ng/ $\mu\text{L}$  for the anti-IgA antibody was established using the as-prepared plasmonic chip. Real-time observation of *P. pastoris* cells omit on this substrate showed a red shift of 6.9 nm in absorbance spectra over a 12-hour period.

### 3 CHAPTER 3 : HYPERSPECTRAL IMAGING WITH LSPR OBSERVATION FOR SINGLE NEUTROPHILS CELLS

In this chapter, simple microengraving cell monitoring method for neutrophil extracellular traps (NETs) released from single neutrophils has been realized using a perforated polydimethylsiloxane (PDMS) microwell array (MWA) sheet on a plasmon chip platform. Study shows that, an imbalance between NETs formation and the succeeding degradation (NETosis) are considered associated with autoimmune disease and others. Thus, an alternative platform that can conduct monitoring of this activity on single cell level at minimum cost but with great sensitivity is greatly desired. By manipulating the MWA structure, single neutrophil cell can be isolated and induce for activation using PMA solution as shown in Figure 3-1. In this study, the nanostructure plasmonic response was placed inside MWA for real time monitoring response depending on the NETosis progression. Under observation using a LSPR substrate enhanced with hyperspectral imaging system that allows high-throughput screening, significant release of NETs from neutrophils cells was observed and reported.

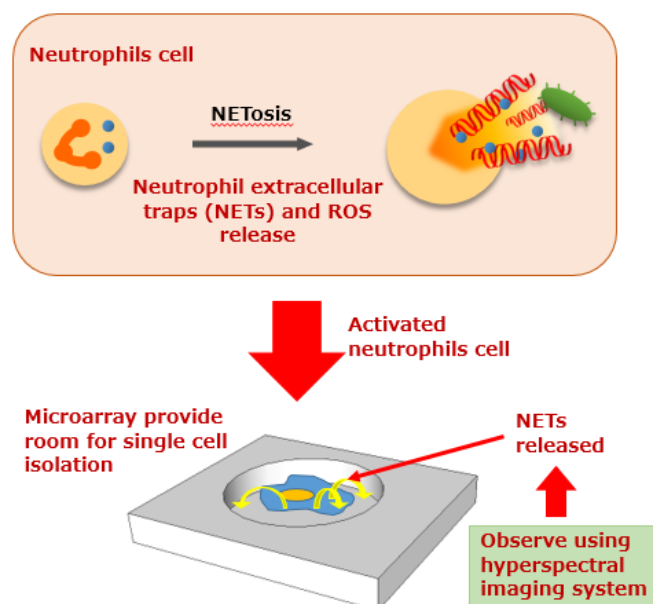


Figure 3-1 : Activated neutrophils cell are isolated using microwell enhanced LSPR substrate.



### 3.1 Introduction

Neutrophils have been considered for a long time as the principal soldiers of the innate immune system against invading pathogens. As primary immune cells to migrate to a site of inflammation, several defense mechanisms can be enacted to combat the spread of the disease through phagocytosis of pathogens, degranulation, cytokine production, and formation of neutrophil extracellular traps (NETs)[30, 82, 83] as shown in . Researcher Takei et al.[32] in 1996 has discovered that a pathway of cellular death that is different from apoptosis and necrosis. Further investigation, Brinkmann et al.[33] produced a report in 2004 states that the mesh-like structure of NETs is found to be composed of histones and highly decondensed chromatin fibers[82] with varying diameters of 15 nm to 17 nm.

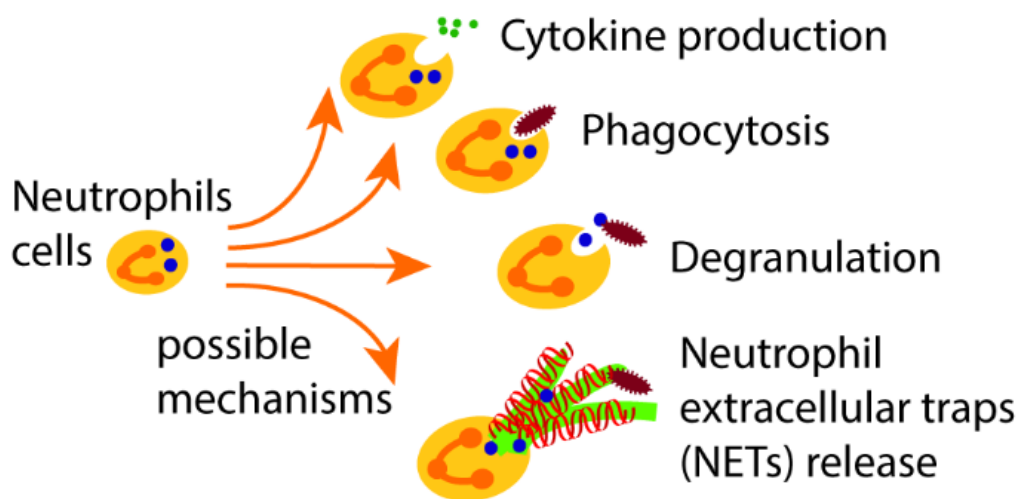


Figure 3-2 : Possible mechanisms of neutrophils cell.

Though the framework of activation pathway is still under investigation, NETs are known to be released by activated neutrophils that form a fibrous network assembled from nuclear and granular components with larger size range[32]. This leads to the great potential of NETs as physical and antimicrobial barriers that first extracellularly restricts and then kills the pathogens at the site of inflammation. They can stay in the bloodstream for 6—8 hours and in tissues for 7 days[30]. However, this unique composition and characteristics of NETs are prone to be considered by our body as a threat. NETs are found in a variety of conditions contributor aside from infection such as malignancy,

atherosclerosis, and autoimmune diseases including rheumatoid arthritis (RA), systemic lupus erythematosus (SLE), anti-neutrophil cytoplasmic antibodies (ANCA)- associated vasculitis (AAV), psoriasis, and gout[84]. An imbalance between NET formation and the succeeding degradation are considered associated with autoimmune disease and its pathogenesis[84]. If left untreated or diagnosed late, prolonged exposure to NETs-related cascades associated to the autoimmunity could lead to systemic organ damage[84].

Evaluating if a patient has an autoimmune disease is conventionally performed with antinuclear antibody using immunofluorescence assay which requires at least 2 weeks to process due to the range of types associated to certain autoantibodies[85]. Aside from the long required time for this test and the cost; repeated dye staining is needed due to photobleaching effect and spectral overlap limited by available colors. A current emerging technology known as Cytometry by time-of-flight (CyTOF) provides excellent cytoplasmic proteins tabulation in cell profiling as an alternative for this cell analysis purpose[86]. CyTOF method allows an extra stretch in a number of detection compared to fluorescence-based conventional flow cytometers; about 18 parameters of antigen. CyTOF uses transition elements isotopes as label surface markers with specific antibodies tag before introducing into the sample cells. Cells are further vaporized inside a coupled plasma (ICP) before the isotope-bound-cell entities are analyzed using time-of-flight mass spectroscopy. Even though this type of single cell analysis provides higher number of specific antibody detection, CyTOF method requires cells to be fixed before analysis, causing particular cells not available for continuous test acquisition[87].

Another technology that is directly targeted for NETs study is Reactive Oxygen Species (ROS) measurement that is generated by activated NADPH oxidase. Commonly used methods for this purpose are spectrophotometry and electrochemiluminescence[88]. However, their high activity, very short lifespan and extremely low concentration, makes ROS measurement a remaining challenge for researchers[89]. With this in mind, a localized surface plasmon resonance (LSPR) detection with

integrated PDMS micro through-hole layer as microwells has been assembled that enables time-lapse single cell-level measurement and has the capability for continuous monitoring.

Most conventional cell analyses methods involve bulk studies of cells that are considered having similar phenotypes. However, this type of study only provides the average values of the responses from highly heterogeneous populations of cells[62, 90, 91]. This approach can easily overlook unique cell responses which are important in leading to unique discoveries that could elucidate the cell behavior pathway[92]. Observation of any abnormal responses could provide new insights for early detection of infectious diseases, imbalanced protein secretion and for regular healthcare[93] as illustrated in Figure 3-3. Therefore, it is highly crucial for researchers to focus on single cell analyses for studying intrinsic cellular responses.

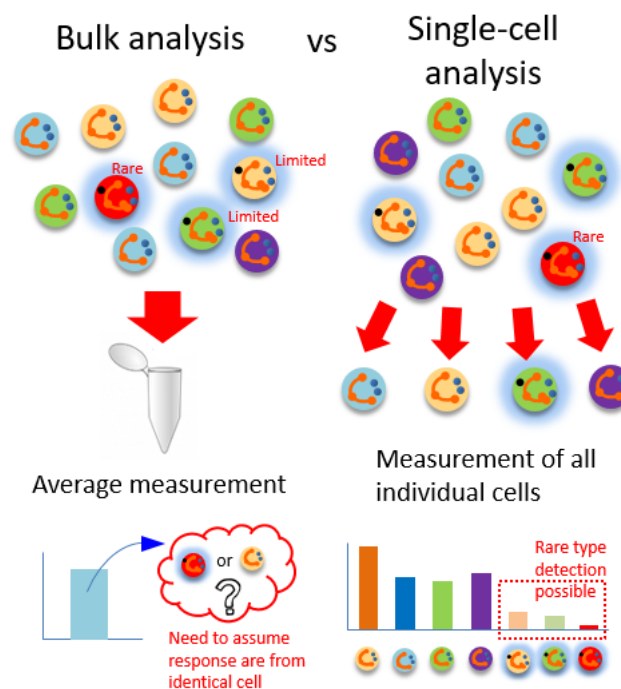


Figure 3-3 : Single cell analysis provide individual response.

LSPR-based biosensor has emerged as a promising technique for rapid detection of biomolecules, with great potential in diagnostic and point-of-care testing (POCT) applications[48-50, 52]. This is made possible due to the interactions of biomolecules and sensing surface during the progression of LSPR. LSPR occurs when the frequency of the incident electromagnetic radiation

matches the natural frequency of the electron cloud around the noble metal (e.g. gold, silver, copper) nanostructures, which leads to resonant oscillations of the electrons and sharp absorption of light at this frequency[51, 53]. Any variation in the refractive index (RI) near the nanoparticle surface due to biomolecules attachment, will lead to instantaneous changes in the LSPR-induced absorption peak wavelength. This could then provide high sensitive and real-time proteomic sensing capability[54, 55].

As LSPR-based techniques may not require any multiple fluorescence staining procedures or secondary antibodies, they are highly favorable for real-time cell monitoring applications. Real-time monitoring of cells enables spontaneous cytoplasmic protein detection and monitoring at any given spatiotemporal domain. In addition, several studies have an emphasis on LSPR-based techniques for biomolecule detection through antigen-antibody interactions and protein surface binding kinetics[56-59, 92]. More recently, LSPR-based observation of cellular activity aided by integration with microfluidics has also been reported which aid in doing high-throughput analyses[60, 94, 95].

In this work, fabricated chip is comprised of a perforated polydimethylsiloxane (PDMS) sheet that forms the MWA and a gold-capped nanopillar-structured cyclo-olefin polymer (COP) substrate that serves as the LSPR sensing platform. The MWA is prepared by thermal imprinting of an uncured PDMS between two silicon wafers with one surface having microposts pattern. This preparation method resulted in an easier fabrication process and a higher production repeatability compared to our previous study[96]. PDMS possesses a clear, non-toxic, and inert behavior on biological sample proving to be an excellent material to be used in various microfluidic applications. The use of the PDMS here allows forming inexpensive arrays of densely packed microwells to isolate individual cells into specific confinement.

The microwell structures allow one to study any secreted proteomes released within the space without interfering with and to other cells using an optical observation instrument such as a hyper-spectral imaging system. The addition of hyper-spectral imaging platform provides a rapid, high-throughput, and continuous observation of heterogeneous responses of each individual cell.

The LSPR substrate is also fabricated initially by thermal imprinting to produce the nanopillar structures on a COP film using a nanoporous anodic aluminum oxide (AAO) as mold. The substrate is then sputtered with gold (Au) to complete the LSPR substrate. The high-density arrays of nanoporous structure dimension can be formed by precisely controlling the anodizing parameters such as anodizing potential[96], substrate temperature, electrolyte solution[97] and pre-treatment of the alumina substrate. This has been used in LSPR-based sensing applications in our previous reports[96], including the multiplex screening of protein interactions using a hyperspectral imaging system[51]. Here, in order to assess the performance of the fabricated plasmon chips, their optical properties and the capacity to isolate single cells were investigated. Finally, the extent of fibril and NET release from neutrophils isolated on the chips were studied using the aforementioned hyperspectral imaging system.

In the current study, neutrophils obtained from whole-blood samples from healthy human donors were trapped, isolated, and stimulated on a novel microwell array (MWA) plasmon sensing chip without using pre immobilization of covalent interaction for NETs capturing purpose. Trapped single neutrophils cell inside MWA undergoes activation with phorbol 12-myristate 13-acetate (PMA)[32] which is a protein kinase C (PKC) agonist to activate NADPH-oxidase and reactive oxygen species (ROS) production[98]. Depending on the nature of the stimulus NADPH-oxidase can stimulate both apoptosis and suicidal NETosis [98]. However, how ROS contribute to NETosis remains uncertain. Upon activation, the neutrophils will flatten and attach to the contacting surface ground and will lose its lobular morphology. Neutrophil elastase (NE) translocates to the nucleus upon escaping from azurophilic granules. It partially degrades certain histones causing chromatin decondensation to occur. Though the role remains unclear, myeloperoxidase (MPO) also assist NE in driving chromatin decondensation. Finally, the cell membrane ruptures and expel its mass of chromatin forming the NETs into the surrounding. There are other NETosis pathways but this is the prevailing view[99]. Inspired by this mechanism, specific built-in plasmonic sensing structure within each microwell will be responsible for spectral shift due to change in RI value as release of NETs when observed in time lapsed

manner for 2 – 4 hours time. The LSPR shift are expected to be observed as a redshift signal the substrate surface is completely covered by the released material as shown in Figure 3-4.

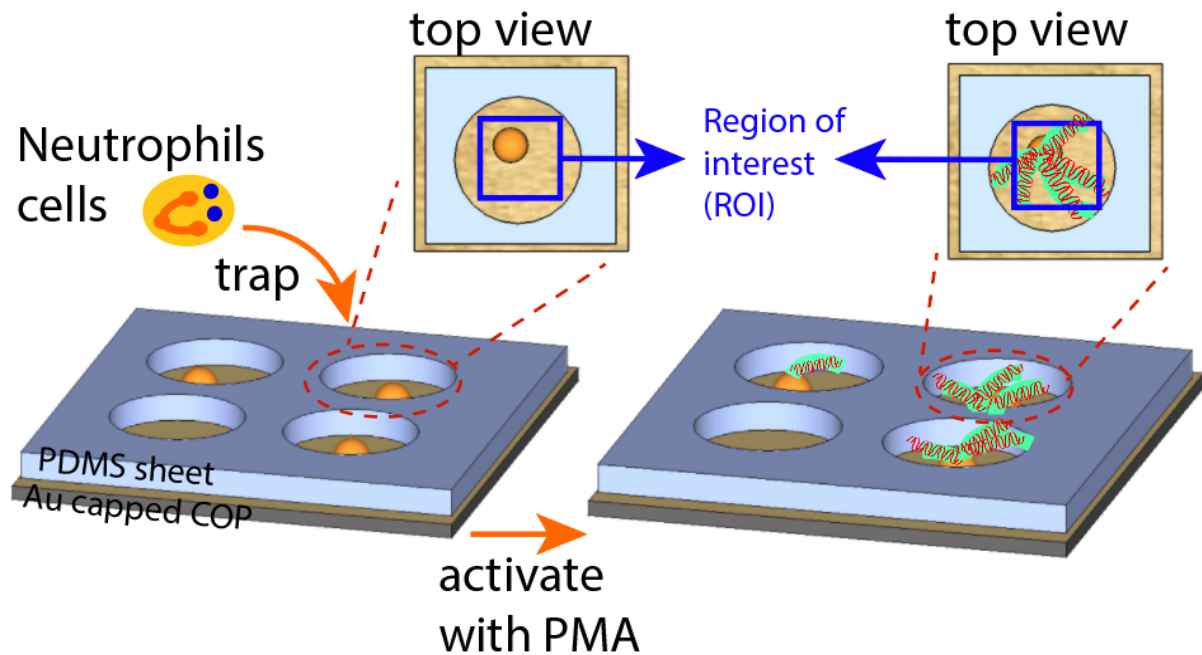


Figure 3-4 : Neutrophils cells are trapped into microwell array before stimulated with PMA solution. Released NETs are observed using LSPR sensing chip.

The focus of this study is the detection of the release of NETs from an observed isolated population but this platform is expected to be applicable to NET degradation monitoring as well. With this capability, an alternative method for NET related autoimmune disease testing platform has been realized. This report covers the assembly process of the chip and the initial results that indicate that our plasmon chips could provide in situ proteomic analysis and straightforward option for continuous high-throughput single-cell monitoring, not only limited to neutrophils but possibly for other types of cells as well.

## 3.2 Material and methods

### 3.2.1 Fabrication of the gold sputtered plasmonic substrate

Self-organized nanoporous AAO mould was prepared for nanopillar structure formation on COP substrate. In this study, the nanoporous AAO mould was fabricated using a two-step anodizing method[100], which has been detailed in our previous reports[51, 76, 77, 101, 102]. High purity

Aluminum substrate with 4 mm thickness was annealed, parallel grained, acetone sonicated and then strip etched using chromic acid (Wako, Japan) before used. The first anodizing step was performed in 0.3

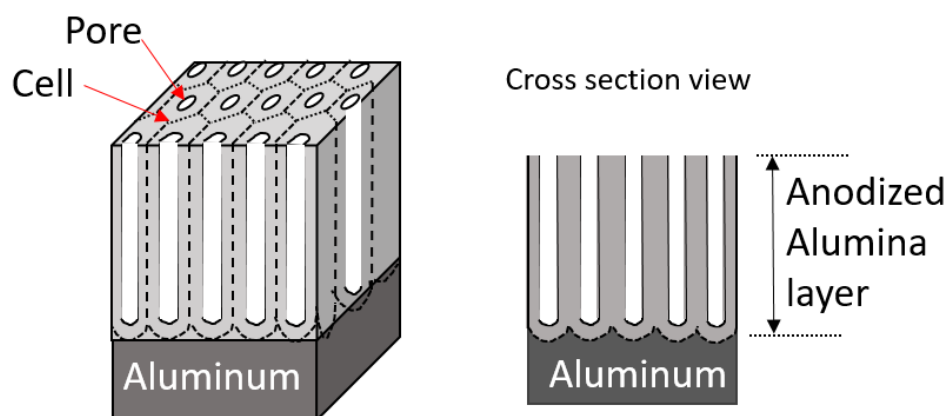


Figure 3-5 : Anodic porous alumina structure (AAO) mold.

M oxalic acid at 80 V and 0 °C for 1 hour, before etching in an aqueous solution containing phosphoric acid (1.16%, w/v) and chromic acid (5%, w/v) for 30 minutes at 70 °C. The second anodizing procedure was conducted at 60 V for 50 seconds and then exposed to a post-etch procedure in 0.23 M phosphoric acid for 12.5 minutes at 40 °C to widen the nanoporous structures. Porous structure of alumina on top of aluminium are illustrated in Figure 3-5.

Next, the nanoporous AAO mould was used to emboss its reverse pattern on a COP film (Zf-14, Zeon Corp., Japan) using thermal nanoimprinting (X-300H, SCIVAX Corp.). A fresh COP film (7.5 cm x 2.5 cm) was placed on top of the prepared aluminum oxide mold before being sandwiched between two identical 4" inch silicon wafers. This allows uniform pressure distribution on COP film during thermal imprint method. Later, a hydraulic pressure of 2 MPa was applied while the temperature was kept constant at 160 °C for 10 minutes under vacuum condition. The transformed pattern on the COP film surface was further deposited with a 68 nm layer of gold using a magnetron sputtering (ACS4000, ULVAC system) for faster and homogenous coating. The substrate was subsequently cut into smaller pieces (1 x 1 cm) and kept in a dry box until further use.

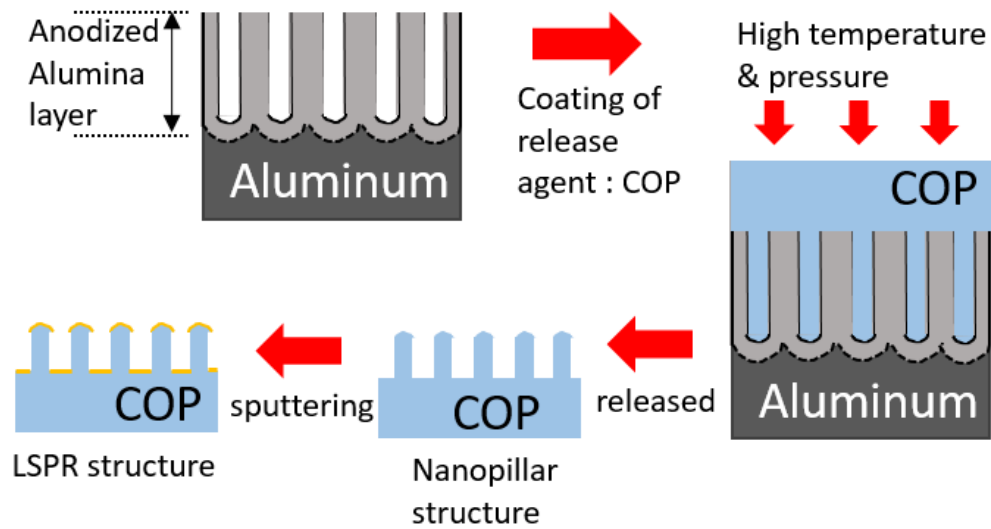


Figure 3-6 : Preparation of LSPR substrate using nanoimprint method.

### 3.2.2 Fabrication of PDMS microwell array (MWA) sheet

Here, PDMS sheets with a varied thickness range of 30  $\mu\text{m}$ , 60  $\mu\text{m}$ , and 90  $\mu\text{m}$  were prepared. Each sheet was designed to have perforated microwell array structures with diameter of 60  $\mu\text{m}$  and 100  $\mu\text{m}$  pitch as shown in Figure 3-7.

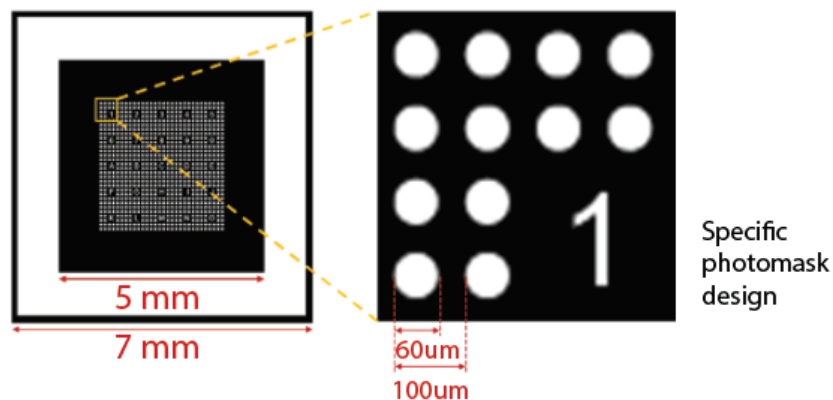


Figure 3-7 : Photomask design with microwell diameter 60 $\mu\text{m}$  and pitch 100 $\mu\text{m}$ .

MWA sheets were prepared using a thermal imprinting procedure that utilizes a fabricated SU-8-patterned-based mold. To produce the mold, a specific photomask design was photolithographically transferred on a 60  $\mu\text{m}$ -thick layer of SU-8 negative photoresist (SU-8 3050, MicroChem Corp., USA)



coated on a silicon wafer. The unexposed region was removed using SU-8 developer (MicroChem Corp., USA) resulting to the structure in Figure 3-8.

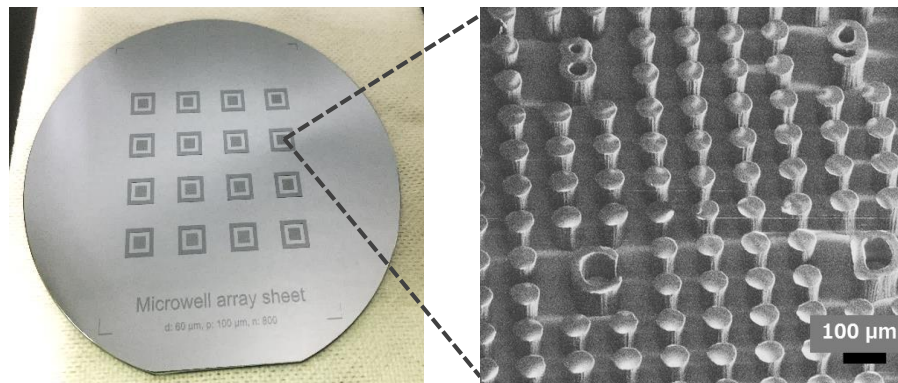


Figure 3-8 : SU8 mold coated on silicon wafer.

The PDMS base agent (Silpot 184, Dow Corning Toray, Japan) was mixed with a curing agent in a 10:1 ratio before being degassed under vacuum. Uncured PDMS was coated onto the SU-8 mold, and then covered with a Teflon sheet (As One, Japan) as shown in Figure 3-9. About 0.4 MPa of pressure was applied at 90 °C for 2 hours on this arrangement in thermal nanoimprinting (X-300H, SCIVAX Corp.).

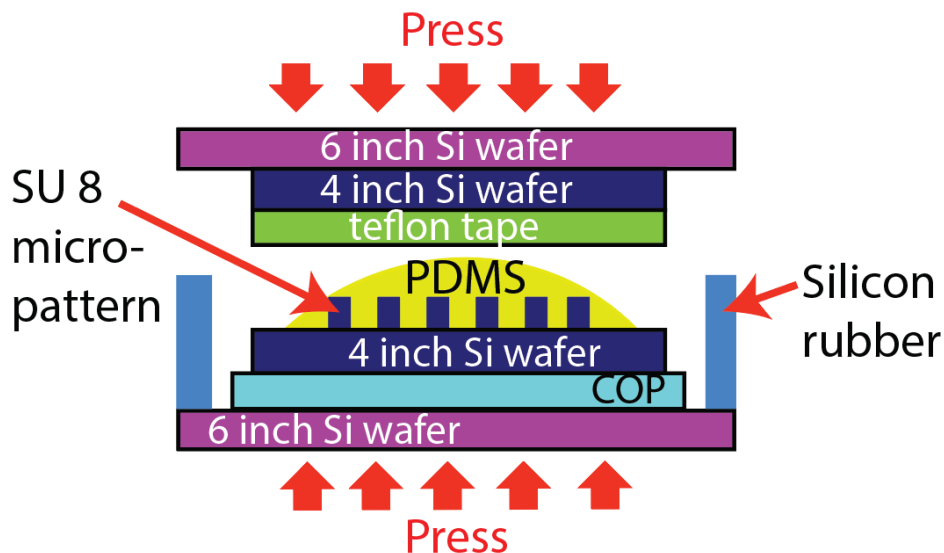


Figure 3-9 : PDMS material was injected into SU8 micro pattern before apply heat & pressure.

Then, the hardened and perforated PDMS sheet was carefully removed from the SU-8 mold as shown in Figure 3-10 and was temporarily placed on a cover glass (Matsunami Glass, Japan).

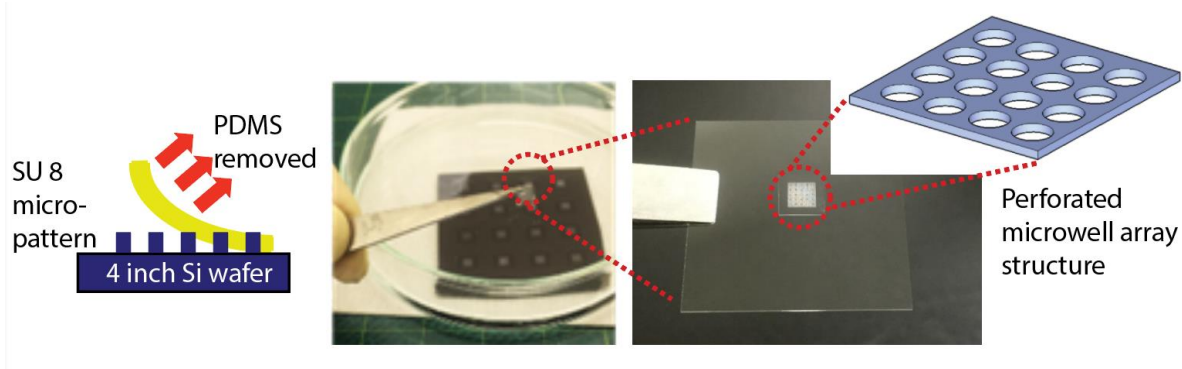


Figure 3-10 : Cured PDMS layer was carefully removed to form perforated microwell array.

### 3.2.3 Assembly of MWA plasmon chips

Gold-sputtered plasmonic substrates were combined with PDMS MWA sheets in this study for isolating single cell and observing their release of fibrils and NETs. MWA sheets, as prepared in the previous section, were trimmed into 7 x 7 mm size pieces and then placed on top of gold sputtered plasmonic substrates as shown in Figure 3-11. Silicone flow guards were placed around the assembled plasmonic chips to prevent any leakage of cell suspensions during observation.

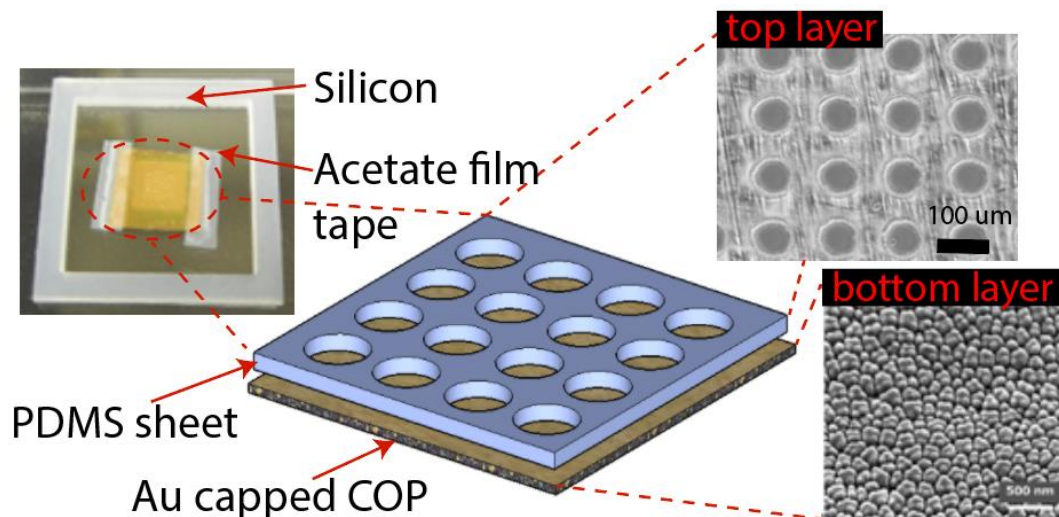


Figure 3-11 : The full assembly of plasmon chip with perforated layer on top and plasmonic substrate at the bottom.

### 3.2.4 Optimization of MWA sheet thickness

The as-prepared PDMS MWA sheets with thicknesses of 30 µm, 60 µm, and 90 µm were used to identify the optimum microwell height for single cell isolation by trapping fluorescent beads. About

150  $\mu\text{L}$  of a solution containing fluorescent beads ( $\phi = 15 \mu\text{m}$ , Thermo Fisher Scientific, USA) with excitation and emission wavelengths of 468 nm and 508 nm, respectively was dispersed in 0.1 % Tween 20 (Polyoxyethylene (20) Sorbitan Monolaurate, Wako, Japan) and was dropped on assembled MWA plasmon chips and allowed to sediment. After 30 minutes, excess beads were washed away and then the trapped beads were observed under a microscope to investigate the bead trapping capability and the presence of bubble formation with varying MWA sheet thickness.

### 3.2.5 Hyperspectral imaging system

The configuration and operation procedure of hyperspectral imaging observation system [51] are as shown below in Figure 3-12. The optical imaging system in this study consists of a tunable bandpass filter (TBPf system), halogen light source (MegaLight 100, Mitutoyo), air-cooled charged-coupled device (CCD) camera (BU-50LN, BITRAN Corp.) and an inverted microscope (IX 81, Olympus). Incident light from the source passes through the substrate and to a 10x magnification lens (NA: 0.4, Olympus). Incident

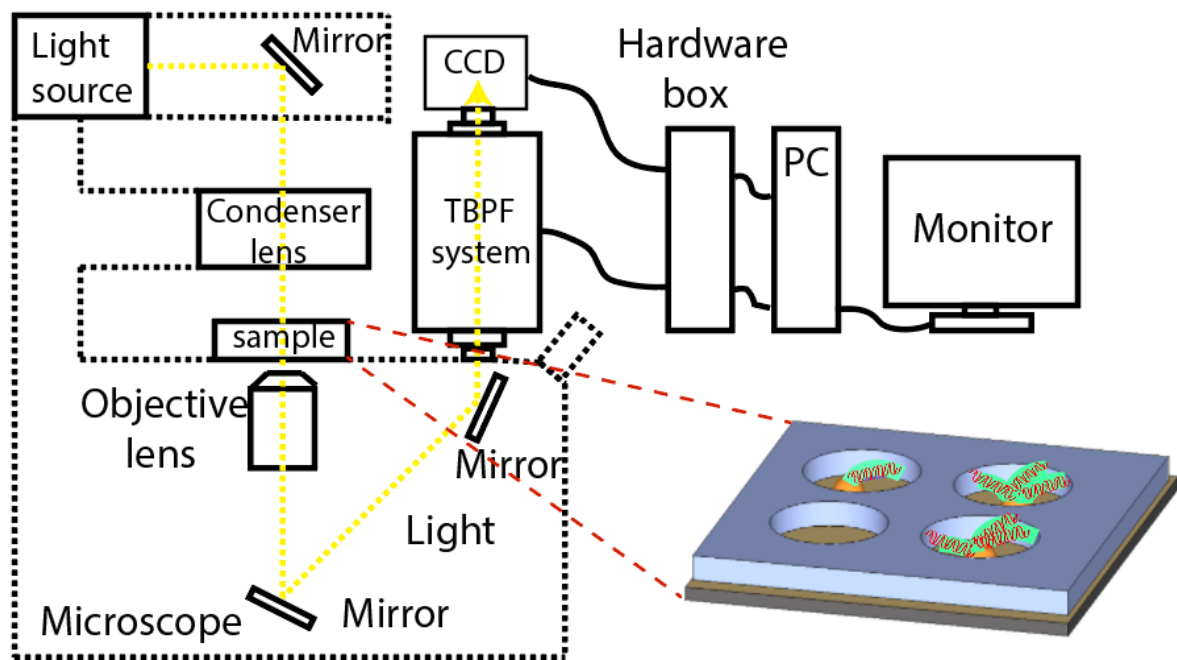


Figure 3-12 : Hyperspectral imaging system setup.

Later, images from the plasmon chip are acquired and recorded by conducting on-frame image acquisition for each 0.5 nm interval between wavelengths of 540 to 700 nm, semi-automatically as

shown in Figure 3-13. Although the maximum imaging size capability is about 580 x 772 pixels, the region of interest (ROI) was fixed at 30 x 30 pixels. All imaging responses were managed using a custom-made LabVIEW (National Instrument Corp.) program. The entire wavelength measurement takes less than one minute to complete.

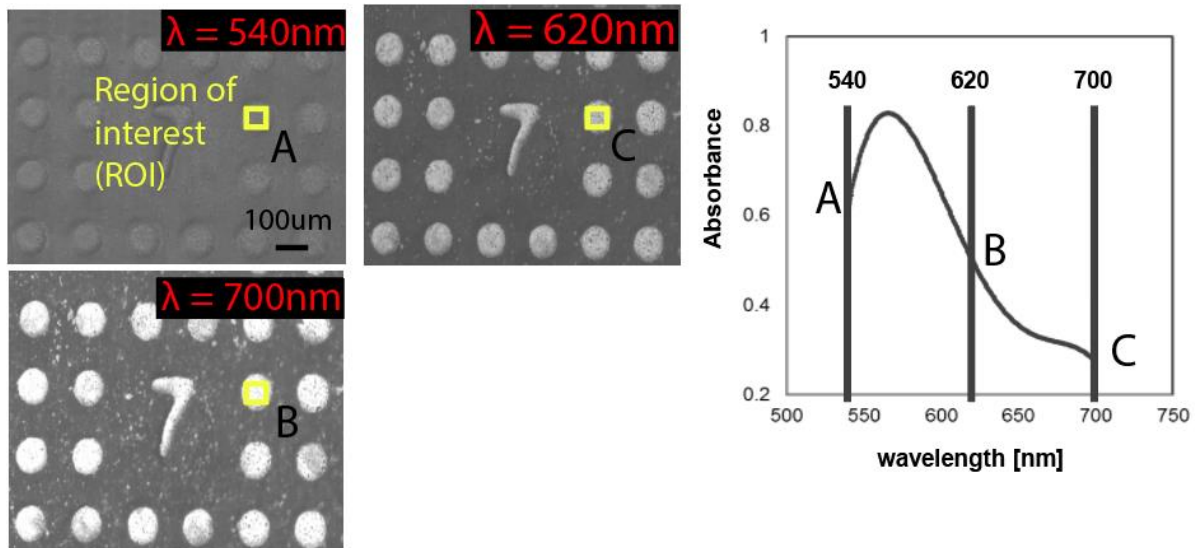


Figure 3-13 : Substrate image corresponding to TBP system in graph representative with wavelength 540nm to 700nm and interval 0.5nm.

### 3.2.6 Extraction of neutrophils from raw blood

About 5 mL of human blood was withdrawn from a healthy donor who gave his informed consent before the study was initiated. All procedures performed to harvest the cells are in compliance with the guidelines and regulations set by the Research Ethics Committee of Osaka University for the medical research targeting humans. Raw blood was collected in a sterilized vacutainer containing anti-coagulants and kept in an incubator for facility transfer purposes. Collected blood samples were processed within 15 minutes after collection. The total procedure has been illustrated in Figure 3-14.

Collected raw blood was transferred to a sterilized centrifuge tube before adding 5 mL of blood cell separation solution, Polymorphprep (Alere Technologies AS, Norway). This tube was subjected to density gradient centrifugation at 400 G and 18 °C for 35 minutes (no brake was applied at the end). Four noticeable layers were formed: plasma, mononuclear cells (MC), polymorphonuclear leukocytes

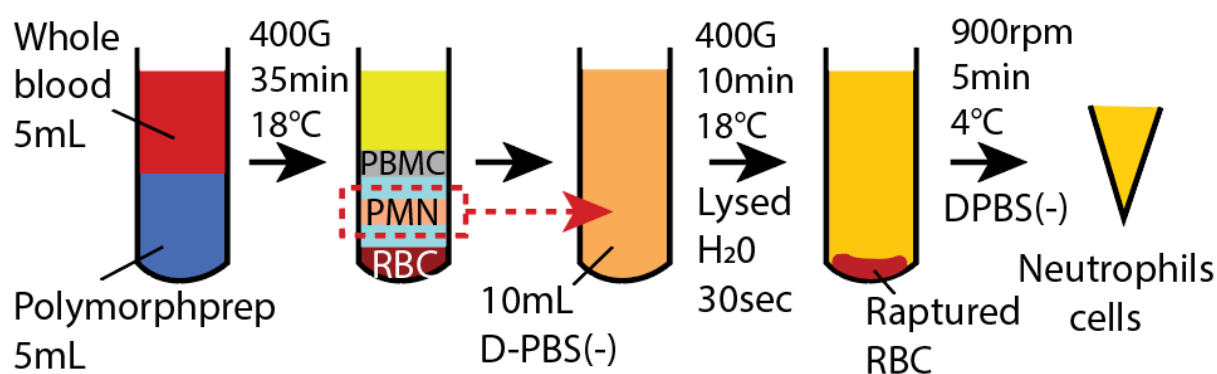


Figure 3-14 : Isolation procedure for neutrophil cells from raw blood.

(PMN) and erythrocytes (in descending order). The PMN layer was then extracted to a new sterilized centrifuge tube. D-PBS(-) was added to this tube until the final volume was 10 mL in total. A second centrifuge procedure was applied for 10 minutes for further PMN purification. The collected sediment pellet was then lysed using 1 mL distilled water by constant vortexing for exactly 30 seconds before diluting with D-PBS(-) to a total volume of 10 mL. This solution was then subjected to a third centrifugation and collection procedure. Finally, the cell suspension concentration was adjusted with D-PBS(-) prior to a full blood count procedure using a calibrated blood cell analyzer (XT-2000i, Sysmex, Japan). All usage of cell suspensions was restricted to within 6 hours of extraction for optimum observation results.

### 3.2.7 Neutrophils isolation using MWA plasmon chips

The neutrophil trapping and isolation capability of as-prepared MWA plasmon chips were evaluated by fluorescence imaging of cells trapped in the chips' microwells for various cell suspension concentrations. Prepared cell suspensions were adjusted to concentrations of 2.0, 4.0, 6.0 and  $8.0 \times 10^5$  cells/mL with D-PBS(-). Meanwhile, MWA plasmon chips were treated with oxygen plasma (PDC 21, Yamato Science, Japan) at 200 W for 10 seconds to induce hydrophilicity on the chip surface. About 150  $\mu$ L of each cell suspension was dispensed on a series of plasmon chips and incubated for 30 minutes as shown in Figure 3-15. Excess cells were washed with D-BPS(-) before introducing 4% paraformaldehyde (Wako, Tokyo, Japan) for 20 minutes to fix cells and disable any further release of biomolecules. About 5 $\mu$ M of fluorescence staining agent (SYTOX Green, Thermo Fisher Scientific, USA)



was introduced for 5 minutes before washing with D-PBS(-). The isolation of neutrophils was evaluated based on high contrast imaging from a confocal laser microscopy system (A1Rsi, Nikon, Japan) and Plan Apo 10x objective lens (NA: 0.45, Nikon, Japan) as shown in Figure 3-16.

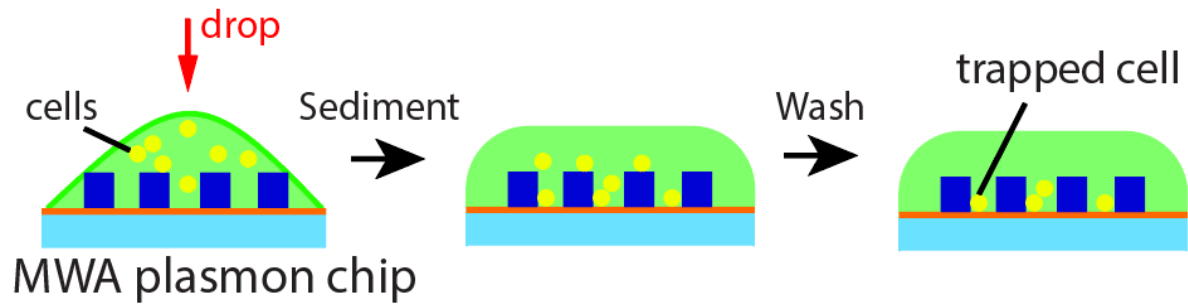


Figure 3-15 : Cell trapping observation.

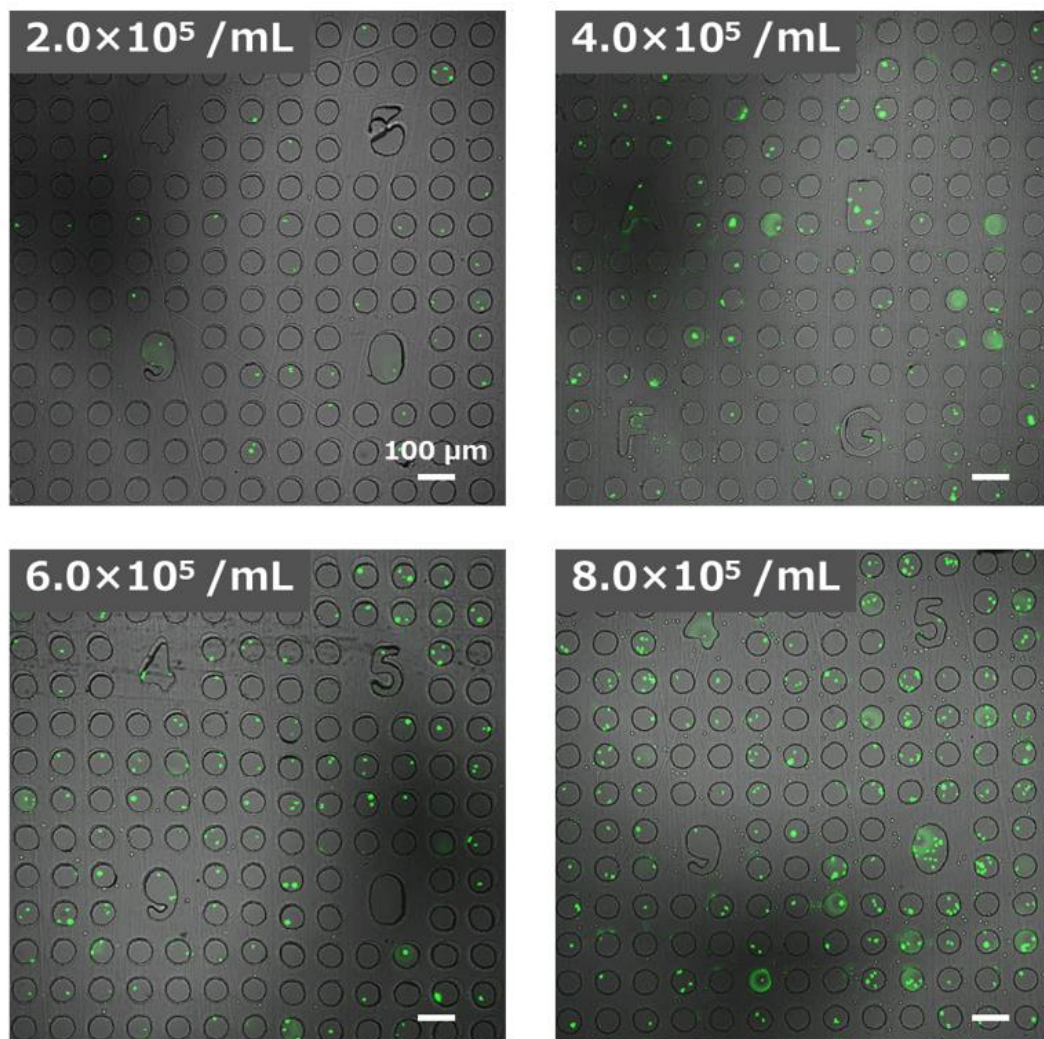


Figure 3-16 : MWA plasmon chips trapping capability.

### 3.2.8 Verification of PMA induced neutrophils of fibril release

The as-prepared neutrophil suspensions ( $1.5 \times 10^5$  cells/mL) were used to study their release of fibrils under the presence of 100 nM PMA (Sigma Aldrich, USA) for 2 hours and 4 hours. Extracellular structures were observed using fluorescence imaging at the end of each time period studied. Cells in D-PBS(-) with the same concentration served as the control. Each test suspension was dispensed separately at equal volume on a plane glass slide with surface treated with 0.001% poly-L-lysine (Wako, Japan). The surfaces were labelled as PMA(+)\_2h, PMA(+)\_4h, PMA(-)\_2h and PMA(-)\_4h.

At the end of each time period, cell suspensions on the glass slide were fixed using 4% paraformaldehyde (Wako, Japan) for 15 minutes. The solution was washed off before staining the fixed cells with SYTOX green for 5 minutes. The stained cells were observed using the same confocal laser microscope system (A1Rsi, Nikon) with different setting of Plan Apo 60x objective lens (NA: 1.4 with oil immersion, Nikon). Based on the obtained images from each time period, the fibril sizes were analyzed. Each preparation and observation procedure was conducted with minimal disturbance to the cell suspensions.

### 3.2.9 Real-time LSPR observation of neutrophil extracellular traps (NETs)

The as-prepared MWA plasmon chips were used to observe the real-time NET release of neutrophils using our hyperspectral imaging system. Suspensions (150  $\mu$ L) containing about  $6.0 \times 10^5$  cells/mL of neutrophils were dispensed on sterilized MWA plasmon chips. The LSPR responses from neutrophils in each chip were evaluated at 2 hours and 4 hours after exposing the cells to 100 nM PMA solution. Cells in DPBS(-) with the same concentration served as the control. The observed periods were labeled as PMA(+)\_2H, PMA(+)\_4H, PMA(-)\_2H and PMA(-)\_4H. The LSPR responses from each 30 individual neutrophils cells trapped in MWA plasmonic chip were recorded and analyzed. To confirm that the measured LSPR signal is indeed from the NETs released, the cells in the chips were fixed at the end of the measurement, stained with SYTOX green, and observed using the hyperspectral imaging system.

### 3.3 Results and discussion

#### 3.3.1 Optimization of MWA plasmon chips

The PDMS sheet with perforated microwell was successfully fabricated as shown in Figure 3-10 indicates that the setting used in the thermal imprinting procedures is at optimum. More importantly, the LSPR substrate with estimated width ranging between 140–150 nm and gap about 15 nm and having homogenous pillar dome shape Figure 3-11 retained its characteristic LSPR spectra even with the addition of the PDMS sheet. The observed absorption peak of the LSPR substrate is at  $\approx 560$  nm.

MWA sheets with several thicknesses (30, 60, 90  $\mu\text{m}$ ) were fabricated using the procedure described earlier. Figure 3-17 shows that the percentage of microwells containing zero beads decreases as the MWA sheet thickness increases (30  $\mu\text{m}$ : 52%, 60  $\mu\text{m}$ : 44%, 90  $\mu\text{m}$ : 23%). Prior to washing, it was observed that all microwells contain microbeads. This suggests that, as the MWA sheet thickness increases, it is less likely for the trapped microbeads to be washed away. The washing of the beads outside the microwells don't show dependence on the thickness of the MWA sheet. However, increasing the sheet thickness also led to an increase of bubble formation inside the microwells: 26% and 41% of microwells were found to contain bubbles for MWA sheets with thicknesses of 60  $\mu\text{m}$  and 90  $\mu\text{m}$ , respectively. On the other hand, the 30  $\mu\text{m}$  sheet was found to contain no bubbles. This indicates that with an increase of height-to-diameter ratio, the air bubbles are easier to be trapped. This bubble formation problem was not observed when D-PBS(-) was used. This is related to the innate characteristic of a surfactant-containing solution that forms a thin plug deposit in a microchannel as a trailing film under low pressure[103]. As for the percentage of microwells containing single trapped bead, a decreasing trend with increasing sheet thickness (30  $\mu\text{m}$ : 31%, 60  $\mu\text{m}$ : 29% and 90  $\mu\text{m}$ : 22%) was observed as shown in Figure 3-17. Since the 30  $\mu\text{m}$  sheet showed the highest percentage of wells containing zero trapped beads and the 90  $\mu\text{m}$  sheet showed the highest percentage of wells containing air bubbles, the 60  $\mu\text{m}$  MWA sheet was selected to be used in subsequent experiments. In addition, the percentage of microwells containing single trapped beads was almost the same for the 60  $\mu\text{m}$



sheet as it was for the 30  $\mu\text{m}$  sheet. Therefore, the optimized PDMS MWA thickness was determined to be at 60  $\mu\text{m}$ .

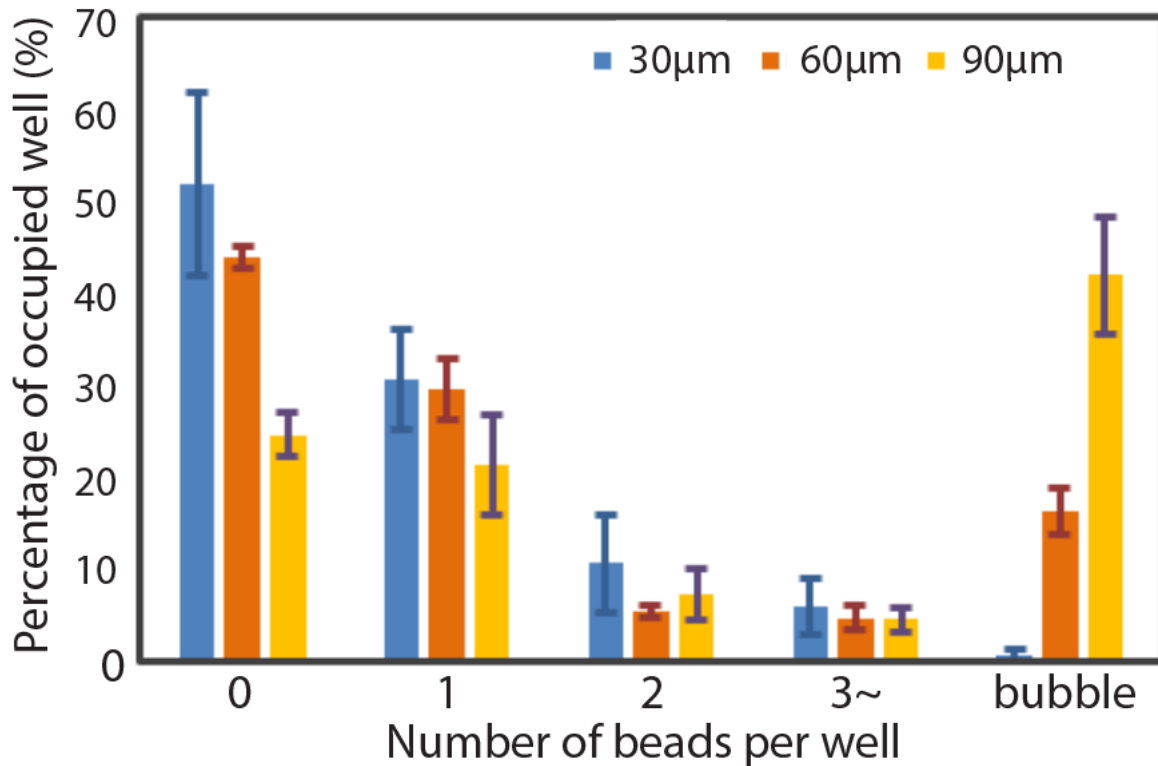


Figure 3-17 : Beads trapping capacity of varies thickness range of 30  $\mu\text{m}$ , 60  $\mu\text{m}$  and 90  $\mu\text{m}$ .

### 3.3.2 Neutrophil isolation capability

Suspensions of neutrophils at various concentration (2.0, 4.0, 6.0 and  $8.0 \times 10^5$  cells/mL) were used to determine the optimum cell concentration for isolation of single cells in the as-prepared MWA plasmon chips. Figure 3-18 illustrates the result of the tests. The percentage of the microwells that were able to trap cells increased from 25.7% to 82.4% as the neutrophil cell concentration was increased. The increase in the number of cells per milliliter provides a higher possibility for cells to be isolated within the chips' microwells. On the other hand, single cell isolation showed a gradual increase as the cell concentration increases before slightly dropping at the highest concentration of  $8.0 \times 10^5$  cells/mL. Figure 3-18 also illustrates the single cell isolation percentage of each tested concentration:  $2.0 \times 10^5$  cells/mL (16.6%),  $4.0 \times 10^5$  cells/mL (28.5%),  $6.0 \times 10^5$  cells/mL (36.3%) and  $8.0 \times 10^5$  cells/mL (34.5%). From this study, it was found that the MWA plasmon chip shows the highest

single cell isolation capability for the neutrophil suspension of  $6.0 \times 10^5$  cells/mL with an average of 36.3% of wells being able to trap single cells ( $\sigma = 2.72\%$ ,  $N=3$ ). Therefore, the neutrophil suspension was determined to be the optimum at this concentration for use in subsequent experiments.

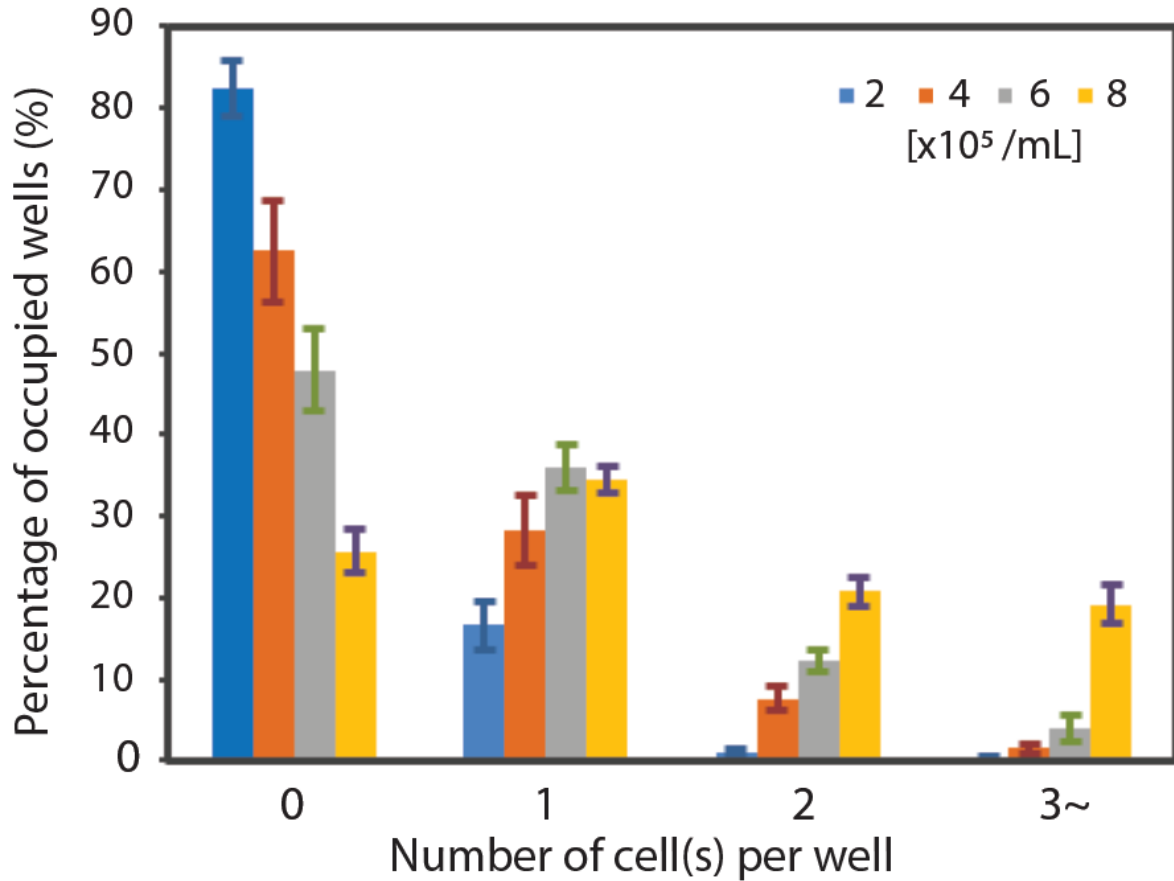


Figure 3-18 : Neutrophils trapping efficiency using 60  $\mu\text{m}$  thick MWA PDMS sheet.

### 3.3.3 PMA induced fibril release from neutrophils

Gold Neutrophils incubated with PMA solution undergo activation of nicotinamide adenine dinucleotide phosphate (NADPH) oxidase, an enzyme that produces reactive oxygen species (ROS), which in turn would result in activation of a protein – arginine deiminase 4 (PAD4)[98]. Activated PAD4 leads to chromatin decondensation with help from neutrophil elastase (NE) and myeloperoxidase (MPO) granules[99]. Chromatin is released into the cytosol and combines with cytosolic proteins. Within the first 4 hours of stimulation e.g. by PMA, it releases extracellular fibril or neutrophil extracellular traps (NETs), which can trap and disarm pathogens[33, 37, 99].

Full blood counts revealed that over 90% of neutrophils were successfully collected using the previously mentioned protocol Figure 3-14. The collected neutrophils were then incubated with PMA solution to observe fibril release using fluorescence staining. Figure 3-19 shows the fluorescence images of neutrophils at 2 hours and 4 hours after incubation in PMA and in D-PBS(-) solutions; denoted as PMA(+) and PMA(-), respectively. The initial fluorescence image shows that on average, cells have areas no bigger than  $101 \mu\text{m}^2$  ( $\sigma = 27.3 \mu\text{m}^2$ ,  $N = 30$ ). The sizes remain almost the same for PMA(+)\_2h, with a mean observed area of  $113 \mu\text{m}^2$  ( $\sigma = 20.4 \mu\text{m}^2$ ,  $N = 30$ ). However, neutrophils shows fibril formation after 4 hours of incubation, with cells in PMA(+)\_4h showing size between  $314 - 758 \mu\text{m}^2$  (mean =  $376 \mu\text{m}^2$ ,  $\sigma = 157 \mu\text{m}^2$ ,  $N = 30$ ). On the other hand, the neutrophils' sizes in PMA(-)\_2h and PMA(-)\_4h remain unchanged from their initial values. The results for PMA(+)\_4h, as seen in Figure 3-19, show similar structures and time-dependent characteristics that match with the above description.

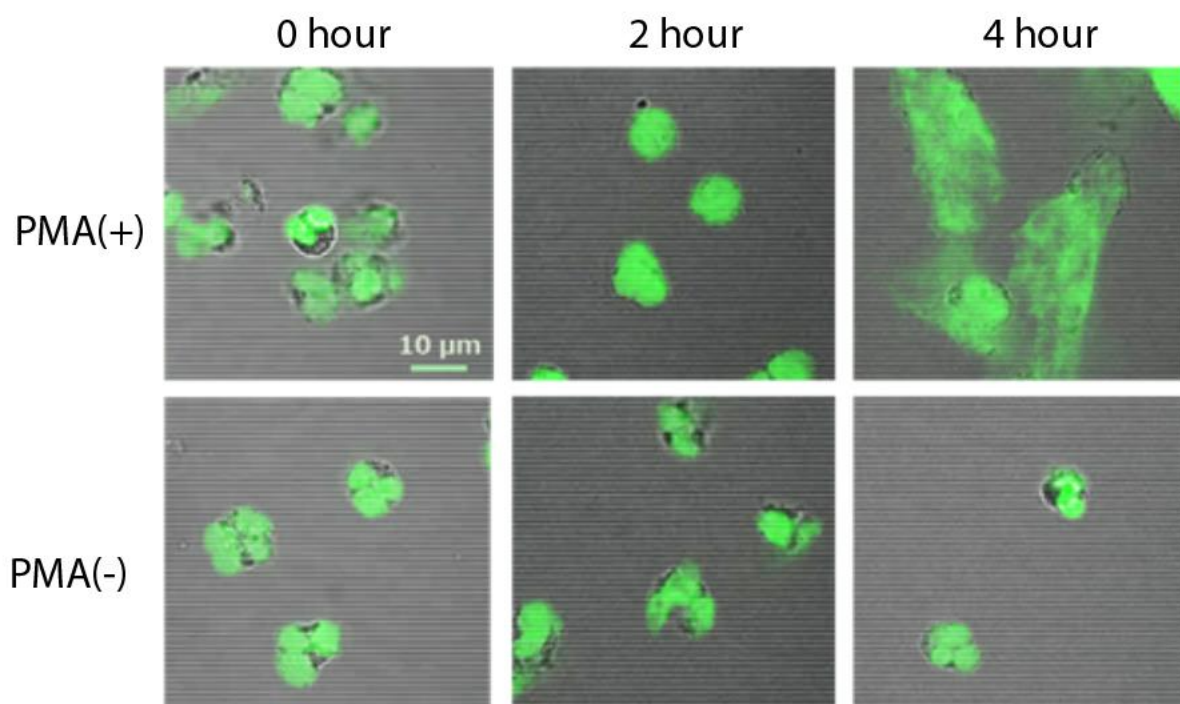


Figure 3-19 : The fibril releases from neutrophils cells under stimulation of PMA and D-PBS(-) solutions.

### 3.3.4 Real-time LSPR imaging observation of neutrophils

Suspensions containing neutrophils were introduced to MWA plasmon chips and stimulated by PMA solutions before observation under our hyperspectral imaging system. Neutrophils incubated in D-PBS(-) was used as the control in this study. A chronological observation was performed at 2 hours and 4 hours after incubation with PMA and D-PBS(-); denoted as PMA(+) and PMA(-), respectively. Figure 3-20 shows the acquired and processed spectroscopic images of the 30 x 30-pixel (22.5 x 22.5  $\mu\text{m}^2$ ) region of interest. The LSPR absorption peak shifts of 30 random cells were analyzed and also presented in Figure 3-20. The color intensity of the points in the graph indicates the number of overlapping points.

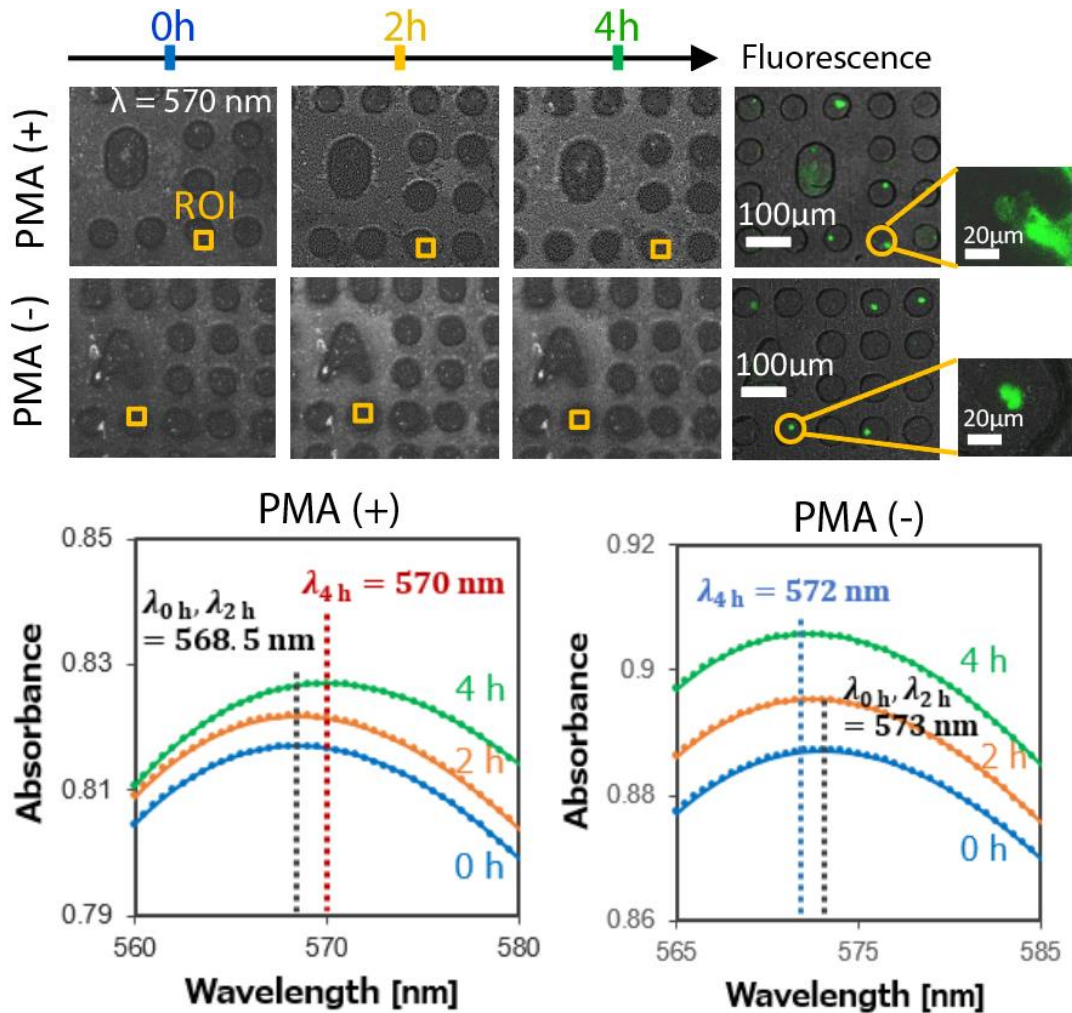


Figure 3-20 : Real time LSPR observation of single neutrophils cells with PMA (+) and PMA (-) at 570 nm wavelength from initial to 4 hours.

The average absorption peak wavelengths for PMA stimulated neutrophils at each measurement time are PMA(+)\_0h = 568.5 nm, PMA(+)\_2h = 568.5 nm and PMA(+)\_4h = 570.0 nm. A redshift of  $\Delta\lambda = 1.5\text{nm}$  was observed after 4 hours of incubating the neutrophils with PMA. This redshift was largely due to the increase in the neutrophils fibril release that cause changes in the refractive indices inside their respective microwells. As the fibrils cover the surface, an increase in refractive index is expected resulting to the observed redshift of absorption peak. For confirmation, the neutrophils stained by SYTOX green fluorescence image in PMA(+)\_4h shows an expanded released NET that is consistent with Figure 6b. On the other hand, neutrophils incubated with D-PBS(-) showed an average absorption peak wavelengths of 573 nm, 573 nm and 572 nm for PMA(-)\_0h, PMA(-)\_2h and PMA(-)\_4h, respectively. An average blue shift of  $\Delta\lambda = 1\text{nm}$  was also observed.

A blue shift is expected when there is a decrease in refractive index on the observed surface. This observed phenomenon is associated to the shrinking of the cells as they undergo cell death and possible detachment from the contact surface. In addition, though not explored in this study, the blue shift of the absorption spectra can be monitored to determine the degradation of the NETs with a different stimulus. This can be proven useful in future NETosis studies for the elucidation of activation and degradation pathways.

Further analyses of 30 cell samples show similar absorption peak shifts, as summarized in the scattergram in Figure 3-21. About 13.3% of neutrophils in PMA(+)\_2h show red shift in peak absorbance. This figure increases to 36.7% for neutrophils in PMA(+)\_4h. Meanwhile, the neutrophils in D-PBS(-) demonstrate no change after 2 hours in the observed average absorption peak wavelength. There was a slight increase of about 6.7% for neutrophils with redshifted absorption peak wavelength after 4 hours which indicates the release of NETs or the swelling of cells that increases the initially covered area. A different activation pathway of NETs must have been triggered which could be related to ROS production but this was not explored in the current study. More importantly, the majority of the cells in D-PBS(-) produced blue shifted absorption peaks which indicate that most cells didn't

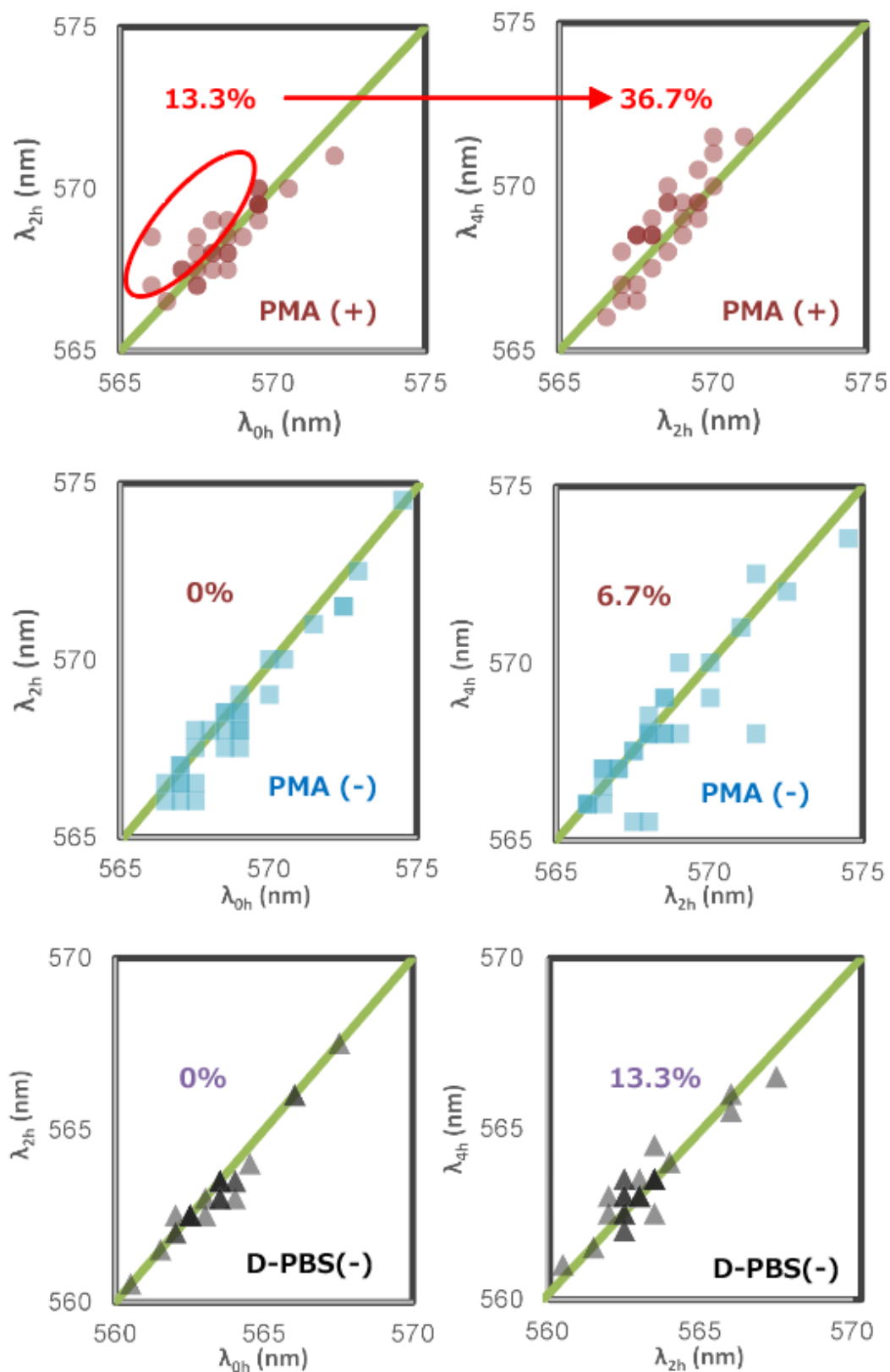


Figure 3-21 : Real time monitoring for 30 single cell neutrophils in PMA (+), PMA (-) and control D-PBS(-).

release NETs and that a decrease in cell size or detachment from the contact surface occurred. These result clearly indicate that the MWA plasmonic chips used in this study can be utilized for real-time and label- free analyses of fibril and NET release from neutrophils and can clearly demarcate them from inactive neutrophils.

To demonstrate that the observed absorption peak shift is specific to the NETs released, a MWA plasmon chip was tested with D-PBS(-) only. It can be observed in Figure 3-21 that no significant shift of absorption peak spectra was observed after 2 hours of exposure to D-PBS(-). However, redshifted absorption peaks were observed after 4 hours. This is associated with the uncured PDMS silicone oil from the MWA sheets that seep out as the time progresses. This problem has already been minimized based on the several washing attempt. It is important to note that the absorption peak observed and the corresponding shifted peak fall below 565 nm which is lower than the observed peaks from the case of neutrophils. This indicates that the effect of the peak shift caused by the oil can be considered insignificant and that the observed peak shifts from NETs are specific.

### 3.4 Conclusion

MWA sheets integrated with plasmonic sensing capability for studies of single neutrophils have been successfully investigated using our hyperspectral imaging system. The fabrication of the MWA layer using PDMS has allowed for trapping of single neutrophils before continuous analysis using LSPR. The thickness of the PDMS MWA sheet has been optimized with 60  $\mu\text{m}$  thickness for greatest single cell isolation with minimal trapped bubbles. The optical image of the MWA sheets showed the successful fabrication of smooth perforated sheets based on the optimized procedure. The best single neutrophil isolation using the as-prepared MWA plasmonic chips was achieved for a concentration of  $6.0 \times 10^5$  cells/mL, with 36.3% trapping capability of single cells; 105 microwells with single cell available for study. Investigations under a confocal microscope revealed that neutrophils stimulated by 100nM PMA solution show significant release of extracellular fibrils and NETs after 4 hours with maximum observed areas between 314 - 758  $\mu\text{m}^2$ . Average LSPR absorption peak wavelengths showed a red

shift of  $\Delta\lambda = 1.5\text{nm}$  as neutrophils released NETs. This redshift was observed from 36.7% of imaged cells after 4 hours of stimulation. In addition, the platform allows the identification of inactive neutrophils based on the blueshifted absorption peak. Also, the degradation of the NETs could be studied which could further expand the application of this detection platform. With these, a label-free plasmon chip for high-throughput single cell detection of released NETs has been realized that could aid in studying NETosis for autoimmune disease detection and pathogenesis elucidation. This platform can also be proven useful for other studies with cell behavioural traits that can affect the optical density of the surrounding environment like stem cell differentiation, tumor cell release progression, co-culture screening, cell growth and death monitoring, and many other more.



## 4 CHAPTER 4 : LUMINOL BASED ECL FOR ROS DETECTION FROM NEUTROPHILS CELLS.

### 4.1 Introduction

Neutrophils cells possess important task as first line of defence in immune system, protecting human from external intruder such as pathogens and other kind of toxics substance. Being most abundant cells among leukocyte cells (about 40% to 70%), it is obviously plays important role guarding through blood vessel seeking any trace of chemotaxis such as interleukin-8 (IL-8), C5a, fMLP, leukotriene B4 and others. Being in constant in mobile allows neutrophils cells moves and reach narrow site of imflammation where other cells not able to penetrate. Regular neutrophil cells contains nucleus that divided into 2 – 5 loops where it is interconnected through chromatin. Young neutrophil contains primary azurophilic granules that provide capability to generate myeloperoxidase that been used to kill pathogens by possessing the ability to break down pathogens protein and cell wall. The secondary granule in present as the cell getting matured over time.

The neutrophils cells able to migrate to the side of inflammation for pathogens elimination or cytokine production[29]. There are several differentiation mechanisms that been reported on neutrophils including phagocytosis, degranulation, cytokine production and neutrophil extracellular traps (NETs) formation [30] as shown in Figure 4-1. The function reaction of neutrophils that travel

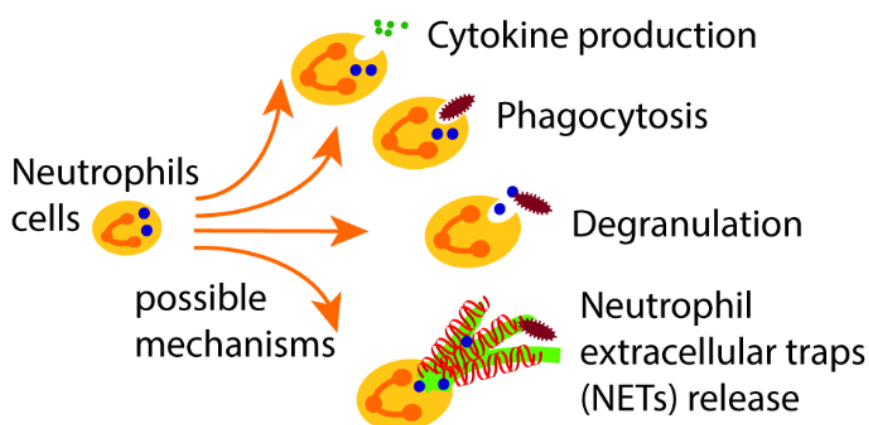


Figure 4-1 : Mechanism pathway of neutrophils differentiation.

inside blood vessel following chemotaxis substance perform adhesion (activated), then migration (diapedesis) into tissues reaching the site of inflammation[31]. In the mechanism of phagocytosis, microbes are engulfed inside neutrophils cell before azurophilic granules perform breaking down processes before undergoes apoptosis. As host cell, neutrophil also able to undergoes other possible differentiation mechanisms by releasing its granules targeting pathogens which is known as degranulation.

Another interesting pathway mechanism including release of NETs fibril into surrounding to eliminate pathogens more effectively. As discovery of Takei et al. [32] in 1996, it was reported that with activation of PMA solution, new possible pathway of chromatin reduction differentiation was observed. This report was further supported by Brinkmann et al. [33] and named it as NETosis. There are 3 suggested model of NETosis as reported, the suicidal NETosis is the most domain, even though their molecular reaction is still in enquiry.

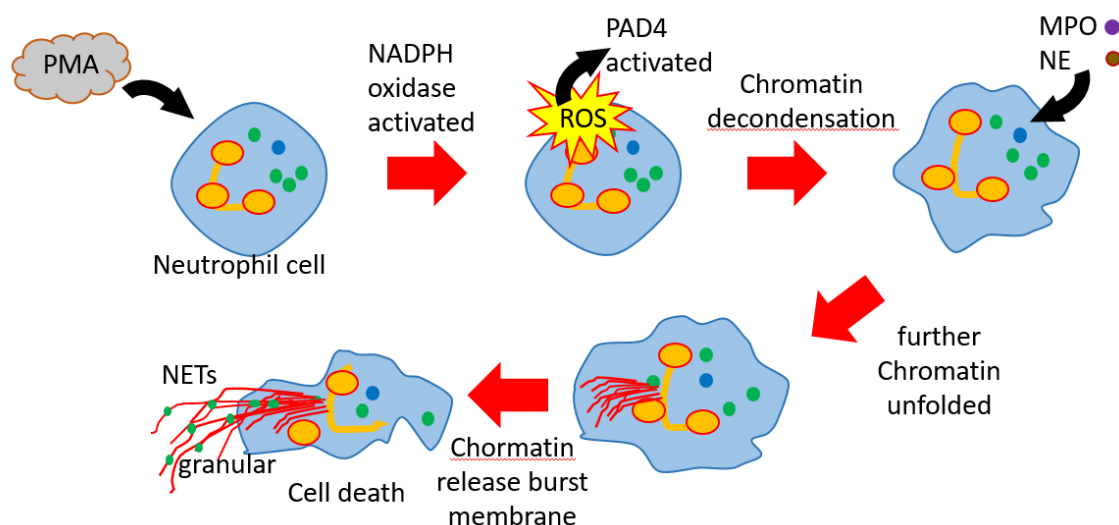


Figure 4-2 : Suicidal NETosis mechanism by neutrophil cell.

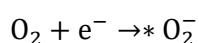
For suicidal NETosis to formed, the nicotinamide adenine dinucleotide phosphate (NADPH) oxidase inside neutrophils cell was activated within hours of introduction of PMA stimulant as shown in Figure 4-2. This allows for production of reactive oxygen species (ROS) causing activation of protein arginine deiminases (PAD4) resulting chromatin decondensation to occur[37]. The formation of ROS

is highly dependable here for chromatin decondensation [38-40] and also behave as second messenger by promoting the gradual separation and loss of nuclear membrane [30]. At this moment, the neutrophils elastase (NE) and myeloperoxidase (MPO) are migrated to help further boost the unfolding of chromatin decondensation. Chromatin starts to agglomerate into cytosol and become decorated with granule toxins and cytoplasmic proteins. Finally, NETs are released through cell membrane pores and cell begin to lysis or apoptosis. As mention earlier, formed NETs has antimicrobial characteristic where pathogen will be eliminated.

Another important neutrophil cell depended substance is ROS formation during activation mechanisms for microbes elimination through suicidal NETosis formation. Recent study shows ROS plays important role as both intra and intercellular messenger during chromatin decondensation [38-40] and also as cell signalling. Most of the ROS are generated due to electron transport in atomic oxygen with two unpaired electrons in valence band. The sequent reduction of oxygen with addition of free electrons into valence leads for formation of ROS in form of mainly superoxide which acts as precursor for hydrogen peroxide, hydroxyl radical, hydroxyl ion and nitric oxide.

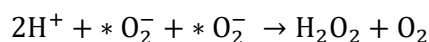
Studying the ROS production in form of superoxide and other species is crucial since it play important role during NETosis production and as cell signalling. However, excess/incompetent amount of ROS secretion has reported causing emerging of autoimmune disease such as systemic lupus erythematosus (SLE), diabetic or vasculitis inflammation disease. Therefore, it is essential to monitor the amount of ROS in their biological cell setting for improvement in prolonging patient's healthcare.

The formation of molecular oxygen ( $O_2$ ) produce superoxide ( $*O_2^-$ ) and becoming precursor for most of the other type of ROS[41]. The reduction equation are as follows;

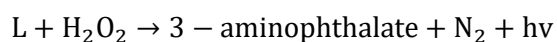
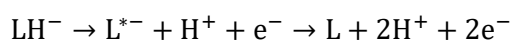


Due to the stability level of  $*O_2^-$  are estimated very low (half-life about 1 - 4 $\mu$ s)[42], this radical needs to dismutase into more stable species. Dismutation of superoxide produces hydrogen peroxide

(H<sub>2</sub>O<sub>2</sub>) which have half-life of > 1ms. The equations involve are as follows. Since the hydrogen peroxide radical is stable, it is possible to be used as key for quantification of ROS.



Electrochemiluminescence (ECL) showing promising analytical tool in various field. It is related to the light where excited luminophere is detected when successful reaction happen with the help low electric potential (voltage). In general, luminol based ECL can become successful candidate to measure present of ROS with the very high sensitivity range. The potential scheme of reaction for detection are as follows;



In this study, a simple Luminol based ECL chip was fabricated with microwell array to quantify the amount of ROS (the H<sub>2</sub>O<sub>2</sub>) amount released by neutrophil cell. The obtain result represent, ROS can be measured using luminol based ECL method.

## 4.2 Fabrication of Luminol based ECL biosensor

The fabricated luminol based ECL biosensor was prepared with 4 dedicated layers. The main, bottom layer works as working electrode while top layer of ITO glass will act as counter electrode. The illustration of full assemble electrode are shown in Figure 4-3.

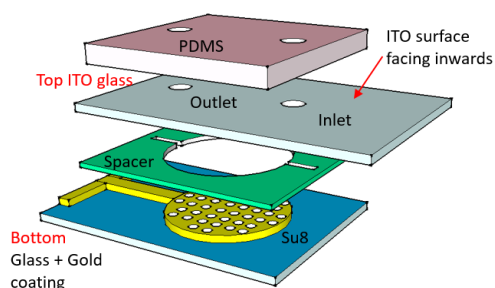


Figure 4-3 : The full assemble of microwell enhance luminol based ECL setup.

For bottom layer, it starts with microscopy glass. To make desire electrode contact on the glass, it need to be sputtered with 10nm of Titanium and 90nm of gold. However, before going any further, the glass needs to be pre cleaned using ultrasonic bath in acetone for 10 minutes. This allows to remove unwanted impurities on the glass. On the same time, specific design of acrylic sheet was cut using laser cutter as shown in Figure 4-4. The sheet was then placed on the cleaned glass before sputtering procedure of titanium for 10 nm and gold for 90nm height. Titanium was used to enhance the sticking possibility of the gold particles on the surface of glass. Otherwise, gold tend to easily

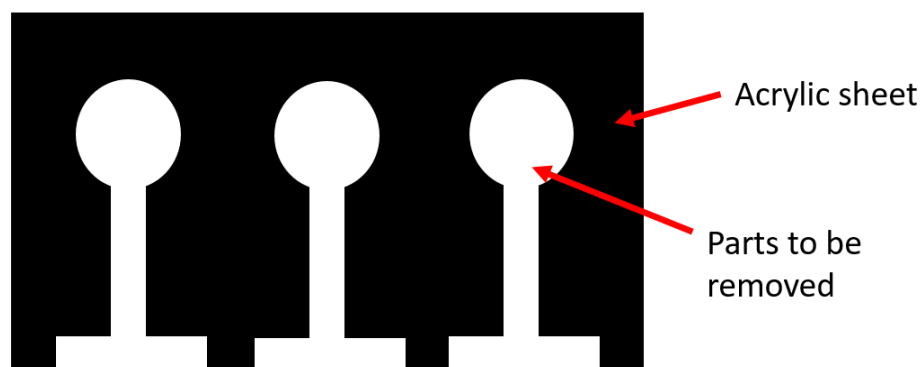


Figure 4-4 : The specific design using acrylic sheet.

removed by nail scratching. Then, the acrylic sheet was removed after coating exposed the needed electrode design. Exposed glass area will be coated with desired coating while the unexposed area will be null. Later, for microwell array enhancement, SU8 3010 photoresist was spin coated on the prepared electrode glass at speed 2000 rpm forming about 30  $\mu\text{m}$  even thickness. The SU8 coated glass was pre bake at 95  $^{\circ}\text{C}$  for almost 5 minutes. This will allow the photoresist to curd. Then, specific design of photomask was placed on the top of the glass and allow to be exposed at for 4 seconds.

After expose, the glass substrate was then post bake at 65  $^{\circ}\text{C}$  for 1 minutes and at 95  $^{\circ}\text{C}$  for 2 minutes. This double step heating allows to reduce any possible crack due to sudden temperature change. Then it was developed with SU8 developer for 35 second under constant irrigation. This provide microwell structure to emerge on the surface of the electrode as shown in Figure 4-3.

For the spacer, PET material with double side sticking ability was purchased. The height was fix at 50  $\mu\text{m}$  that will represent distance between top and bottom electrode. The PET material tape was further cut with specific design for allowing channel for solution flow. As the spacer been cut, it is essential to use adequate laser power fix at 40% capacity and speed at 16% for optimum cutting performance. Prepared spacer can further sandwich between working and counter electrode.

Next in line, inward facing ITO glass. There are two independent holes with diameter of 0.8 mm was milled using ultrasonic miller with space between two holes of 7.7 mm. This hole was made to allow solution flow onto both sandwiched electrodes, capsulated by sticking PET spacer. The hole was made carefully without crack or tilted holes.

To support inlet holder, PDMS material with thickness of 1.5 mm was premade with 10:1 ratio. After curd at 80  $^{\circ}\text{C}$  at 2hours, the PDMS sheet was cut into almost ITO glass size. Then, simple oxygen plasma cleaning was carried out to put it together PDMS sheet and non ITO side glass. All prepared material was assemble as shown in Figure 4-3.

#### 4.3 ECL imaging using microarray electrode

The prepared substrate was then used to optimize the suitable range of parameter to use in this study. The experimental setup of the luminol enhance ECL are as follows.

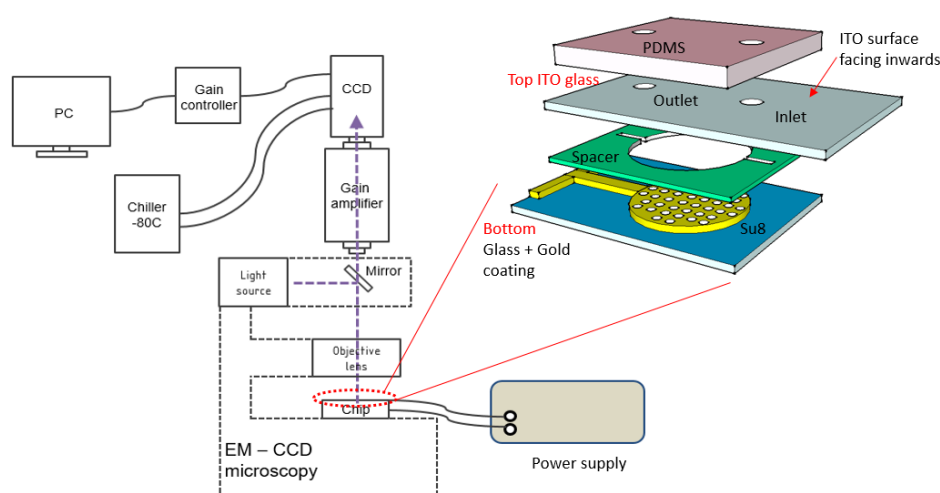


Figure 4-5 : The experimental setup of microwell enhanced luminol based ECL substrate.

In this study, the Electro multiplier – charge coupled device (EM-CCD) was setup. Chiller was set at -80 °C to counter heat produced inside the CCD equipment during photon detector. In this setup, gain controller was used to increase overall gain of photomultiplier tube. This allow for high sensitivity detection of photon produced due to the ECL reaction. Prepared substrate was placed on the substrate holder and solution was injected. The Luminol solution was fixed at 100  $\mu$ M, otherwise stated. Separate H<sub>2</sub>O<sub>2</sub> solution was diluted with 200 mM Borate – NaOH buffer solution with fixed pH value of 9, into suitable range from 1mM to 1pM range.

#### 4.3.1 Effect of Ph buffer

In order to understand the working environment of possible reaction, the Ph range of 200 mM Borate – NaOH buffer was tested. The pH value was set at 7.84, 8.0, 8.5 and 9.02. The solution used was fixed at 100mM Lumniol solution and 100  $\mu$ M H<sub>2</sub>O<sub>2</sub> solution. To test this situation, constant DC value of 1.7V was used. The reading obtain are shown in Figure 4-6. It is found that light base situation higher than pH 8.5 are preferred over near neutral based buffer. Therefore, Borate – NaOH buffer solution with pH value of 9 will be fixed for entire experiment in future.

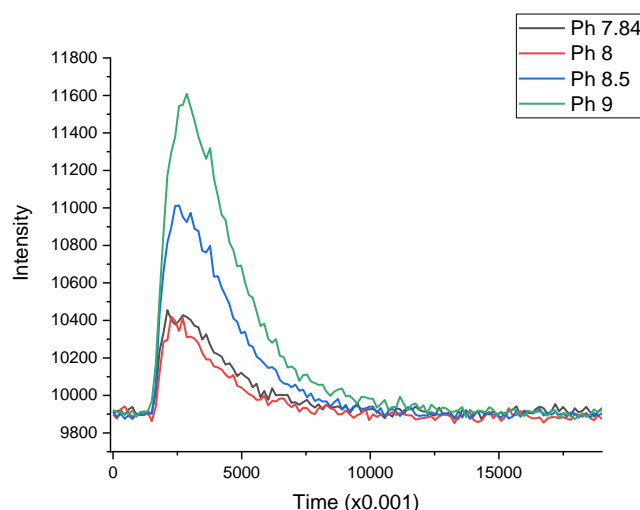


Figure 4-6 : pH response in range of 7.84, 8, 8.5 and 9.02.

#### 4.3.2 Peak versus area under the curve analysis for continuous testing

In order to determine where luminance response detected in form of intensity can be analysed on either peak value or area under the curve. This situation provide further understand and option selection in further analysis. The device was prepared and solution of 100mM of  $H_2O_2$  with 100mM of luminol was insert into the device. In this experiment, the voltage was set at low (1.1V DC) to avoid destructive situation on the surface of the working electrode. After each analysis, the surface was washed with 1mL buffer solution before insert luminol solution. The performance of the chip was observed as shown in Figure 4-7.

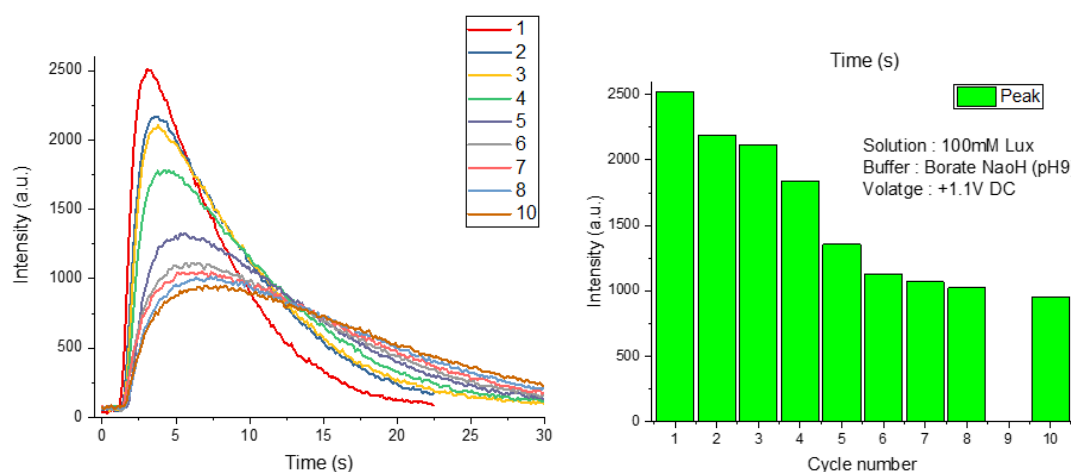


Figure 4-7 : Repetition performance at 10 cycle.

Table 6 : The peak analysis for 10 repeated cycle.

Cycle	Peak	Change
1	2524	0
2	2191	-3.33
3	2117	-0.74
4	1839	-2.78
5	1357	-4.82
6	1126	-2.31
7	1068	-0.58
8	1023	-0.45
10	952	-0.71

Graph shows that the quenching activity of luminance was observed for first 30 second. Most of the activity was perform between this range. The cycle repetition shows peak value drop steadily



between 1-4% for the first 6 cycles. The drop was become more less after the 7<sup>th</sup> cycle to 10<sup>th</sup> cycle where it maintains below than 0.7%. This has been shown in Table 6.

On the other hand, the area under the curve was observed for each cycle as shown in Figure 4-8.

The area was measured and represented with peak analysis as shown in Figure 4-9.

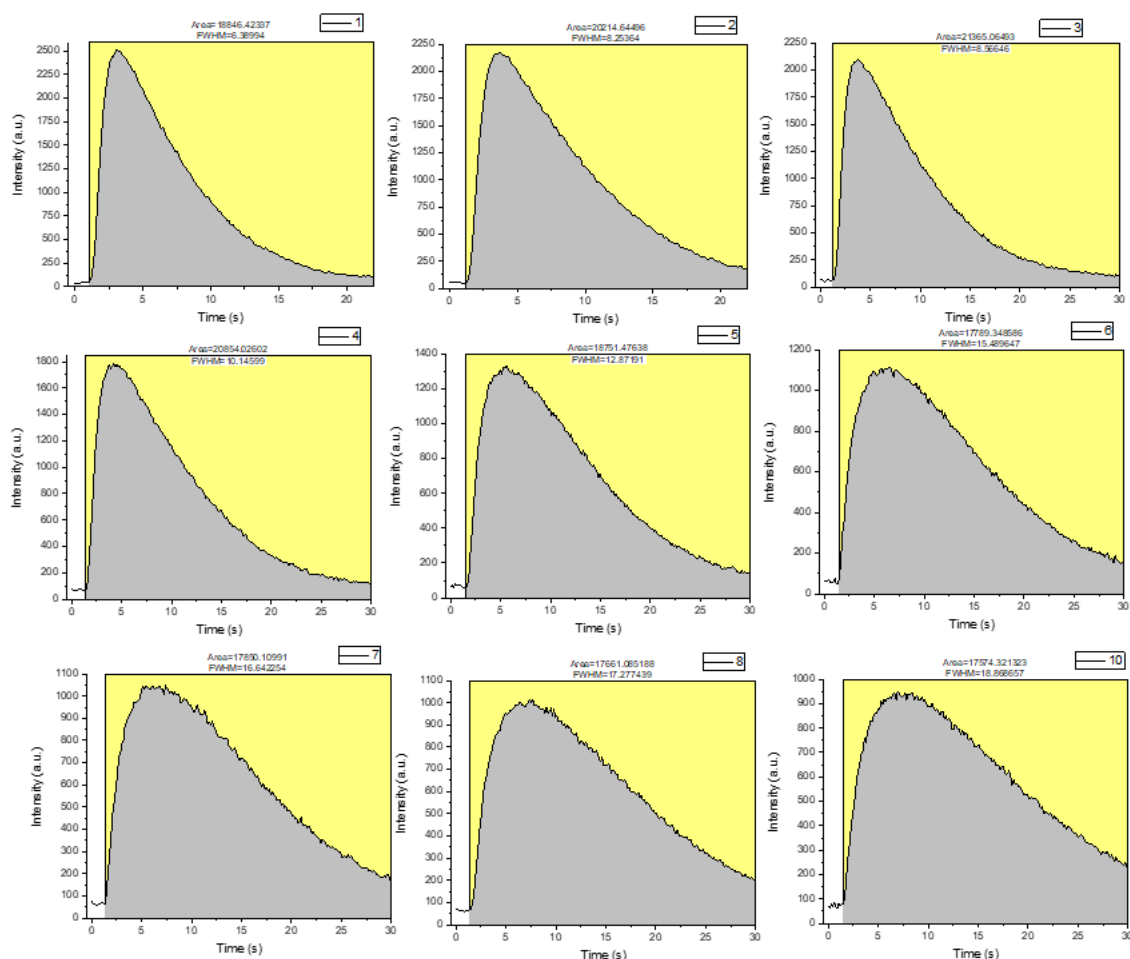


Figure 4-8 : The area under curve representation of 10<sup>th</sup> cycle.

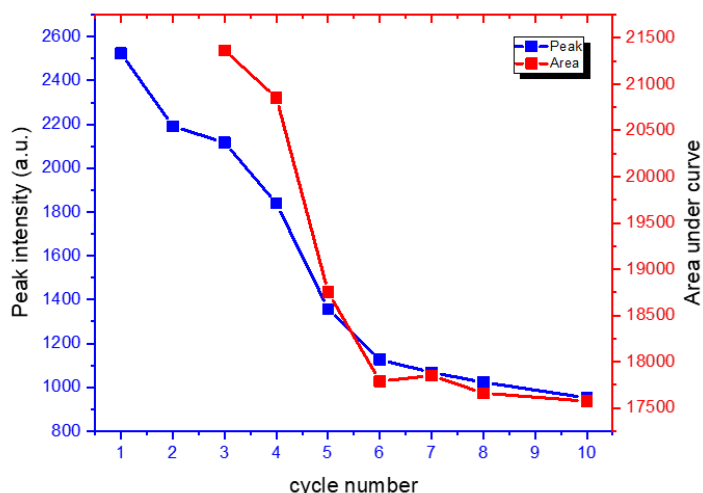


Figure 4-9 : The peak versus area under curve analysis.

The figure Figure 4-9 shows that area under curve was observed to drop significantly after 4<sup>th</sup> cycle with 21% of drop. Then on the 5<sup>th</sup> cycle, the almost 9% drop was found before stabilized after 6<sup>th</sup> cycle. Such situation provides huge fluctuation to the data analysis. Because of this situation, the peak analysis is much more preferable compare to the area under the curve analysis. From onwards, only peak value will be used in further analysis.

#### 4.3.3 Effect of potential voltage

In this study the effect of DC potential voltage over fixed amount of 100 mM luminol was tested to understand its reaction prepared solution was diluted with 200mM Borate NaOH buffer. Here, the response from 1.1 V to 1.7 V was recorded and represented in the graph as shown in the Figure 4-10. The response shows the peak value increases as the voltage increase. Even though at 1.7V DC, the highest peak was observed, the surface of electrode was found small air bubble was created due to electrolysis of water process. Therefore, to minimized the possibility of the bubble creation, middle voltage at 1.4V DC was used entire experiment.

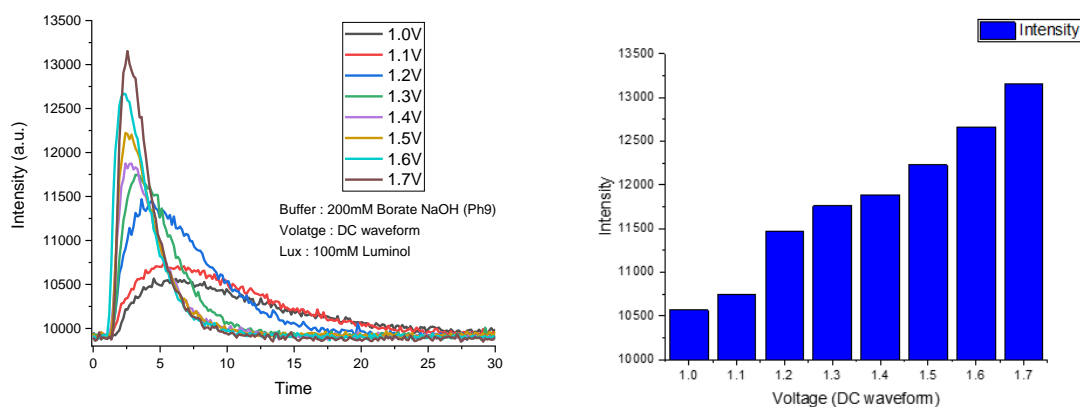


Figure 4-10 : The potential response of DC voltage from 1.0 V to 1.7V.

#### 4.3.4 Effect of alternative current (AC) by altering the frequency

In this study the effect of AC potential voltage over various frequency range. The buffer was fixed at 100 mM luminol was tested to understand its reaction. Here, the response from 1.7 V was recorded and represented in for of graph. It is found that the suitable frequency range is in between 0.3Hz to 1 Hz. The DC shows more constant response over AC value.

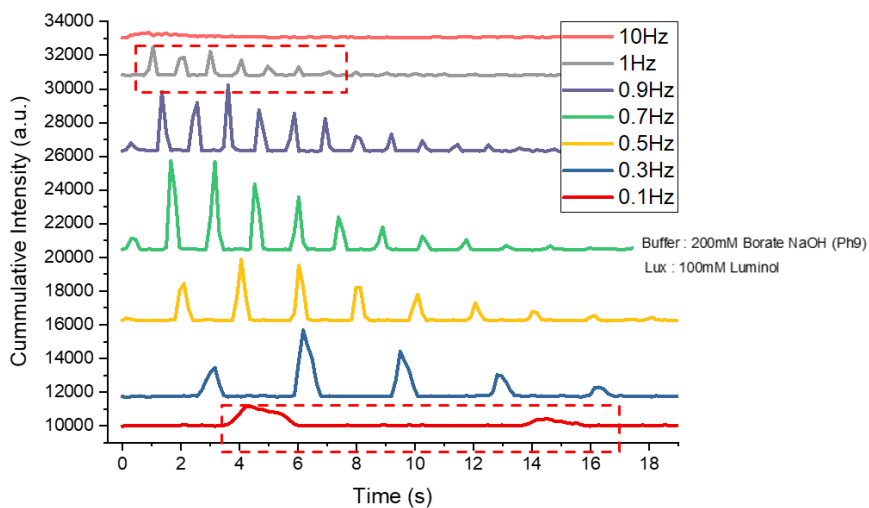


Figure 4-11 : The frequency based AC response.

#### 4.3.5 Effect of H<sub>2</sub>O<sub>2</sub> concentration

In this study the effect of H<sub>2</sub>O<sub>2</sub> solution over various frequency range. The buffer was fixed at 100 mM luminol was tested to understand its reaction. Here, the response from 1.4 V was recorded and

represented in for of graph. It is found that that 1.4V shows better low detection compared to other potential voltage. The limit of detection for this 10 nM.

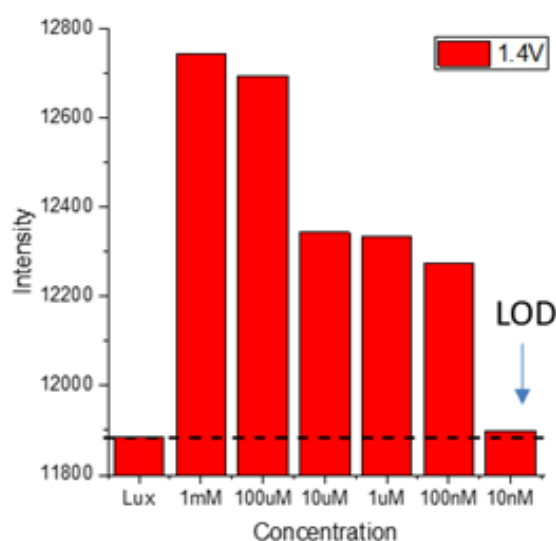


Figure 4-12 : The limit of detection of lumniol based ECL for 1.4V DC.

#### 4.4 Real time monitoring of neutrophils cells

##### 4.4.1 Neutrophil cell preparation

About 5 mL of human blood was withdrawn from a healthy donor who gave his informed consent before the study was initiated. All procedures performed to harvest the cells are in compliance with the guidelines and regulations set by the Research Ethics Committee of Osaka University for the medical research targeting humans. Raw blood was collected in a sterilized vacutainer containing anti-coagulants (hprene) and kept in an incubator for facility transfer purposes. Collected blood samples were processed within 15 minutes after collection. The total procedure has been illustrated in Figure 4-13. Collected raw blood was transferred to a sterilized centrifuge tube before adding 5 mL of blood cell separation solution, Polymorphprep (Alere Technologies AS, Norway). This tube was subjected to density gradient centrifugation at 400 G and 18 °C for 35 minutes (no brake was applied at the end). Four noticeable layers were formed: plasma, mononuclear cells (MC), polymorphonuclear leukocytes

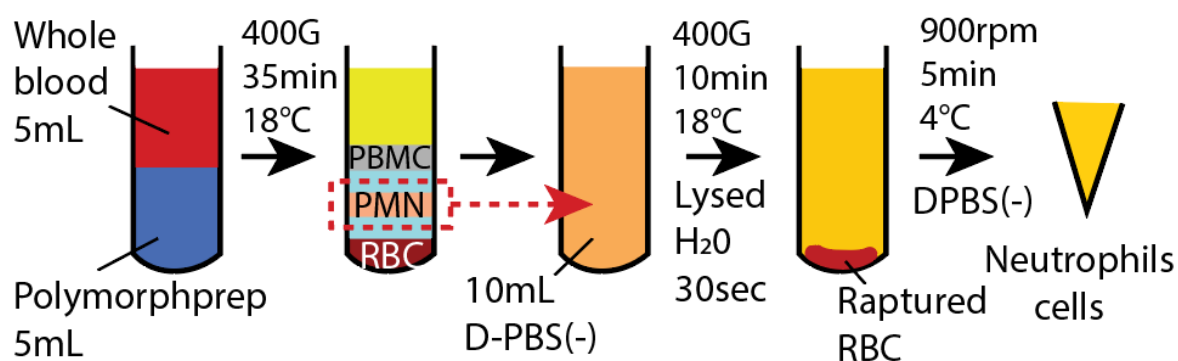


Figure 4-13 : Neutrophil cell isolation from raw blood.

(PMN) and erythrocytes (in descending order). The PMN layer was then extracted to a new sterilized centrifuge tube. Dulbecco's phosphate-buffered saline (D-PBS(-), Wako, Japan) was added to this tube until the final volume was 10 mL in total. A second centrifuge procedure was applied for 10 minutes for further PMN purification. The collected sediment pellet was then lysed using 1 mL distilled water by constant vortexing for exactly 30 seconds before diluting with D-PBS(-) to a total volume of 10 mL. This solution was then subjected to a third centrifugation and collection procedure. Finally, the cell suspension concentration was adjusted with D-PBS(-) prior to a full blood count procedure using a calibrated blood cell analyzer (XT-2000i, Sysmex, Japan). All usage of cell suspensions was restricted to within 6 hours of extraction for optimum observation results.

#### 4.4.2 Real time neutrophil observation

Prepared neutrophil cell (concentration  $2.0 \times 10^5$  cells/mL) was then injected into the prepared substrate. The potential was set at 1.4V DC. The solution was set with ratio 1:1. The response shows that at 10 minutes, there are slight increase about (4.45%) in intensity measurement, while at 30 minutes, the value dropped about 1.2% in term intensity. This drop of value may contributed decrease amount of luminol inside the substrate. Further investigation is needed to maintain similar luminol concentration inside chamber.

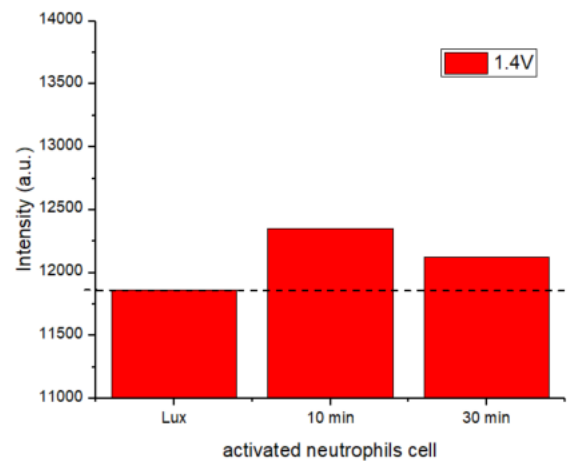


Figure 4-14 : The real time ROS ( $H_2O_2$ ) measurement from activated neutrophil cell.

## 5 CHAPTER 5 : CONCLUSION AND FUTURE WORK.

### 5.1 Conclusion

In this work, neutrophil cells were activated with PMA solution for NETs and ROS detection using microwell assist, LSPR observation and luminol based ECL quantification. The NETosis phenomena has cause change in physical appearance with the release of fibril type chomatin with granular histones into the surrounding for microbes elimination though phagocytosis. The protein releases into surrounding leads to refractive index around plasmonic substrate to change. This allows NETs quantification by observing the time based absorbance wavelength shift. On the other hand, the ROS release during NETosis has been quantified with present of co-reactance of oxide luminol pore with the help of small potential voltage. The excited radical managed to drop to ground state by releasing luminance which has been detected by photon detector. Details conclusion by chapter are as follows.

In the chapter 2, the hierarchical hybrid micro-nanostructures with plasmonic sensing capabilities have been successfully fabricated on a single-COP-film substrate via one-step NIL method. This was realized by combining a nanoporous alumina mold with an SU-8 spacer to form a hybrid mold for NIL. With this exquisite design, this substrate is capable of single cell isolation and LSPR detection. The diameter and height of the SU-8 spacer were optimized to obtain the best conditions for smooth de-embossing of the imprinted COP films. Morphological observation by SEM revealed the formation of microwells with a diameter of 70  $\mu\text{m}$  and a pitch of 500  $\mu\text{m}$  along with dome-shaped nanostructures of 190 nm diameter. The gold-sputtered COP film omit exhibits plasmonic properties, with the LSPR-induced absorption peak wavelength red shifting in response to an increases in the local refractive index. The bulk sensitivity of this substrate was found to be 274 nm/RIU. A limit of detection of 10 ng/ $\mu\text{L}$  for the anti-IgA antibody was established using the as-prepared plasmonic chip. Real-time observation of *P. pastoris* cells omit on this substrate showed a red shift of 6.9 nm in absorbance spectra over a 12-hour period.

For chapter 3, the MWA sheets integrated with plasmonic sensing capability for studies of single neutrophils have been successfully investigated using our hyperspectral imaging system. The fabrication of the MWA layer using PDMS has allowed for trapping of single neutrophils before continuous analysis using LSPR. The thickness of the PDMS MWA sheet has been optimized with 60  $\mu\text{m}$  thickness for greatest single cell isolation with minimal trapped bubbles. The optical image of the MWA sheets showed the successful fabrication of smooth perforated sheets based on the optimized procedure. The best single neutrophil isolation using the as-prepared MWA plasmonic chips was achieved for a concentration of  $6.0 \times 10^5$  cells/mL, with 36.3% trapping capability of single cells; 105 microwells with single cell available for study. Investigations under a confocal microscope revealed that neutrophils stimulated by 100nM PMA solution show significant release of extracellular fibrils and NETs after 4 hours with maximum observed areas between 314 - 758  $\mu\text{m}^2$ . Average LSPR absorption peak wavelengths showed a red shift of  $\Delta\lambda = 1.5\text{nm}$  as neutrophils released NETs. This redshift was observed from 36.7% of imaged cells after 4 hours of stimulation. In addition, the platform allows the identification of inactive neutrophils based on the blueshifted absorption peak. Also, the degradation of the NETs could be studied which could further expand the application of this detection platform. With these, a label-free plasmon chip for high-throughput single cell detection of released NETs has been realized that could aid in studying NETosis for autoimmune disease detection and pathogenesis elucidation. This platform can also be proven useful for other studies with cell behavioural traits that can affect the optical density of the surrounding environment like stem cell differentiation, tumor cell release progression, co-culture screening, cell growth and death monitoring, and many other more.

The chapter 4, provide the data analysis of luminol based ECL substrate with enhanced microwell trapping capability. With this method, cell can be trapped into confident area and then observed it ROS response over certain amount of time. This is useful for further study of ROS release from neutrophil cells. In this study, it found that the highest peak value obtain was using pH 9 buffer rather than other pH value. The suitable analysis method was fixed using peak analysis over area under curve



with 1.4V DC shows the most significant value. The observation of  $\text{H}_2\text{O}_2$  concentration, the LOD was found at 10nM concentration. For real time neutrophil monitoring, it was found that the response shows that at 10 minutes, there are slight increase about (4.45%) in intensity measurement, while at 30 minutes, the value dropped about 1.2% in term intensity. This drop of value may have contributed decrease amount of luminol inside the substrate.

## 5.2 Future remarks

In this work, the prepared LSPR substrate and luminol based ECL plays important role for label free quantification of activated neutrophil cells. The LSPR substrate able to quantify trapped cells with real time benefit up to 4 hours. However, the trapping efficiency was found about 36.3% which need to be improved better. It is suggested to be capsulated with microfluidic channel where cells are able to regulate its flow speed and channel height. This might allow lower rate of cell rebound (came out) from microwell during washing or loading procedure.

The quantification of ROS release from activated neutrophil cell using luminol based ECL was found sensitive and provide huge advantage that not able to be achieved though LSPR observation technique. This allows very low quantification of  $\text{H}_2\text{O}_2$  at 10nM at DC 1.4V to be achieved. However, the quantification value was found low. The sensitivity needs to be improve by introducing luminol integrated with nanoparticle for higher successful integration, causing higher sensitivity.

## 6 Reference

- [1] M. Cremer, *Ueber die Ursache der elektromotorischen Eigenschaften der Gewebe, zugleich ein Beitrag zur Lehre von den polyphasischen Elektrolytketten*. R. Oldenbourg, 1906.
- [2] W. R. Heineman and W. B. Jensen, "Leland C. Clark Jr. (1918–2005)," *Biosensors and Bioelectronics*, vol. 21, no. 8, pp. 1403-1404, 2006.
- [3] G. G. Guilbault and J. G. Montalvo, Jr., "A urea-specific enzyme electrode," *J Am Chem Soc*, vol. 91, no. 8, pp. 2164-5, 1969.
- [4] N. Bhalla, P. Jolly, N. Formisano, and P. Estrela, "Introduction to biosensors," *Essays Biochem*, vol. 60, no. 1, pp. 1-8, 2016.
- [5] C. S. Ezeonu, R. Tagbo, E. N. Anike, O. A. Oje, and I. N. Onwurah, "Biotechnological tools for environmental sustainability: prospects and challenges for environments in Nigeria-a standard review," *Biotechnol Res Int*, vol. 2012, p. 450802, 2012.
- [6] D. N. Stratis-Cullum, "Current Trends in Ubiquitous Biosensing," *Journal of Analytical & Bioanalytical Techniques*, vol. S7, no. 0, pp. -, 2013.
- [7] K. J. Odenthal and J. J. Gooding, "An introduction to electrochemical DNA biosensors," *Analyst*, 10.1039/B701816A vol. 132, no. 7, pp. 603-10, 2007.
- [8] P. Banerjee and A. K. Bhunia, "Mammalian cell-based biosensors for pathogens and toxins," *Trends Biotechnol*, vol. 27, no. 3, pp. 179-88, 2009.
- [9] Y. Fang, "Label-Free Biosensors for Cell Biology," *International Journal of Electrochemistry*, vol. 2011, pp. 1-16, 2011.
- [10] A. Diercks, H. Kostner, and A. Ozinsky, "Resolving cell population heterogeneity: real-time PCR for simultaneous multiplexed gene detection in multiple single-cell samples," *PloS one*, vol. 4, no. 7, pp. e6326-e6326, 2009.
- [11] J. S. Marcus, W. F. Anderson, and S. R. Quake, "Microfluidic Single-Cell mRNA Isolation and Analysis," *Analytical Chemistry*, vol. 78, no. 9, pp. 3084-3089, 2006.
- [12] W. J. Blake, M. Kærn, C. R. Cantor, and J. J. Collins, "Noise in eukaryotic gene expression," *Nature*, vol. 422, p. 633, 2003.
- [13] M. N. Teruel and T. Meyer, "Parallel Single-Cell Monitoring of Receptor-Triggered Membrane Translocation of a Calcium-Sensing Protein Module," *Science*, vol. 295, no. 5561, pp. 1910-1912, 2002.
- [14] M. B. Elowitz, A. J. Levine, E. D. Siggia, and P. S. Swain, "Stochastic Gene Expression in a Single Cell," *Science*, vol. 297, no. 5584, pp. 1183-1186, 2002.

- [15] J. E. Ferrell Jr, "The Biochemical Basis of an All-or-None Cell Fate Switch in *Xenopus* Oocytes," *Science*, vol. 280, no. 5365, pp. 895-898, 1998.
- [16] S. Lindström and H. Andersson-Svahn, "Miniaturization of biological assays — Overview on microwell devices for single-cell analyses," *Biochimica et Biophysica Acta (BBA) - General Subjects*, vol. 1810, no. 3, pp. 308-316, 2011.
- [17] K. M. McKinnon, "Flow Cytometry: An Overview," *Current Protocols in Immunology*, vol. 120, no. 1, pp. 5.1.1-5.1.11, 2018.
- [18] A. Gross, J. Schoendube, S. Zimmermann, M. Steeb, R. Zengerle, and P. Koltay, "Technologies for Single-Cell Isolation," *International Journal of Molecular Sciences*, vol. 16, no. 8, p. 16897, 2015.
- [19] P. O. Krutzik and G. P. Nolan, "Fluorescent cell barcoding in flow cytometry allows high-throughput drug screening and signaling profiling," *Nature Methods*, Article vol. 3, p. 361, 2006.
- [20] J. P. Nolan and L. A. Sklar, "The emergence of flow cytometry for sensitive, real-time measurements of molecular interactions," *Nature Biotechnology*, vol. 16, p. 633, 1998.
- [21] M. Deutsch *et al.*, "A novel miniature cell retainer for correlative high-content analysis of individual untethered non-adherent cells," *Lab on a Chip*, 10.1039/B603961H vol. 6, no. 8, pp. 995-1000, 2006.
- [22] E. Ostuni, C. S. Chen, D. E. Ingber, and G. M. Whitesides, "Selective Deposition of Proteins and Cells in Arrays of Microwells," *Langmuir*, vol. 17, no. 9, pp. 2828-2834, 2001.
- [23] J. R. Rettig and A. Folch, "Large-Scale Single-Cell Trapping And Imaging Using Microwell Arrays," *Analytical Chemistry*, vol. 77, no. 17, pp. 5628-5634, 2005.
- [24] S. Lindström, R. Larsson, and H. Andersson Svahn, "Towards high-throughput single cell/clone cultivation and analysis," *ELECTROPHORESIS*, vol. 29, no. 6, pp. 1219-1227, 2008.
- [25] D. D. Chaplin, "Overview of the immune response," *Journal of Allergy and Clinical Immunology*, vol. 125, no. 2, pp. S3-S23, 2010.
- [26] T. Kurosaki, K. Kometani, and W. Ise, "Memory B cells," *Nature Reviews Immunology*, Review Article vol. 15, p. 149, 2015.
- [27] N. P. Restifo and L. Gattinoni, "Lineage relationship of effector and memory T cells," *Current Opinion in Immunology*, vol. 25, no. 5, pp. 556-563, 2013.
- [28] W. M. Nauseef and N. Borregaard, "Neutrophils at work," *Nature Immunology*, Review Article vol. 15, p. 602, 2014.
- [29] E. Kolaczowska and P. Kubes, "Neutrophil recruitment and function in health and inflammation," *Nature Reviews Immunology*, Review Article vol. 13, p. 159, 2013.

- [30] V. Delgado-Rizo, M. A. Martinez-Guzman, L. Iniguez-Gutierrez, A. Garcia-Orozco, A. Alvarado-Navarro, and M. Fafutis-Morris, "Neutrophil Extracellular Traps and Its Implications in Inflammation: An Overview," *Front Immunol*, vol. 8, p. 81, 2017.
- [31] G. Rothe and M. Klouche, "Phagocyte Function," in *Methods in Cell Biology*, vol. 75: Academic Press, 2004, pp. 679-708.
- [32] H. Takei, A. Araki, H. Watanabe, A. Ichinose, and F. Sendo, "Rapid killing of human neutrophils by the potent activator phorbol 12-myristate 13-acetate (PMA) accompanied by changes different from typical apoptosis or necrosis," (in eng), *J Leukoc Biol*, vol. 59, no. 2, pp. 229-40, 1996.
- [33] V. Brinkmann *et al.*, "Neutrophil Extracellular Traps Kill Bacteria," *Science*, vol. 303, no. 5663, pp. 1532-1535, 2004.
- [34] R. H. Pires, S. B. Felix, and M. Delcea, "The architecture of neutrophil extracellular traps investigated by atomic force microscopy," *Nanoscale*, 10.1039/C6NR03416K vol. 8, no. 29, pp. 14193-14202, 2016.
- [35] F. H. Pilsczek *et al.*, "A Novel Mechanism of Rapid Nuclear Neutrophil Extracellular Trap Formation in Response to *Staphylococcus aureus*," *The Journal of Immunology*, vol. 185, no. 12, pp. 7413-7425, 2010.
- [36] A. B. Al-Khafaji, S. Tohme, H. O. Yazdani, D. Miller, H. Huang, and A. Tsung, "Superoxide induces Neutrophil Extracellular Trap Formation in a TLR-4 and NOX-dependent mechanism," *Molecular medicine (Cambridge, Mass.)*, vol. 22, pp. 621-631, 2016.
- [37] S. K. Jorch and P. Kubes, "An emerging role for neutrophil extracellular traps in noninfectious disease," *Nat Med*, Review vol. 23, no. 3, pp. 279-287, 2017.
- [38] H. D. Lewis *et al.*, "Inhibition of PAD4 activity is sufficient to disrupt mouse and human NET formation," *Nature Chemical Biology*, vol. 11, p. 189, 2015.
- [39] P. Li, M. Li, M. R. Lindberg, M. J. Kennett, N. Xiong, and Y. Wang, "PAD4 is essential for antibacterial innate immunity mediated by neutrophil extracellular traps," *The Journal of Experimental Medicine*, vol. 207, no. 9, pp. 1853-1862, 2010.
- [40] V. Papayannopoulos, K. D. Metzler, A. Hakkim, and A. Zychlinsky, "Neutrophil elastase and myeloperoxidase regulate the formation of neutrophil extracellular traps," *The Journal of Cell Biology*, vol. 191, no. 3, pp. 677-691, 2010.
- [41] J. F. Turrens, "Mitochondrial formation of reactive oxygen species," *The Journal of Physiology*, vol. 552, no. 2, pp. 335-344, 2003.
- [42] R. Mittler, "ROS Are Good," *Trends in Plant Science*, vol. 22, no. 1, pp. 11-19, 2017.
- [43] S. M. Yoo and S. Y. Lee, "Optical Biosensors for the Detection of Pathogenic Microorganisms," *Trends in Biotechnology*, vol. 34, no. 1, pp. 7-25, 2016.

- [44] A. J. Haes and R. P. Van Duyne, "A nanoscale optical biosensor: sensitivity and selectivity of an approach based on the localized surface plasmon resonance spectroscopy of triangular silver nanoparticles," *J Am Chem Soc*, vol. 124, no. 35, pp. 10596-604, 2002.
- [45] J. C. Riboh, A. J. Haes, A. D. McFarland, C. Ranjit Yonzon, and R. P. Van Duyne, "A Nanoscale Optical Biosensor: Real-Time Immunoassay in Physiological Buffer Enabled by Improved Nanoparticle Adhesion," *The Journal of Physical Chemistry B*, vol. 107, no. 8, pp. 1772-1780, 2003.
- [46] R. Shiwaku *et al.*, "A Printed Organic Circuit System for Wearable Amperometric Electrochemical Sensors," *Scientific Reports*, vol. 8, no. 1, p. 6368, 2018.
- [47] L. S. Dolci, S. Zanarini, L. Della Ciana, F. Paolucci, and A. Roda, "Development of a new device for ultrasensitive electrochemiluminescence microscopy imaging," *Anal Chem*, vol. 81, no. 15, pp. 6234-41, 2009.
- [48] B. R. Oh *et al.*, "Multiplexed Nanoplasmonic Temporal Profiling of T-Cell Response under Immunomodulatory Agent Exposure," *ACS Sensors*, vol. 1, no. 7, pp. 941-948, 2016.
- [49] S. S. Acimovic *et al.*, "LSPR chip for parallel, rapid, and sensitive detection of cancer markers in serum," *Nano Letters*, vol. 14, no. 5, pp. 2636-41, 2014.
- [50] P. Chen *et al.*, "Multiplex serum cytokine immunoassay using nanoplasmonic biosensor microarrays," *ACS Nano*, vol. 9, no. 4, pp. 4173-81, 2015.
- [51] H. Yoshikawa, M. Murahashi, M. Saito, S. Jiang, M. Iga, and E. Tamiya, "Parallelized label-free detection of protein interactions using a hyper-spectral imaging system," *Analytical Methods*, 10.1039/C5AY00738K vol. 7, no. 12, pp. 5157-5161, 2015.
- [52] T. Endo, S. Yamamura, N. Nagatani, Y. Morita, Y. Takamura, and E. Tamiya, "Localized surface plasmon resonance based optical biosensor using surface modified nanoparticle layer for label-free monitoring of antigen–antibody reaction," *Science and Technology of Advanced Materials*, vol. 6, no. 5, pp. 491-500, 2005.
- [53] B. R. Oh *et al.*, "Integrated nanoplasmonic sensing for cellular functional immunoanalysis using human blood," *ACS Nano*, vol. 8, no. 3, pp. 2667-76, 2014.
- [54] F. Fernandez, O. Garcia-Lopez, E. Tellechea, A. C. Asensio, and I. Cornago, "LSPR Cuvette for Real-Time Biosensing by Using a Common Spectrophotometer," *IEEE Sensors Journal*, vol. 16, no. 11, pp. 4158-4165, 2016.
- [55] M. Bhagawati, C. You, and J. Piehler, "Quantitative real-time imaging of protein-protein interactions by LSPR detection with micropatterned gold nanoparticles," *Analytical Chemistry*, vol. 85, no. 20, pp. 9564-71, 2013.
- [56] T. Huang, P. D. Nallathamby, and X. H. Xu, "Photostable single-molecule nanoparticle optical biosensors for real-time sensing of single cytokine molecules and their binding

- reactions," *Journal of the American Chemical Society*, vol. 130, no. 50, pp. 17095-105, 2008.
- [57] T. Endo, K. Kerman, N. Nagatani, Y. Takamura, and E. Tamiya, "Label-free detection of peptide nucleic acid-DNA hybridization using localized surface plasmon resonance based optical biosensor," *Analytical Chemistry*, vol. 77, no. 21, pp. 6976-84, 2005.
  - [58] G. Bellapadrona *et al.*, "Optimization of localized surface plasmon resonance transducers for studying carbohydrate-protein interactions," *Analytical Chemistry*, vol. 84, no. 1, pp. 232-40, 2012.
  - [59] K. M. Mayer *et al.*, "A label-free immunoassay based upon localized surface plasmon resonance of gold nanorods," *ACS Nano*, vol. 2, no. 4, pp. 687-92, 2008.
  - [60] J. Breault-Turcot and J. F. Masson, "Nanostructured substrates for portable and miniature SPR biosensors," *Analytical and Bioanalytical Chemistry*, journal article vol. 403, no. 6, pp. 1477-84, 2012.
  - [61] M. Y. Berezin and S. Achilefu, "Fluorescence lifetime measurements and biological imaging," *Chemical Reviews*, vol. 110, no. 5, pp. 2641-84, 2010.
  - [62] P. K. Chattopadhyay, T. M. Gierahn, M. Roederer, and J. C. Love, "Single-cell technologies for monitoring immune systems," *Nature Immunology*, vol. 15, no. 2, pp. 128-35, 2014.
  - [63] N. Yoshimoto *et al.*, "An automated system for high-throughput single cell-based breeding," *Scientific Reports*, Article vol. 3, p. 1191, 2013.
  - [64] L. Judith, M. N. Sergey, and M. L.-M. Luis, "Sensing using plasmonic nanostructures and nanoparticles," *Nanotechnology*, vol. 26, no. 32, p. 322001, 2015.
  - [65] M. P. Raphael, J. A. Christodoulides, J. B. Delehanty, J. P. Long, and J. M. Byers, "Quantitative imaging of protein secretions from single cells in real time," *Biophysical Journal*, vol. 105, no. 3, pp. 602-8, 2013.
  - [66] S. Y. Chou, P. R. Krauss, and P. J. Renstrom, "Imprint of sub - 25 nm vias and trenches in polymers," *Applied Physics Letters*, vol. 67, no. 21, pp. 3114-3116, 1995.
  - [67] S. Chou, P. R. Krauss, W. Zhang, L. Guo, and L. Zhuang, "Sub-10 nm imprint lithography and applications," *Journal of Vacuum Science and Technology B*, vol. 15, no. 6, pp. 2897-2904, 1997.
  - [68] F. Buyukserin, M. Aryal, J. Gao, and W. Hu, "Fabrication of polymeric nanorods using bilayer nanoimprint lithography," *Small*, vol. 5, no. 14, pp. 1632-6, 2009.
  - [69] P.-S. Lee, O.-J. Lee, S.-K. Hwang, S.-H. Jung, S. E. Jee, and K.-H. Lee, "Vertically Aligned Nanopillar Arrays with Hard Skins Using Anodic Aluminum Oxide for Nano Imprint Lithography," *Chemistry of Materials*, vol. 17, no. 24, pp. 6181-6185, 2005.

- [70] J. Chen *et al.*, "UV-nanoimprint lithography as a tool to develop flexible microfluidic devices for electrochemical detection," *Lab on a Chip*, 10.1039/C5LC00515A vol. 15, no. 14, pp. 3086-94, 2015.
- [71] Y. Song *et al.*, "AC Electroosmosis-Enhanced Nanoplasmofluidic Detection of Ultralow-Concentration Cytokine," *Nano Letters*, vol. 17, no. 4, pp. 2374-2380, 2017.
- [72] L. A. Walsh, J. L. Allen, and T. A. Desai, "Nanotopography applications in drug delivery," *Expert Opinion on Drug Delivery*, vol. 12, no. 12, pp. 1823-7, 2015.
- [73] B. Bilenberg *et al.*, "Topas-based lab-on-a-chip microsystems fabricated by thermal nanoimprint lithography," *Journal of Vacuum Science and Technology B*, vol. 23, no. 6, pp. 2944-2949, 2005.
- [74] A. W. Martinez, S. T. Phillips, G. M. Whitesides, and E. Carrilho, "Diagnostics for the developing world: microfluidic paper-based analytical devices," *Analytical Chemistry*, vol. 82, no. 1, pp. 3-10, 2010.
- [75] R. Pelton, "Bioactive paper provides a low-cost platform for diagnostics," *TrAC Trends in Analytical Chemistry*, vol. 28, no. 8, pp. 925-942, 2009.
- [76] M. Saito *et al.*, "Novel gold-capped nanopillars imprinted on a polymer film for highly sensitive plasmonic biosensing," *Analytical Chemistry*, vol. 84, no. 13, pp. 5494-500, 2012.
- [77] S. Jiang, M. Saito, M. Murahashi, and E. Tamiya, "Pressure free nanoimprinting lithography using ladder-type HSQ material for LSPR biosensor chip," *Sensors and Actuators B: Chemical*, vol. 242, pp. 47-55, 2017.
- [78] L. Huang, Y. Chen, Y. Chen, and H. Wu, "Centrifugation-Assisted Single-Cell Trapping in a Truncated Cone-Shaped Microwell Array Chip for the Real-Time Observation of Cellular Apoptosis," *Analytical Chemistry*, vol. 87, no. 24, pp. 12169-76, 2015.
- [79] W. Aoki *et al.*, "Comprehensive characterization of secreted aspartic proteases encoded by a virulence gene family in *Candida albicans*," *Journal of Biochemistry*, vol. 150, no. 4, pp. 431-8, 2011.
- [80] A. Gonzalez-Quintela *et al.*, "Serum levels of immunoglobulins (IgG, IgA, IgM) in a general adult population and their relationship with alcohol consumption, smoking and common metabolic abnormalities," *Clinical and experimental immunology*, vol. 151, no. 1, pp. 42-50, 2008.
- [81] S. Rodriguez-Segade *et al.*, "High serum IgA concentrations in patients with diabetes mellitus: age-wise distribution and relation to chronic complications," *Clinical Chemistry*, vol. 42, no. 7, pp. 1064-7, 1996.
- [82] M. J. Kaplan and M. Radic, "Neutrophil extracellular traps: double-edged swords of innate immunity," *J Immunol*, vol. 189, no. 6, pp. 2689-95, 2012.

- [83] C. Rosales, N. Demaurex, C. A. Lowell, and E. Uribe-Querol, "Neutrophils: Their Role in Innate and Adaptive Immunity," *J Immunol Res*, vol. 2016, p. 1469780, 2016.
- [84] K. H. Lee *et al.*, "Neutrophil extracellular traps (NETs) in autoimmune diseases: A comprehensive review," *Autoimmun Rev*, vol. 16, no. 11, pp. 1160-1173, 2017.
- [85] M. J. Fritzler, A. Wiik, M. L. Fritzler, and S. G. Barr, "The use and abuse of commercial kits used to detect autoantibodies," *Arthritis Res Ther*, vol. 5, no. 4, pp. 192-201, 2003.
- [86] S. C. Bendall, G. P. Nolan, M. Roederer, and P. K. Chattopadhyay, "A deep profiler's guide to cytometry," *Trends Immunol*, vol. 33, no. 7, pp. 323-32, 2012.
- [87] S. C. Bendall *et al.*, "Single-Cell Mass Cytometry of Differential Immune and Drug Responses Across a Human Hematopoietic Continuum," *Science*, vol. 332, no. 6030, pp. 687-696, 2011.
- [88] R. Sharma, S. Roychoudhury, N. Singh, and Y. Sarda, "Methods to Measure Reactive Oxygen Species (ROS) and Total Antioxidant Capacity (TAC) in the Reproductive System," in *Oxidative Stress in Human Reproduction* Cham: Springer International Publishing, 2017, pp. 17-46.
- [89] L. A. Pavelescu, "On reactive oxygen species measurement in living systems," *J Med Life*, vol. 8 Spec Issue, no. Spec Issue, pp. 38-42, 2015.
- [90] L. E. Kippner, J. Kim, G. Gibson, and M. L. Kemp, "Single cell transcriptional analysis reveals novel innate immune cell types," *PeerJ*, vol. 2, p. e452, 2014.
- [91] D. Wang and S. Bodovitz, "Single cell analysis: the new frontier in 'omics'," *Trends Biotechnol*, vol. 28, no. 6, pp. 281-90, 2010.
- [92] J. R. Heath, A. Ribas, and P. S. Mischel, "Single-cell analysis tools for drug discovery and development," *Nat Rev Drug Discov*, Review vol. 15, no. 3, pp. 204-216, 2016.
- [93] M. Bengtsson, A. Stahlberg, P. Rorsman, and M. Kubista, "Gene expression profiling in single cells from the pancreatic islets of Langerhans reveals lognormal distribution of mRNA levels," (in eng), *Genome Res*, vol. 15, no. 10, pp. 1388-92, 2005.
- [94] A. E. Cetin *et al.*, "Handheld high-throughput plasmonic biosensor using computational on-chip imaging," *Light Sci Appl*, Original Article vol. 3, p. e122, 2014.
- [95] A. F. Coskun, A. E. Cetin, B. C. Galarreta, D. A. Alvarez, H. Altug, and A. Ozcan, "Lensfree optofluidic plasmonic sensor for real-time and label-free monitoring of molecular binding events over a wide field-of-view," Article vol. 4, p. 6789, 2014.
- [96] T. Kinpara *et al.*, "A Picoliter Chamber Array for Cell-Free Protein Synthesis," *The Journal of Biochemistry*, vol. 136, no. 2, pp. 149-154, 2004.
- [97] G. D. Sulka, "Highly Ordered Anodic Porous Alumina Formation by Self-Organized Anodizing," in *Nanostructured Materials in Electrochemistry*, A. Eftekhari, Ed.: Wiley-VCH Verlag GmbH & Co. KGaA, 2008, pp. 1-116.



- [98] A. Karlsson, J. B. Nixon, and L. C. McPhail, "Phorbol myristate acetate induces neutrophil NADPH-oxidase activity by two separate signal transduction pathways: dependent or independent of phosphatidylinositol 3-kinase," *Journal of Leukocyte Biology*, vol. 67, no. 3, pp. 396-404, 2000.
- [99] K. D. Metzler, C. Goosmann, A. Lubojemska, A. Zychlinsky, and V. Papayannopoulos, "A myeloperoxidase-containing complex regulates neutrophil elastase release and actin dynamics during NETosis," *Cell Rep*, vol. 8, no. 3, pp. 883-96, 2014.
- [100] M. Hideki and S. Masahiro, "Fabrication of Gold Nanodot Array Using Anodic Porous Alumina as an Evaporation Mask," *Japanese Journal of Applied Physics*, vol. 35, no. 1B, p. L126, 1996.
- [101] H. Ha Minh *et al.*, "Immobilization of Gold Nanoparticles on Aluminum Oxide Nanoporous Structure for Highly Sensitive Plasmonic Sensing," *Japanese Journal of Applied Physics*, vol. 49, no. 6S, p. 06GM02, 2010.
- [102] R. A. M. Ali *et al.*, "One-step nanoimprinted hybrid micro-/nano-structure for in situ protein detection of isolated cell array via localized surface plasmon resonance," (in English), *Japanese Journal of Applied Physics*, vol. 57, no. 3S2, p. 03EC03, 2018.
- [103] N. M. Kovalchuk, E. Roumpea, E. Nowak, M. Chinaud, P. Angeli, and M. J. H. Simmons, "Effect of surfactant on emulsification in microchannels," *Chemical Engineering Science*, vol. 176, pp. 139-152, 2018.

## List of publications

1. Riyaz Ahmad Mohamed Ali, Wilfred Villariza Espulgar, Wataru Aoki, Shu Jiang, Masato Saito, Mitsuyoshi Ueda and Eiichi Tamiya. One-step nanoimprinted hybrid micro-/nano-structure for in situ protein detection of isolated cell array via localized surface plasmon resonance. Japanese Journal of Applied Physics, 2018, 57, 03EC03.
2. Riyaz Ahmad Mohamed Ali, Daiki Mita, Wilfred Espulgar, Masato Saito, Hyota Takamatsu, Hiroyuki Yoshikawa, Masayuki Nishide and Eiichi Tamiya. Single cell analysis of neutrophils by microscopic LSPR imaging system. Analyst (under review).
3. Riyaz Ahmad Mohamed Ali, Wilfred Espulgar, Masato Saito, Hyota Takamatsu, Hiroyuki Yoshikawa and Eiichi Tamiya. Luminol based electrochemiluminescence monitoring of active human neutrophils cells. (in preparation).

## List of attended scientific conference

1. Riyaz Ahmad Mohamed Ali, Masato Saito, Mizuho Murahashi, Eiichi Tamiya. "Development of micro- and nano-structured LSPR chip for label free single cell assay". The 77<sup>th</sup> Japan society of Applied Physics Autumn meeting, Toki Messe (Niigata Convention Center), 13-16 September 2016. (Poster presentation).
2. Riyaz Ahmad Mohamed Ali, Masato Saito, Mizuho Murahashi, Eiichi Tamiya. "Development of nano/micro- structured plasmonic chip for single cell array application". The 64<sup>th</sup> Japan society of Applied Physics Spring meeting, Pacifico, Yokohama, 14-17 March 2017. (Oral presentation).
3. Riyaz Ahmad Mohamed Ali, Masato Saito, Mizuho Murahashi, Eiichi Tamiya. "Study of nano/micro- structured plasmonic chip for label free cell array application". The 3<sup>rd</sup> Kansai branch – applied physics society meeting 2017, Nakanoshima Center, Osaka, 24 February 2017. (Poster presentation).
4. Riyaz Ahmad Mohamed Ali, Masato Saito and Eiichi Tamiya. "Study of hybrid micro/nano plasmonic structure for single cell array application". The 9<sup>th</sup> International conference on molecular electronics & bioelectronics, Kanazawa, Japan, 26-28 June 2018. (Poster presentation).
5. Riyaz Ahmad Mohamed Ali, Masato Saito and Eiichi Tamiya. "Nanoplasmonic enhanced micro-structured chip for single cell sensing application". The 78<sup>th</sup> Japan society of Applied Physics Autumn meeting, Fukuoka International Congress Center, 5-8 September 2017. (Poster presentation).
6. Riyaz Ahmad Mohamed Ali, Masato Saito and Eiichi Tamiya. "AC electro-osmosis enhanced microwell array for cell maneuver assist application". The 65<sup>th</sup> Japan society of Applied Physics Spring meeting, Nishi – Waseda campus, Waseda University, 17-20 March 2018. (Poster presentation).
7. Riyaz Ahmad Mohamed Ali, Mazumder Joyotu, Masato Saito and Eiichi Tamiya. "Luminol based electrochemiluminescence biosensor for in situ reactive oxygen species quantification". The 12<sup>th</sup> Symposium on Biorelevant Chemistry, CSJ, Osaka University, 9-11 September 2018. (Poster presentation).

## Acknowledgement

This thesis become into reality with lots of love and kind support from many individuals. With this accomplishment, it an honour to express my gratitude to all special people who had supported and travelled with me along the way carving each words making this dissertation a dream come true. I am tremendously fortunate to have such a wonderful family who constantly provide their time for me.

First, I would like to give express my sincerest gratitude and appreciation to my professor, Professor Dr Eiichi Tamiya, who had initially provide me, one of the greatest opportunity in my lifetime to pursue doctoral degree under his keen supervision in the Land of the Rising Sun, Japan. Whenever there is cliff-hanger situation regrading my research, Professor Tamiya never failed to impress with his brilliant ideas or new perspective approach what could change the course immediately into its direction. Not only enriched with research knowledge, Professor Tamiya's passion for world issue and his deep understanding of Japanese tradition keep me amazed. His word of wisdom and encouragement, grows an interest inside me to keep exploring some new branch of study.

My research journey could not be smooth without the help from Dr. Masato Saito, Dr. Hiroyuki Yoshikawa, Dr. Wilfred Espulagar, Dr. Luo Xi, Dr. Hyota Takamatsu, Dr. Masayuki Nishide, Prof Dr Quamrul Hassan, Dr. Wataru Aoki, Mr. Joyotu Mazumder and Mr. Daiki Mita. Numerous time, this research has travel at pace as like in roller coaster, but with the morale support and research guidance, this study has progress and reached its objective.

I would like to express my love to my family member; Mr Mohamed Ali, Ms. Mumtaj Begum, Mr. Mohamed Rafiq, Mr. Kamal Batcha, Ms. Raseena Sanofer and little master Raaif Ahmad, who never miss prayer and thought for me and being my backbone though this stay and study. Also, my lab members, Ms. Araki, Chen, Zhu, Jonathan, Hoori, Okajima, Ono, Toma, Ide and other members who made lots of colourful memories in my life.

Special acknowledgement to the Malaysian Ministry of Education and Universiti Tun Hussein Onn Malaysia (UTHM) who provide me financial support to keep me survive for the entire study. Also I

would like to express my gratitude to Prof (retired) Dr Zainal Abidin, AP Dr Rosli Omar, AP Dr Nafarizal Nayan, AP Dr Muhammad Mahadi, AP Dr Babul Salam, Dr Jais Lias, Ms. Masnani, Mr Hazwaj and others (the list will be long) who provide me the guidance, technical and morale support from Malaysia to me.

Thank you..

Empty page